

Viscoelasticity of Filled Elastomers: Determination of Surface-Immobilized Components and their Role in the Reinforcement of SBR-Silica Nanocomposites

DISSERTATION

zur Erlangung des akademischen Grades

doctor rerum naturalium

(Dr. rer. nat.)

genehmigt durch

die Naturwissenschaftliche Fakultät II

Institut für Physik

der Martin-Luther-Universität

Halle-Wittenberg

vorgelegt von

M. Sc. Anas Muftaba

geboren am 03.04.1980 in Lahore, Pakistan

Halle (Saale), January 15th, 2014

Gutachter:

1. Prof. Dr. Thomas Thurn-Albrecht
2. Prof. Dr. Manfred Klüppel
3. Prof. Dr. Rene Androsch

Öffentliche Verteidigung: July 3rd, 2014

In loving memory of my beloved Sister

Rabbia

“She will be in my Heart ξ by my Side for the Rest of my Life”

Contents

1	Introduction	1
2	Theoretical Background	5
2.1	Elastomers	5
2.1.1	Fundamental Theories on Rubber Elasticity	7
2.2	Fillers	10
2.2.1	Carbon Black	12
2.2.2	Silica	12
2.3	Filled Rubber Reinforcement	15
2.3.1	Occluded Rubber	16
2.3.2	Payne Effect	17
2.3.3	The Kraus Model for the Strain-Softening Effect	18
2.3.4	Filler Network Reinforcement	20
3	Experimental Methods	29
3.1	Dynamic Mechanical Analysis	29
3.1.1	Temperature-dependent Measurement (Temperature Sweeps)	31
3.1.2	Time-Temperature Superposition (Master Curves)	31
3.1.3	Strain-dependent Measurement (Payne Effect)	33
3.2	Low-field NMR	34
3.2.1	Theoretical Concept	34
3.2.2	Experimental Details	39
4	Optimizing the Tire Tread	43
4.1	Relation Between Friction and the Mechanical Properties of Tire Rubbers	46
4.2	Usage of $\tan \delta$ As Loss Parameter	48
4.2.1	Theoretical Approach	49
4.2.2	Experimental Indication	52

4.3	Tire Optimizing Parameters and their Relation to Viscoelastic Behavior and Friction	54
4.3.1	Wet Traction	54
4.3.2	Rolling Resistance	55
4.3.3	Summary	57
5	Sample Mixing and Processing	59
5.1	Rubber Mixing and Processing	60
5.2	Vulcanization	61
5.3	Morphological Analysis by TEM	63
6	Results	65
6.1	Filler Reinforcement	65
6.2	Frequency-Dependent Mechanical Response of the Composite	68
6.2.1	Master Curve Construction of the Filled Composite Following WLF Procedure	70
6.2.2	Master Curves For Nanocomposites	71
6.3	Evaluation of Immobilized Fractions in Composites	75
6.4	Factors Contributing to Reinforcement	79
6.4.1	Quantification of Crosslink Density of Nanocomposites in Absolute Units	79
6.4.2	Filler Network	83
6.4.3	Occluded Rubber	88
6.5	Viscoelasticity of Filler Network	89
6.6	Parameters Influencing Energy Dissipation in Filled Rubbers	93
7	Conclusion	97
A	Isothermal Frequency Sweeps (80 phr Silica-filled)	101
	Bibliography	103

Chapter 1

Introduction

Elastomers containing nano-sized fillers like carbon black or silica with large filler surface area are of central importance for different fields of application. An automobile tire is a field of standard application where such composite materials are extensively used. The optimization of elastomer composites containing nanoparticle for tire treads is a conventional problem and of major importance for the performance of tires. [1–5] This is primarily a three-parameter optimization problem since rolling resistance, wet grip and abrasion result in different requirements regarding the mechanical properties of an elastomer nanoparticle composite. Most relevant for wet grip and rolling resistance is the dissipation in different frequency ranges. [6–8] While the wet grip is determined by the relaxation behavior at high frequencies and small strain amplitudes, the rolling resistance is, according to experimental studies on realistic road surfaces and related simulations, connected with the dissipation at lower frequencies [9–11]. Due to instrumental limitations, estimation of high frequency dissipation is not possible. In order to estimate high frequency relaxation and dissipation in the filled elastomer, the optimization of the tire is often based on existing experience, extended screening experiments and empirical rules based on time-temperature superposition principle. This is due to the fact that there are various effects on the microscopic scale influencing the dissipation behavior in parallel which are still not well understood from the scientific point of view. Although this is known since decades, a predictive understanding of the parameters influencing application relevant quantities like fuel consumption, CO₂ emission, abrasion or braking behavior of tires is, however still missing. The optimization of composite materials for tire applications touches fundamental scientific questions in the field of soft matter science like those for the origin of the glass transition, [12–19] the influence of spatial confinement effects, [20–23] constraints at interfaces, [24–28]

and network topology [29–32] on the dynamics of polymers. This shows nicely that there is a close relation between basic research in the field of soft matter science and traditional applications of filled elastomers in tires. From that perspective it seems important to understand and quantify effects influencing the relaxation dynamics of filled elastomers based on real/applied systems and modern techniques to characterize network topology, mesostructure and confined dynamics of composite materials.

Many decades of research have been devoted to understand the strong synergistic effect of particles dispersed on level of nanometers and above, not only their interactions among themselves but also with the polymer matrix [33–36]. High reinforcement has been desired characteristic for those products and defined as enhanced modulus, stiffness, rupture energy, tear strength, tensile strength, abrasion resistance, fatigue resistance and cracking resistance [37, 38]. A number of hydrodynamic (volumetric argument) and molecular network mechanisms have been proposed to explain the phenomenon of filler reinforcement. The hydrodynamic theory of Einstein-Smallwood established a relationship between the volume concentration of filler and the observed increased modulus. A strain-induced softening effect of filled vulcanizates has been extensively studied and modeled by Payne and Kraus [39–42], attributed this effect arises due to the simultaneous breakdown and formation of filler-filler bonds. A concept of jammed particle network due to the flocculation of primary filler aggregates has been presented by Heinrich and Klüppel [8, 43–45]. Flocculation studies consider the small strain mechanical response of the uncrosslinked composites and demonstrate that a relative movement of the particles takes place that depends on particle size, molar mass of the polymer as well as polymer-filler and filler-filler interaction. Hence they proposed that the strong reinforcement at small mechanical deformations arises due to a kinetic cluster-cluster aggregation (CCA) mechanism of filler particles in the rubber matrix to form a filler network. A range of models has been reported to explain the mechanical measurements relying only on the presence of strong polymer-filler interactions [34, 46–51]. The mechanically active nanoparticle network can be thought of as being connected by elastic chains that connect the particles, thus assuming the particles to be “giant crosslinks” [52, 53]. The temperature dependent mechanical reinforcement has often been explained by more specific interactions arising from “glassy” (precisely: immobilized) polymer fractions [34, 54–56] that likely exhibit a glass transition temperature gradient [57–59].

The models assuming the formation of glassy polymer bridges between the filler particles are among the most widely accepted ones. However, there is no clear consensus concerning its relevance in actual, technologically relevant elastomers [60]. Numerous

theoretical studies [46, 61–63] and experiments [28, 55, 56, 64–67] have been conducted on model systems where particular care has been taken to enhance the polymer-filler interactions and the homogeneous distribution of the fillers within the matrix. In some cases, the “glassy layers” have been observed directly on model systems by NMR [28, 67] or by DSC or by other experimental techniques [57, 65, 68, 69]. In other cases, to explain the temperature- and frequency-dependent mechanical [55, 64] or dielectric [56, 65] data, glassy layers has been assumed. However, significant amounts of immobilized polymer have either not been observed directly at all, or have not been directly related to mechanical properties in the same sample. A previous, well-cited study of Tsagaropoulos and Eisenberg [64] has shown a second, high-temperature peak in the mechanical loss tangent ($\tan \delta$) in different types of non-crosslinked polymers filled with silica nanoparticles. This second peak was interpreted as an increased glass transition temperature of adsorbed polymer chains on the filler surfaces. This interpretation was later challenged by Robertson and coworkers [70] and it has been nicely proved that the second $\tan \delta$ peak is attributed to a terminal flow rather than a second alpha relaxation process. This example demonstrates the danger of such indirect interpretations.

The extensive and convincing experimental work of Montes, Lequeux, Long, and coworkers [28, 58, 67, 71] precisely demonstrate and explain the temperature- and frequency-dependent mechanical properties based on experimentally determined glassy polymer around the filler particles. Therefore, their model [54] is based on the presence of glassy layer around the fillers particles and strong reinforcement is obtained when glassy layers of the fillers overlaps, forming a glassy bridge between adjacent filler particle. The dynamics of breaking and rebirth of glassy bridges account for the nonlinear Payne and Mullins effects. These mechanisms account also for dissipative properties of filled elastomers under nonlinear mechanical deformations. However these studies are based upon a rather idealized model material characterized by tailored and particularly strong polymer-filler interaction. Nevertheless the finite-element simulation work of Gusev [61] proposed the similar phenomenon that only minute amounts of increased- T_g material (down to the sub-percent level) located remotely in the gaps between or around filler particles can already explain the enhanced storage modulus and the additional dissipation in filled elastomers.

In this thesis a combination of mechanical and NMR spectroscopy is presented in technologically relevant silica-filled Styrene-butadiene rubber (SBR) samples. For the first time in these systems, a direct correlation between enhanced mechanical properties and quantitative detection of immobilized-component within the matrix is demonstrated. The mechanical shear spectroscopy was used on samples filled with different amount of

silica nanoparticles, to measure not only fixed-frequency storage and loss modulus at different temperatures but to construct the master curves over the extended frequency range. We observed the relaxatory nature of the filler-induced reinforcement effect [72] from the shear measurements only in high silica-filled composites. This relaxatory nature of composite was regarded as a characteristic feature of a percolating solid phase in matrix called a filler network. The filler network contribution ΔG to the plateau modulus above the percolation threshold was separated by using an analysis of the sample's linear and non-linear response [72]. Proton low-field NMR was used for a direct molecular observation of immobilized components of the matrix as a function of temperature at different filler loadings. The magic-sandwich echo (MSE) was used to study the polymer relaxation at short time scales i.e., less than 0.2 ms [28,57]. By using MSE-refocused free induction decay (FID), a precise information of polymer dynamics near the filler surfaces was obtained as an immobilized fraction of the matrix which is observed as a function of temperature and the filler fraction. The NMR-observable immobilized fraction quantifies the mechanically rigid component of the elastomeric matrix (modulus $\approx 10^9$ Pa), assumed to be confined within the filler network. In short, by combining the results obtained from the mechanical analysis and the NMR, it is concluded that the filler network holds viscoelastic properties.

This systematic study helps to gain deeper insights into phenomena determining the properties of filled elastomers and potentially contributes to a more efficient optimization of such materials.

Chapter 2

Theoretical Background

2.1 Elastomers

Elastomers belong to a class of polymers which has ability to undergo large reversible-elastic deformations i.e., after stretching, they return to their original shape in a reversible way. Raw elastomers consist of long polymer chains which can flow under the applied strain. In order to make elastomers mechanically more useful, a process named vulcanization/ curing is usually carried out. Figure 2.1 shows the polymer structure before and after the vulcanization process. This process involves the conversion of a raw rubber into a network due to the formation of crosslinks, chemical bonds or bridges by using curing systems like sulfur based and/ or peroxide based systems. During the process, a viscous entanglement of long chain molecules is converted into a three dimensional elastic network by insertion of crosslinks.

The overall usage of the rubber in the world is estimated around 15 million metric ton [73]. This amount of usage is further divided between natural rubber, which accounts for 35% of global consumption, and synthetic rubber, of which styrene-butadiene rubber (SBR) accounts for 18%. Nearly 75% of the rubber consumption goes to tire industry. In this regard, Natural rubber usage has increased significantly in modern radial tires. The reason for the increase is due to improved strength, lower tire temperatures dissipated under given load conditions, and lower tire rolling resistance to get better fuel efficiency. SBR was the first successful commercial grade of synthetic rubber, which was then named as Buna S in the 1930s in Germany [74]. Today, SBR ranks first in world annual production of all the synthetic rubbers, which finds extensive applications in manufacturing tire treads, accounting for over 65% of the synthetic rubbers used in tire industry [73]. A typical SBR monomeric unit containing styrene

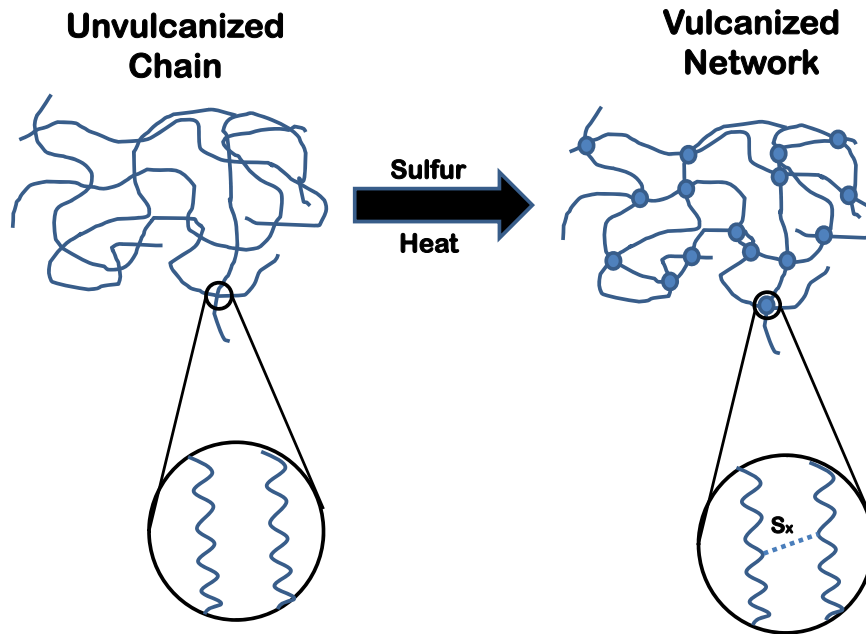


Figure 2.1: Vulcanization process.

and vinyl butadiene monomers is shown in Figure 2.2a.

SBR is a random copolymer of styrene and butadiene (styrene and butadiene can also be polymerized as block copolymer SBS, which is used as thermoplastic elastomer), with a usual styrene content of 23 to 40% [74]. Due to the fact that different arrangement of the monomer within a polymer chain can be possible by the addition of butadiene to the polymer chain, BR as well as SBR could have different microstructures, and the ratio of these different monomeric isomers depends on the polymerization condition. The different microstructures for butadiene are *cis*-1,4, *trans*-1,4, and vinyl, as shown in the following Figure 2.2b. Due to the random distribution of different configurations in the polymer chain of the SBR, there is no regularity and hence they are noncrystalline materials. The macrostructure of a polymeric material, that includes molecular weight, polymer branching, crosslink distribution and crystallite formation, governs the overall thermo-mechanical properties of the elastomers. For SBR with a styrene content of 23.5%, the T_g is usually -50°C , which increases with the addition of styrene and vinyl level. A study of Day and Futamura [73] on the effect of varying vinyl and styrene content in SBR on the final vulcanizate properties, shows i) an increased tensile strength with increasing styrene content ii) vinyl content tends to reduce both tear strength and ultimate elongation, and iii) hysteretic properties are hardly effected by vinyl or styrene content if T_g is constant [73].

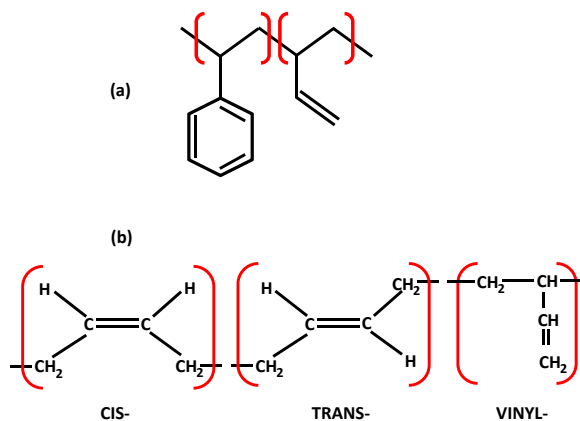


Figure 2.2: (a) Chemical structure of a monomeric unit of the vinyl SBR. (b) Possible configurations for butadiene in SBR and PBD.

SBR can be polymerized either from emulsion or solution, with the products named as ESBR (Emulsion SBR) and SSBR (Solution SBR) respectively. Emulsion polymerization of SBR follows the mechanism of free radical polymerization, leading to a copolymer with a broad MWD (molecular weight distribution), random copolymer composition, and long chain branching [74]. The microstructure is generally not controllable, because the temperature of the polymerization affects the ratio of trans to cis formation. Solution SBR is synthesized in a living anionic polymerization reaction usually initiated by alkyl lithium compounds [73]. This kind of polymerization gives products with narrower MWD and lower T_g than corresponding emulsion polymerized polymers. ESBRs show superior performance in wet traction, while a SSBR with the same styrene content gives lower rolling resistance and better tread wear. The living feature of the solution polymerizations brings a wide degree of freedom to design a polymer microstructure, polymer modification, composition and molecular weight distribution [75].

2.1.1 Fundamental Theories on Rubber Elasticity

The important and unique property of a polymer network is the elasticity. This property is based on the macromolecular construction of the polymers and the ability to alter their configuration by the thermal motions and the external mechanical stress. When a polymer chain is stretched, it has to change its conformation by rotating the covalent bonds along the chain. In this stretched state, the number of possible conformational states is much less. That is to say, entropy is greatly reduced upon stretching. When releasing the external stress, the polymer chain would return to the original coil

state since entropy always favors to be maximized and the polymer chain adopt their entropically favored random-coil conformation [76].

By loading the network under mechanical stress, the polymer chains behave as entropic springs. This can be explained with the help of thermodynamics of the rubbers. According to first law of thermodynamics, the change in internal energy of a polymer system is the sum of all the energy changes: e.g., heat added to the system TdS , work done upon network deformation fdL . Hence the force f applied to deform a network, consists of two contributions:

$$f = \left(\frac{\partial F}{\partial L} \right)_{T,V} = \left(\frac{\partial U}{\partial L} \right)_{T,V} - T \left(\frac{\partial S}{\partial L} \right)_{T,V} \quad (2.1)$$

The first term on the right side of the equality describes how the internal energy changes with the sample length ($f_E = \left(\frac{\partial U}{\partial L} \right)_{T,V}$). While the second contribution is the product of absolute temperature and the rate of change of entropy with sample length ($f_S = T \left(\frac{\partial S}{\partial L} \right)_{T,V}$).

On the contrary to the polymer networks, very small deformations on an atomic scale cause a huge increase of internal energy in solids like crystals, metals and ceramics. The increase of internal energy is several orders of magnitude higher than for comparable deformations of polymer networks. Hence the energetic contribution dominates the total deformational force for such systems. In “ideal polymer networks” however, there is no energetic contribution to elasticity, so $f_E = 0$. The dominance of the entropic part of Eq 2.1 bestows peculiar temperature dependence to the force at constant extension. The network strands lose conformation entropy when stretched making $\frac{\partial S}{\partial L} < 0$ and the force increases with increasing temperature [77].

Several theoretical models have been developed to describe rubber-like elasticity. All the models deal with the fundamental problem concerning the precise description and identification of the microscopic origin of the change in entropy due to deformation of a network. Additionally another problem is defining the distributions of the length of network strands between the crosslinks [78]. Since the precise estimation of the length of network strand is hardly accessible by experiments, many theories for the description of rubber-like elasticity are based on the assumption of ideal, defect-free homogeneous polymer network. The two main network models used are the *Affine model* by Hermans, Flory and Wall [79, 80], and the *Phantom model* by James and Guth [81, 82].

The simplest model that explains the idea of rubber elasticity is the affine network model. The main assumption of this model is an affine deformation: the relative

deformation of each network strand is the same as the macroscopic relative deformation imposed on the whole network. Accordingly the affine length (R_{aff}) is defined as the shortest length scale at which the parts of the network deform proportionally to the deformation of the network as a whole (deform affinely). At length scale shorter than R_{aff} , the deformation is said to be nonaffine and is characterized by the conformations of the individual network chains [76]. Based on the statistical theory of rubber elasticity which utilizes thermodynamic concepts to derive the relationship between stress and strain, the shear modulus G for uniaxial deformations is calculated,

$$G = \frac{nkT}{V} = \nu kT = \frac{\rho RT}{M_c} \quad (2.2)$$

The number of network strands per unit volume (number density of strands) is $\nu = n/V$. In the last equality, ρ is the network density (mass per unit volume), M_c is the number-average molar mass of a network strand, and R is the gas constant. The network modulus increases with temperature because it has entropic origin. The modulus also increases linearly with the number density of network strands $\nu = n / V = \rho N_A / M_c$.

According to the affine model, the network is assumed to be consisting of non-fluctuating elastic crosslinks where the individual network strands are fixed permanently. In contrast to this assumption, the *Phantom Model* states that the crosslinks are free to fluctuate around a mean position and the macroscopic deformation of the network leads to the microscopic deformation of the individual chains only through their ends. However, this model ignored the topological interactions between the neighboring chains. The constrained-junction model uses the similar approach and adds an additional potential constraining the fluctuation of the crosslinks [83]. The central idea of this model is that the fluctuations of the networks strands are changing affinely with the deformations and hence affects the constraining potential too. One of the successful ways to account for the topological interactions between the network chains is the Edward's tube model [84]. In this model the network chain is confined by the neighboring ones to a tube like region. The important question was asked how the diameter of this confining tube changes with the network deformation. Hence this model assumed that the tube diameter changes affinely with the macroscopic deformation of the network. Later the experimental studies [85] did not agree well with the assumptions made in this model. A unified picture of deformation of both phantom and entangled networks was presented in the form of non-affine tube and slip tube model. The above mentioned models as well as the others [86] are used in many studies in order to describe the results

from mechanical and swelling experiments. [87]. However, they reveal problems in the quantitative estimation of measurement results. Other physically more precise models of rubber-like elasticity failed due to an excessive number of free fitting parameters and /or mathematical complexity, therefore often numerical solutions are required to solve these experimental results [77, 88].

2.2 Fillers

Reinforcement of elastomers by the fillers like carbon black or silica plays an important role in the improvement of the mechanical properties of high performance rubber materials. In the dynamic mechanical analysis, the reinforcement is quantified well above the glass transition temperature and defined as the viscoelastic plateau of the storage modulus (G'). The effect of fillers on reinforcement has been systematically studied by Wang [34].

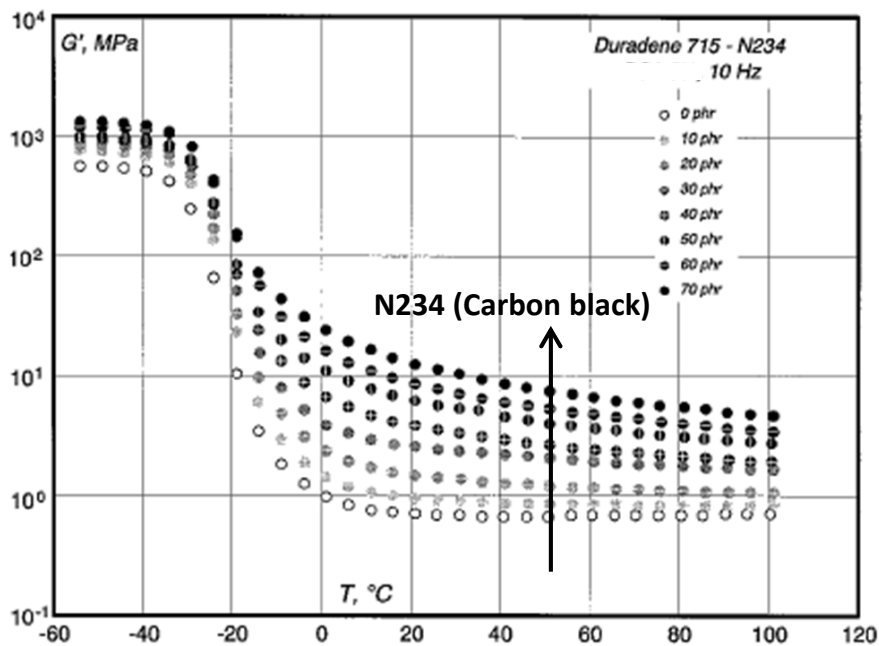


Figure 2.3: Storage modulus as a function temperature for different degree of carbon black fillings. Systematic increase of the plateau modulus (G'_p) with filler indicates the filler-induced reinforcement. Adapted from [34].

In Figure 2.3, it is observed that the G'_p is mildly affected with the addition of fillers at low temperatures in the glassy region. However, at high temperature in the plateau range the G'_p becomes systematically dependent on the filler loadings. This particular

feature shows the filler-induced reinforcement in the soft elastomer matrix. The degree of reinforcement is mainly governed by two effects: (i) the formation of a physically bonded flexible filler network and (ii) strong polymer-filler couplings. Both of these effects originate from the specific surface nature of the filler particles [34,35]. The basic equation used to describe the surface energy of fillers is:

$$\gamma_s = \gamma_s^d + \gamma_s^{sp} \quad (2.3)$$

where γ_s is the surface energy (also called surface tension), γ_s^d is the dispersive component of the surface energy and based on dispersive (van der Waals') forces among the fillers, and γ_s^{sp} is the specific component of the surface energy and it is the sum of polar or hydrogen bond interactions between the fillers. Hence the single most important parameter to enhance reinforcement is the average particle size. Particles having size larger than 1 μm do not have reinforcing capacity due to less interactive surface and they only increase the reinforcement by the simple hydrodynamic effect. Reinforcement can be realized with the filler size smaller than 100 nm [35]. Figure 2.4 highlights the typical dimensions considered for both silica and carbon black fillers.

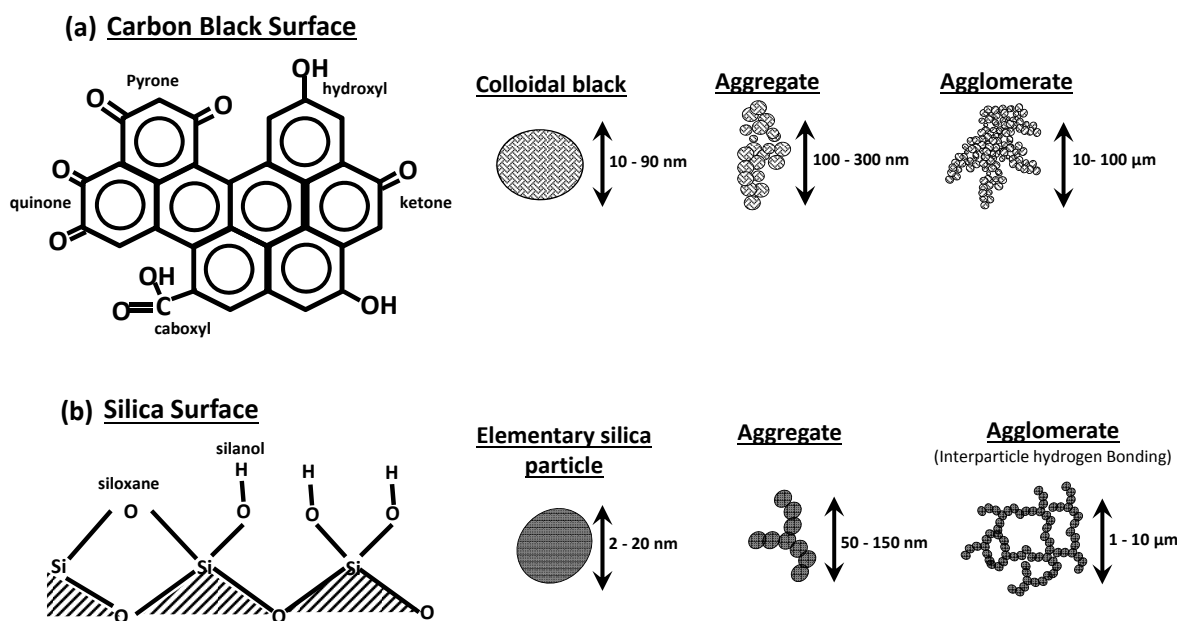


Figure 2.4: Filler morphology and the relevant dimensions of carbon black (a) and silica (b) filler particles.

2.2.1 Carbon Black

Carbon black is frequently used as reinforcing filler in polymers. The incorporation of carbon black into the plastics results in an increase in properties such as mechanical strength, wear resistance and fatigue resistance. The smallest scale individual block formed during the partial combustion of oil or natural gas is called a particle as shown in the Figure 2.4a. A large number of these particles when fused together by Van der Waals attractive forces form aggregates. These primary aggregates flocculate together to form larger secondary agglomerates. According to ASTM (American standards of testing materials) classification, different carbon grades are classified with respect to a four-character code i.e., $Nxyz$. Higher the yz number, higher will be the reinforcement, for instance, N340 is tested more reinforcing grade than N327, while their elementary particle size have same diameter of 26-30 nm. Typically the “N” stands for “Normal curing” which means that this kind of filler do not participate in vulcanization process, “ x ” represents the average size of the elementary particle (ASTM D1765-86), while “ yz ” describes the structure of aggregate [35].

Carbon black has a high dispersive component of the surface energy (γ_s^d) which depends on the surface area of the carbon black and not on the structure [6, 7]. Due to this fact, carbon black particles have strong filler-rubber interaction and weaker filler-filler interaction as compared to the silica fillers, resulting in weaker filler networks. The influence of the presence of carbon black on the dynamic mechanical properties of variety of filled rubbers has been subject of different studies [33, 42, 89–91]. An overview of the earlier work shows that the incorporation of carbon black in different types of rubber gives in most of the cases an increase in the storage G' and loss moduli G'' . Increases in strain amplitude leads to a decrease in storage modulus G' : the so-called Payne effect, has extensively been studied on carbon black filled systems. Wang and Wolff [92] reported that the enhanced mechanical properties depends on the bound rubber content which often realized due to high filler-rubber interactions.

2.2.2 Silica

There are two types of silica: precipitated silica and fumed silica, both produced from different manufacturing methods. Precipitated silica is produced by a controlled precipitation method from the reactions of sodium silicate with acid. The elementary particle size ranges from 10 to 100 nm [93]. Fumed silica is manufactured with relatively expensive method with the particle size of 7-15 nm produced at a high temperature by a reaction of silicon tetrachloride with water vapor [77]. Reinforcing silica particles,

either produced by precipitation process or fumed process, exhibit similar hierarchical structural geometry like carbon black. Particularly in precipitation process, silica elementary particles are linked by a chemical bond and form an aggregate with dimensions of 50-200 nm. As the precipitation is economically feasible process compared to the manufacturing fumed silica, this process is widely used in industry. The hierarchy of the geometrical structure of the silica is shown in Figure 2.4b.

In contrast to the carbon black, the surface characteristics of the precipitated silica result a variety of problems in the use of this material as reinforcing agent, particularly in hydrocarbon elastomer. The surface of hydrated, precipitated silica is largely polar and hydrophilic as a result of its polysiloxane structure (as shown schematically Figure 2.4b) and the presence of several silanol groups [37]. Large amounts of moisture content are also present on the silica surfaces which cause difficulty of achieving rapid wetting and dispersion in rubber. Therefore, elementary spherical particles generally form aggregates and different aggregates due to strong hydrogen bonding form agglomerates. Silica has a strong tendency to form agglomerates as compared to the carbon black due to its high specific component of surface energy (γ_s^{sp}). Therefore in silica, filler-filler interactions are stronger than filler-polymer interaction [6, 7]. The surface interaction of silica surface with non-polar groups of hydrocarbon elastomers is weak compared to the hydrogen-bonding interactions between surface silanol groups in silica itself. Due to this reason, silica filler comparatively give rise to greater reinforcement in polar elastomers like NBR than in nonpolar polymers such as SBR and NR. Moreover silica, when compared to carbon black particles having the same filler size, do not give the similar degree of reinforcement. Studies on silica pointed out that the addition of the silica to a tread material of the tire (usually consists of SBR and BR) on one hand improves the hysteresis but also leads to a loss of tread material i.e, low abrasion resistance [73].

It is common practice to enhance the hydrophobic properties of glass and ceramic surfaces by treatment with different organosilanes [37]. The deficiencies mentioned above in silica filled composites is compensated by the use of silane coupling agent. Remarkable improvements in mechanical properties of silica-filled rubbers are obtained with the use of a coupling agent. The most widely used coupling agent is bis-(triethoxysilylpropyl) tetrasulfide (TESPT) commercially known as Si69. An important prerequisite for a coupling agent is that the molecule should be bifunctional. Coupling agent has a capability to react chemically with both the silica and polymer during the vulcanization process and indirectly form a covalent bond between the filler and the polymer. The reinforcement mechanism by silanization process consist of two

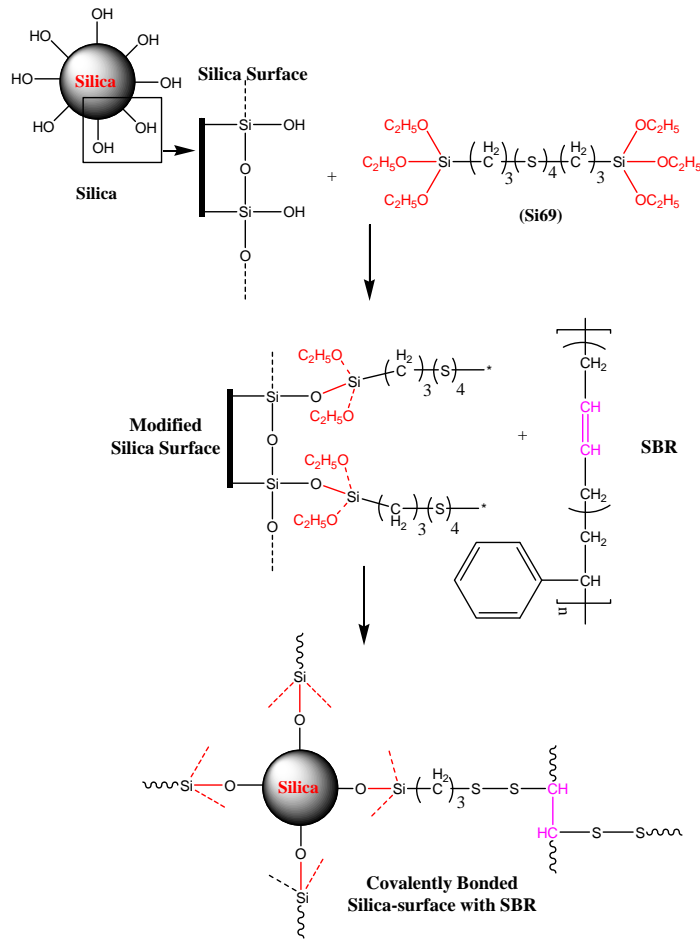


Figure 2.5: Reaction mechanism of silanization [93].

processes: i) the silanization reaction to couple filler with the coupling agent, followed by ii) the formation of chemical bonds between the modified silica surface and the polymer (as shown in Figure 2.5) [77, 93].

Dannenberg and Cotten [37] have shown the remarkable improvement in mechanical properties of a silica-filled styrene-butadiene vulcanizate obtained after using a silane as coupling agent. Chemical bonding of the polymer to the filler surfaces improves dispersion and prevents formation of large scale agglomerates. They mentioned that the result of these effects is to decrease low-strain stiffness or hardness and to improve dynamic properties by minimizing energy-loss processes associated with the breakdown of large agglomerates. High degree of filler dispersion and better surface wetting leads to higher tensile strength.

2.3 Filled Rubber Reinforcement

Particularly it is well known that the addition of fillers in rubbers increases the high temperature plateau modulus (G'_p) of the composite materials [92, 94, 95] and hence it enhances the overall reinforcement. Not only that, particulate fillers also influence the overall temperature-dependent mechanical response of composites [34]. This effect can be observed as the decreasing behavior of the plateau modulus over the whole investigated temperature range (cf. Figure 2.3). However limited focus has been given to understand the underlying physical phenomenon of this decreasing storage modulus. In the following sections, several studies are reviewed to understand the temperature- as well as frequency-dependent mechanical reinforcement in the elastomeric composites.

Hydrodynamic Theories

Several fundamental models can describe the mechanical reinforcement of rubber compounds. Among these, the simplest models involve the hydrodynamic displacement of filler particles. The hydrodynamic effect was first introduced as an increased viscosity of a fluid with dispersed rigid particles by Einstein [96]. Einstein explained this increase in viscosity with an equation relating the viscosity to the filler volume fraction ϕ ,

$$\eta = \eta_0 (1 + 2.5\phi) \quad (2.4)$$

where η_0 is the viscosity of the pure fluid without fillers.

To apply this effect in elastomers, it was assumed that the modulus of the rubber behaves similar to the viscosity of a liquid. This was done by Smallwood [97] considering the assumption that the particles are spherical, dispersed, wetted and under low shear stress. However, in practice the fillers do not meet such ideal conditions and hence further modification was done. For the practical applications, the equation needed to be modified for higher filler fractions where filler-filler interactions are observed. Guth and Gold [98, 99] considered the interactions of the spherical fillers by adding an additional ϕ^2 term in a Einstein-Smallwood equation (Eq. 2.4).

$$G'(\phi) = G'_{unfilled}(1 + 2.5\phi + 14.1\phi^2) \quad (2.5)$$

Several modifications have been done on Guth-Gold Eq 2.5 to account for deviations of the fillers from the ideal case. In real terms, fillers are not spherical but are asymmetric consisting of complex branched structure. In order to consider the effect of filler

shape, aggregates/agglomerate structure or also the occluded rubber on hydrodynamic reinforcement, Medalia [89, 100] introduced the structure factor “ f ” in the Guth-Gold equation and modified the volume fraction ϕ as an effective volume fraction $\phi_{eff} = f\phi$.

$$G'(\phi) = G'_{unfilled}(1 + 2.5f\phi + 14.1f^2\phi^2) \quad (2.6)$$

Another modification of the Einstein-Smallwood equation for typical loadings of fillers up to volume fraction $\phi \approx 0.35$ has been done by Pade approximation [101].

$$G'(\phi) = G'_{unfilled}(1 + 2.5\phi + 5\phi^2) \quad (2.7)$$

The various other models [102, 103] used to predict the hydrodynamic effect have largely developed with the help of experimental data that proposes empirical relationships. Vilgis and Heinrich [8, 46] have extensively reviewed the field of reinforcement and emphasized that no consistent model exists that may be used to explain rubber reinforcement. Eggers and Schümmer [104] studied the Thomas empirical relation [102], who added $10.05\phi^2$ and some constants to the Einstein-Smallwood equation, showing that it fit to a rather broad range of filler loading i.e. $0.1 < \phi < 0.5$, than the previous form of Guth-Gold equation. However, Eggers and Schümmer pointed out in their study that these equations apply only to uncured systems. Once the rubber is vulcanized these models may no longer be applicable.

So far numerous models have been proposed explaining the hydrodynamic reinforcement behavior of filler rubber. However, all these models are specific to certain particular cases or these are often sensitive to a narrow range of filler loadings. Generally, the hydrodynamic effect results in the increase in modulus under conditions of low strain and low filler fraction. When strain increases beyond the critical value, the majority of the modulus is attributed to the rubber itself. When the volume fraction of filler increases, filler-filler interaction increases and forms a filler network. This network causes a reinforcement mechanism different from those above-mentioned hydrodynamic effects.

2.3.1 Occluded Rubber

Another kind of reinforcement often reported in literature is due to “occluded rubber”. Woff, Donnet, Wang and coworkers have published many papers that discuss the hydrodynamic reinforcement of rubbers due to occlusion of rubber within the filler aggregates [92, 105, 106]. It is proposed that the aggregated geometry of filler leads

to some of the rubber 'trapped' within the voids of the aggregates. This trapped or occluded rubber increases the effective volume of filler. Medalia [89, 90] in his earlier work proposed that in a carbon black-rubber system, the rubber which fills the void space within aggregates is occluded and immobilized and thus acts as part of the filler aggregate rather than as part of the deformable matrix. The amount of occluded rubber has been calculated directly from the DBP (n-dibutyl phthalate) absorption value by:

$$\phi_{eff} = 0.5\phi [1 + (1 + 0.02139 (DBP)) / 1.46] \quad (2.8)$$

where ϕ is the actual volume fraction of filler. This relationship still holds as a predictor of the effective volume of carbon black.

The concept of occluded rubber has been used by several authors to account for the effect of carbon black structure on viscoelastic properties. Medalia quantified the occluded rubber using swelling experiments. Kraus and Sambrook [90, 91, 107] treated the occluded rubber contribution to the modulus using tensile experiments. Sambrook attempted to use the volume fraction of carbon black plus occluded rubber in a theoretical based equation for the prediction of Young's modulus. The theoretical ratio of Young's modulus (E_{filled}/E_{gum}) from modified Guth-Gold equation 2.6 was used to interpret the ratio (E_{filled}/E_{gum}) measured experimentally from the initial slope of stress-strain curves using f as a correction factor for occluded rubber. He found that the values of f was not unity but varied from about 0.7 at 20°C to 0.4 at 150°C. He interpreted the decrease in f (occluded rubber) with temperature as a consequence of increased deformability with increasing temperature. The sole argument of the change in the deformability of the occluded rubber with temperature is due to the change in the mobility of the rubber molecules within and /or on the surface of the carbon black aggregates.

2.3.2 Payne Effect

The Payne effect is a particular feature of the stress-strain behavior of rubber, especially rubber compounds containing fillers such as carbon black or silica. It is named after the British rubber scientist A. R. Payne, who made extensive studies of the effect [39–41]. The effect is observed under cyclic loading conditions starting with small strain amplitudes. Above approximately 0.3% strain amplitude, the shear storage modulus (G') shows sigmoidal decline with increasing amplitude. At sufficiently large strain amplitudes (roughly 20% or above), the storage modulus approaches to its lower limit. In contrast to G' , the loss modulus (G'') shows maximum values at a moderate strain

amplitude. After passing through a maximum, the G'' decreases rapidly with further increase in strain. This typical non-linear behavior of decreasing modulus with strain is generally termed as “*Payne Effect*”. Payne mentioned that such behavior of the strain dependence of filled rubber cannot be explained only by the hydrodynamic effect. He interpreted the sigmoidal decrease of G' as a result of a dynamical break-up of the filler network i.e., van der Waals bonds between carbon black aggregates are continuously broken and reformed. So at low deformations, the energetic elastic contribution of the rigid filler network is dominant, whereas at high deformations the filler has only a small remaining effect, which is hydrodynamic and caused by the rubber-filler interaction

The Payne effect depends on the filler content of the material and the temperature and the effect vanishes for unfilled elastomers. Payne and some other researchers [39, 108, 109] studied the effect of temperature and found that the modulus at low deformations ($G'_{\gamma \rightarrow 0}$) decreases with increasing temperature. The magnitude of the decreasing modulus depends on the filler content. However the shear modulus at large strains becomes progressively less dependent on temperature and finally $G'_{\gamma \rightarrow \infty}$ is virtually independent of temperature over the range considered.

It has been widely accepted that the Payne effect is mainly related to the filler network formed in the polymer matrix. Wang [34] argued that the breakdown of the filler network by increasing strain amplitude would release the occluded rubber so that the effective filler volume fraction and hence the modulus will decrease. Hence this mechanism suggests that the Payne effect can serve as a measure of filler networking which originates from filler-filler as well as polymer-filler interaction.

2.3.3 The Kraus Model for the Strain-Softening Effect

The previous section led to a convincing assumption that the strain-dependent softening phenomenon of filled rubber is due to the break-down of the filler network within the elastomer matrix. However, in contrast to this approach, few alternative models have been proposed. Gui et al. postulated that the strain amplitude effect was due to deformation, flow and alignment of rubber molecules attached to the filler particles [110]. Smit [111] has indicated that a shell of a bound rubber (a rigid/immobilized rubber layer at filler interface) of definite thickness surrounds the filler and the non-linearity in the dynamic mechanical behavior is related to the desorption and reabsorption of the hard-glassy like rubber shell around the filler. On similar line of argument, Mair and Göritz suggested a Langmuir-type polymer chain adsorption on the filler surface to explain the Payne effect [52].

Kraus suggested the first phenomenological quantitative model based on agglomeration/deagglomeration of carbon black agglomerate to describe Payne effect [42]. Due to the fact that this model is used extensively in the result section of this thesis, hence the model needs to understand in detail. Kraus assumes that the (van der Waals) carbon black contacts break and reform according to functions, f_b for breaking and f_r for reforming, of strain amplitude γ_0 . Accordingly the rate of breakdown of filler contacts i.e., the amount of network broken per cycle, R_b , is proportional to the number N of existing contacts and to the function f_b .

$$R_b = k_b \cdot N \cdot f_b \quad (2.9)$$

where k_b is the rate constant. Similarly the network reformation rate, R_r , is assumed to be proportional to $N_0 - N$ where N_0 is the number of carbon-carbon contacts at zero amplitude.

$$R_r = k_r \cdot N \cdot f_r \quad (2.10)$$

k_r being the reformation rate constant. Kraus assumed power laws for the functions $f_b = \gamma_0^m$ and $f_r = \gamma_0^{-m}$ with m being a constant. At equilibrium, the two rates are equal ($R_b = R_r$), which gives N as

$$N = \frac{N_0}{1 + (\gamma_0/\gamma_c)^{2m}} \quad (2.11)$$

where γ_c is a characteristic strain given by $(k_r/k_b)^{\frac{1}{2m}}$.

The excess modulus ($G'(\gamma_0) - G'_\infty$) of the agglomeration network at any given strain amplitude is taken as proportional to the existing number of contacts N , so

$$G'(\gamma_0) - G'_\infty = \frac{G'_0 - G'_\infty}{1 + (\gamma_0/\gamma_c)^{2m}} \quad (2.12)$$

Kraus refers a loss mechanism to be due to excess forces between carbon black particles or between particles and the polymeric medium as contacts are broken [42]. The excess loss modulus may then be taken as proportional to the rate of network breakdown, and

$$G''(\gamma_0) - G'' = c \cdot k_b \cdot \gamma_0^m \cdot N \quad (2.13)$$

where c is a constant and G''_{∞} will be equal to $G''(\gamma_0)$ at infinite strain. Taking the values for N from Eq. 2.11 and approximating $N_0 \approx \Delta G'$,

$$G''(\gamma_0) - G''_{\infty} = \frac{C\gamma_0^m \Delta G'}{1 + (\gamma_0/\gamma_c)^{2m}} \quad (2.14)$$

with C being a another constant and the function $G''(\gamma_0)$ has a maximum G''_m at $\gamma_0 = \gamma_{\infty}$, so

$$\frac{G''(\gamma_0) - G''_{\infty}}{G''_m - G''_{\infty}} = \frac{2(\gamma_0/\gamma_c)^m}{1 + (\gamma_0/\gamma_c)^{2m}} \quad (2.15)$$

Kraus used the above equations for storage and loss modulus to the data of Payne and found nice correlation. Moreover, it was found that m and γ_c are fairly independent of polymer, filler (carbon black in that case) and dispersion. In this model, the exponent m is a purely empirical parameter and the physical basis of this parameter is unclear. However, Vieweg et al. [112,113] estimated m and γ_c from Eq. 2.12 for a large number of different carbon blacks dispersed in SBR, BR and NR. He reported the universal value of $m \approx 0.5 - 0.6$ indicating that it is mainly a geometrical factor of the filler network and agglomerates, independent of the specific filler type [114].

2.3.4 Filler Network Reinforcement

One of the effects of the filler addition into a polymer is a remarkable change in the dynamic mechanical properties of the rubber, including storage and loss modulus. Similar to large deformations of the filled composite, the role of filler structure and the corresponding reinforcement becomes important for the understanding of the small-strain dynamical deformation. When a small sinusoidal strain is imposed on a viscoelastic material, either filled or unfilled rubbers, a sinusoidal stress response depends only upon temperature and frequency, independent of the applied deformation. This phenomenon has been investigated in depth especially in relation to rubber products by Wang et al. [34]. The temperature-dependent measurements of the storage G' and the loss modulus G'' shows that for a given polymer-rubber system, both G' and G'' increase with increase in the concentration of the fillers in the rubber. It is interpreted that the addition of filler influence reinforcement ($G'_{plateau}$) and dissipation ($G''_{plateau}$) in different ways i.e., multiple mechanisms may be involved. One of the important mechanism is “filler networking”, which involves its architecture and strength seems to be the main parameter to govern the dynamic behavior of the filled rubber. Other researchers also mentioned that the filler aggregates in the polymer matrix have a tendency to

form agglomerates, especially at high loading, leading to chain-like filler structures or percolating clusters [33,39,114]. These are generally termed secondary structure or, in some cases, filler network.

Models for Filler Networking

A reasonable theoretical basis for understanding the linear viscoelastic properties of reinforced rubbers has been given by Klüppel and Heinrich [8, 43–45]. Flocculation studies, considering the small-strain mechanical response of the uncrosslinked composites during heat treatment, demonstrates that a relative movement of the particles takes place that depends on particle size, molar mass of the polymer, as well as polymer-filler and filler-filler interaction. They concluded that these experimental studies provides an evidence for a kinetic cluster-cluster aggregation (CCA) mechanism of filler particles in a rubber matrix to form a filler network, [43, 45]. According to CCA model, filler network consist of a space filling configuration of CCA clusters with some characteristic mass fractal dimension formed at $\phi > \phi^*$. A schematic view of this structure is shown in Figure 2.6 .

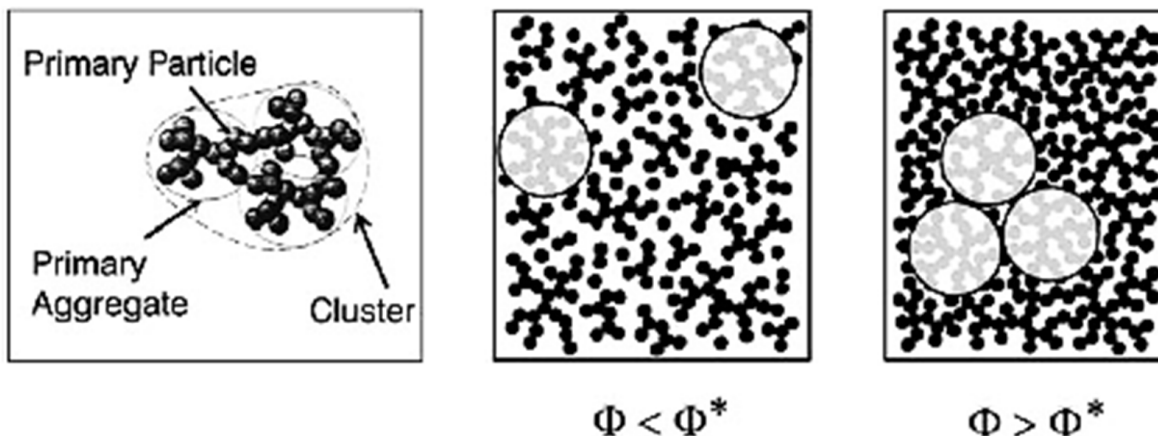


Figure 2.6: Schematic view of kinetically aggregated filler clusters in rubber below and above the percolation threshold ϕ^* : the left side characterizes the local structure of carbon black clusters, build by primary particles and primary aggregates; accordingly, every circle on the right side represents a primary aggregate [43].

The mechanical response of filler networks at small strains depends purely on the fractal connectivity of the CCA clusters. For the small-strain modulus, a power-law behavior with filler content is predicted above the percolation threshold ($\phi > \phi^*$) with an estimated exponent of 3.5. They found this exponent well in accordance with the experimental data of Payne. The predicted power-law behavior is confirmed by a vari-

ety of other experimental data including carbon black and silica-filled rubbers as well as composites with microgels [44, 45].

The consideration of flexible chains of filler particles, by approximating the elastically effective backbone of filler clusters, allows for a micromechanical description of the elastic properties of tender CCA clusters in elastomers. The main contribution of the elastically stored energy in the strained filler clusters results from the bending-twisting deformation of filler-filler bonds. The concept of filler-filler bonds has been extensively discussed by Klüppel by means of ac conductivity and dielectric investigations [65]. From these investigations, he argues that the charge transport above the percolation threshold is limited by a hopping or tunneling mechanism of charge carriers over small gaps of 1 nm between adjacent carbon black particles. From this finding and the observed dependency of the flocculation dynamics on the molar mass of rubber (or amount of bound rubber) [45], a model of filler-filler bonds is developed that is schematically depicted in Figure 2.7.

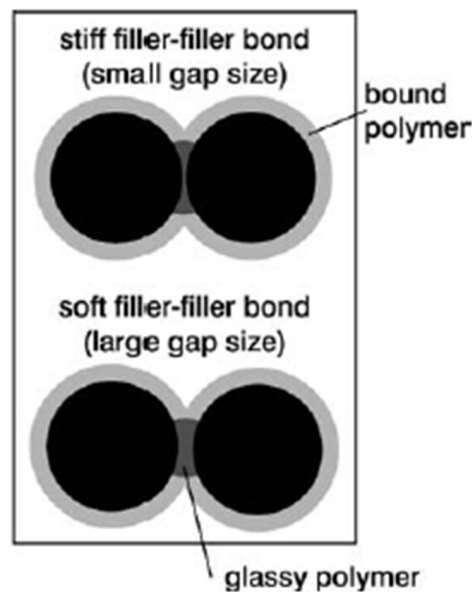


Figure 2.7: Schematic view considering the structure of filler-filler bonds in a bulk rubber matrix. The gap size of neighboring filler particles with confined glassy polymer and the bound rubber layer is indicated.

Following the concept of filler-filler bonds with help of confined glassy polymer bridges, Klüppel [55, 56] has done extensive study dealing the question related to micro-mechanical mechanisms affecting the viscoelastic properties of carbon black and silica-filled elastomer. He shows that the dynamic-mechanical master curves of filled elastomers can be constructed by applying horizontal as well as vertical shift factors.

The complex shifting behavior is said to be related to the superposition of two relaxation processes, i.e. polymer matrix and the filler network. The application of only horizontal shift factor, obtained from the unfilled samples, for the construction of the master curves of the corresponding filled samples leads to a failure of time-temperature superposition (TTS) principle in the small frequency range. The argument for the non-overlapping isotherms is that, with the introduction of fillers as reinforcing agent, the complex interaction between the filler network and the polymer matrix leads to a failure of the TTS principle. The splitting of the low frequencies (high temperature isotherms) curves is regarded as the thermal activation of the filler network, i.e. the temperature dependence of the glassy-like polymer bridges (filler-filler bonds) which results in a significant decrease of storage modulus with increasing temperature. Therefore the two different temperature-dependent vertical shift factors are introduced to construct smooth/continuous master curve of storage G' and loss G'' modulus respectively by shifting each isotherm vertically on modulus axis. Therefore the temperature-dependent vertical shift factors are interpreted in terms of an apparent activation energy associated with the breaking of glassy bridges. This interpretation hence, disregards the relaxatory nature of immobilized polymer components, and amounts to “counting bridges”, i.e., only a certain fraction of them remains active at a given temperature.

Rigid/Immobilized/Glassy Component of the Matrix

The concept of immobilized/glassy/bound rubber is dated back in 1970's when Kaufman et al. introduced the immobile and mobile regions in carbon black filled PB and EPDM composites with the help of measuring spin-spin relaxation time (T_2) from the NMR technique [115]. Later several authors studied the polymer-filler interaction in the elastomer composites [116–119] by using T_2 -relaxometry of NMR experiments on different degree of the filler loadings. The general conclusion of those studies is that in addition to a loosely bound polymer, there is a thin immobilized polymeric layer confined to the filler interface which is regarded as a tightly bound polymer. The difference between tightly and loosely bound polymer is made on the basis of the mobility of the polymer segments close to the point of interaction with the filler particles [69, 116, 117, 120]. The thickness of this interfacial layer is estimated in the range of few diameter of the monomeric unit (≈ 1 -3 nm) [121].

Reinforcement due to Filler-Surface associated Glassy Layer

Based on the findings of rigid/glassy polymeric layer adsorbed to filler surfaces, several other authors interpreted the outstanding mechanical properties of the composites. Vilgis et al. [46] came up with a model based on the localization of the bound polymer near to the heterogeneous surfaces of the filler particles. The argument is based on the fact that the surface of the filler particles is very rough and disordered over the large length scale. The localization of the of polymer at the percolating filler clusters forms significant part of a bound rubber in addition to the filler network formed (at high filler loadings) and hence this phenomenon give rises to a strong reinforcement. Based on the polymer chains mobility at the filler interface, several two phase [34, 47–49, 52] and three phase models [50, 51] are predicted only on the basis of mechanical measurements. Generally they suggested that due to strong polymer-filler interaction, the adsorption of polymer chains on the filler surface give rises to the strong reinforcement and the hysteresis mechanisms in composite [34, 46, 48, 63, 122]. Depending upon the nature of filler and the polymer, the estimated glassy layer thickness is found in the range of 1-10 nm [63, 106]. A precise picture of filler reinforcement and hysteresis is presented with help of FEM simulations by Gusev [61, 123]. A remarkable localization of both storage and dissipation energy was observed, found to occur primarily in the coating layers of immobilized polymer. He emphasized the role of the interfacial phenomena and suggest that the physical (van der Waals) forces responsible for the filler network formation may not necessarily directly affect the reinforcement and the losses but rather indirectly. By way of minute amounts (down to per mille level) of adhesive joints formed from the coating layers of immobilized polymer between the filler particles, one can realize the enhanced storage modulus and the additional dissipation in filled elastomers.

The large and convincing body of work of Long and coworkers [28, 57, 58, 67, 119] is an exception by studying model systems consisting of polymer chains covalently bound to silica particles forming strong polymer-filler interaction. For different degree of filler loadings, temperature dependence of the rigid/glassy fraction is measured by NMR while mechanical properties are studied by using DMA. By comparing NMR and mechanical data, they concluded that the temperature and frequency dependence of the modulus of filled elastomers can be explained by a long-ranged gradient of the polymer matrix glass transition temperature in the vicinity of the particles. The predicted glass transition temperature at a distance z from an interface is described by

$$T_g \approx T_g \left(1 + \left(\frac{\beta}{z} \right)^{1/\nu} \right) \quad (2.16)$$

where T_g is the bulk glass transition temperature of the pure rubber. The exponent $\nu \cong 0.88$ is the critical exponent for the correlation length in 3D percolation. The value of the length β depends on the polymer-filler interactions. For strong interactions, it is of the order 1 nm [67].

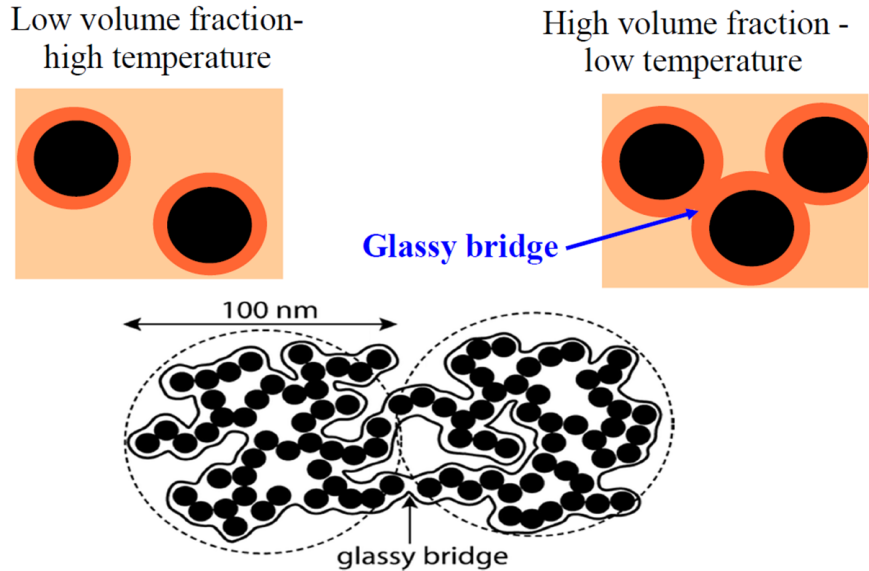


Figure 2.8: (Top) Schematic view Long's model of fillers with glassy layers at (left) low filler volume fraction and/or at high temperature and (right) high filler fraction and/or low temperature forming a glassy bridge between them. (Bottom) Schematic illustration of percolating aggregates of about 100 nm made of primary particles of 10 nm, surrounded by a glassy layer. Adapted from [54].

With these findings and calculations, a model regarding the reinforcement of nanofilled elastomers and thermoplastic elastomers is presented [54]. This model is based on the presence of glassy layers around the fillers as shown in Figure 2.8. Strong reinforcement (defined here as $R(\phi) = G'_{filled}(\phi) / G'_{unfilled}$) is obtained when glassy layers between fillers overlap. Reinforcement is strong when the clusters of fillers and glassy layers percolate. Moreover, it can also be significant even when these clusters do not percolate but are sufficiently large. Under applied strain, the high values of local stress in the glassy bridges reduce their lifetimes. The latter depend on the history, on the temperature, on the distance between fillers, and on the local stress in the material. It is further suggested that the dynamics of breaking and rebirth of glassy bridges account for the nonlinear Payne and Mullins effects. These mechanisms account also for dissipative properties of filled elastomers. This model is then solved numerically by over damped dissipative particle dynamics. The basic ingredients of the model are permanent elasticity, disorder, and excluded volume effects. The solid filler particles are represented by hard spheres randomly distributed in space. Two neighboring filler

particles interact via two distinct forces, which correspond to (a) permanent springs of stiffness $k_\infty = 1$ representing the rubber matrix contribution ($G' = 10^6 Pa$) and (b) nonpermanent springs due to the glassy bridges ($G' = 10^8 Pa$) of much larger stiffness $k_0 \approx 100$, which have finite lifetimes depending on the local history, the local stress at earlier times, and the local glass transition temperature. When the local stress increases, it can lead to a breaking of a glassy bridge.

Criticism on the Glassy Layer Concept

Robertson and coworkers, however believed that in filled polymers, there are different variables to control the reinforcement, such as the size and concentration of the particles, and the nature of the polymer-filler interface. The presence of bound polymer and the introduction of a jammed filler network can enhance the modulus significantly beyond the hydrodynamic effect of particle inclusions, at least for shear and tensile modes of deformation. Therefore glassy bridge/layer should not be considered as a vital ingredient for reinforcement [124]. In a review [4], author cited many literature investigations about the effect of small particles on polymer reinforcement which also affects (increases the polymer Tg) the polymer segmental mobility of polymer chains. This mobility is assessed from the Tg or segmental relaxation times measured by DMA, dielectric or NMR. He mentions that there are published studies that appear to show unambiguously that polymer chains can be immobilized by the presence of small particles, and he thinks that these instances of a “glassy interphase” are representative, or merely special cases of unusually strong and pervasive interactions of filler particles with particular polymers. Certainly the chain segments directly bonded to the filler (e.g., chemisorbed) are immobilized and can function as junctions to increase the effective crosslink density and thus the rubbery modulus. However, a large fraction of directly bonded segments are necessary to obtain an immobilized phase. Robertson critically analyzed the most common NMR approach for characterizing polymer motions in the presence of filler which is to measure proton spin-spin relaxation times (T_2). The author mentions the work of Dutta et al., who found that only the olefinic carbons in SBR were immobilized; indicating that specific interaction at the surface caused the observed immobilization. This is quite different from an interpretation of a “glassy” shell in the interfacial region. One of his study indicates that although silica filler modification can produce high amount of bound rubber ($\approx 71\%$) but this did not alter the glass transition behavior of the SBR [125]. No evidence for the reduced segmental mobility of the polymer was found near the filler for any of the materials he

studied, and he claimed that the model of Long et al. to connect glassy shell concepts with the nonlinear viscoelastic response (Payne effect) may not be applicable to these commercially important filled polymers.

Summary

Several decades of research suggest that the underlying physics of the filler network reinforcement is still not clear. Additionally extensive research has been done on the model filled systems where the polymer-filler interactions have been deliberately enhanced either by filler surface modification or by homogeneous distribution of the fillers in the matrix. Therefore on more practical grounds, a reinforcement study needs to be performed on more technologically relevant elastomer systems.

Chapter 3

Experimental Methods

3.1 Dynamic Mechanical Analysis

Dynamic mechanical analysis is an instrumental technique extensively used to characterize properties of viscoelastic polymeric systems as a function of temperature, time, frequency, stress or a combination of these parameters. It can be simply described as applying a stress or strain to a sample and analyzing the response to obtain phase angle and deformation data [126].

If an applied strain, subjected to the viscoelastic material, varies sinusoidally with time then the response is a sinusoidal stress but will be out of phase with the strain applied, by the phase angle δ , as shown in figure Figure 3.1. This phase lag is due to the excess time necessary for molecular motions and relaxations to occur. The dynamic applied strain ϵ and stress response σ will have the same angular frequency ω which can be mathematically expressed as

$$\text{Input/Program} : \epsilon = \epsilon_0 \sin(\omega t) \quad (3.1)$$

$$\text{Output/Response} : \sigma = \sigma_0 \sin(\omega t + \delta) \quad (3.2)$$

where ω is the angular frequency. Using this notation, the response (stress) can be divided into two components: (i) of magnitude $(\sigma_0 \cos \delta)$ in-phase with the strain and (ii) of magnitude component $(\sigma_0 \sin \delta)$ 90° out-of-phase with the strain and rewritten as

$$\sigma = \sigma_0 \sin(\omega t) \cos \delta + \sigma_0 \cos(\omega t) \sin \delta \quad (3.3)$$

The above equation can be written in terms of shear modulus by dividing shear stress by shear strain and using the symbols G' and G'' for the in-phase (real) and out-of-phase

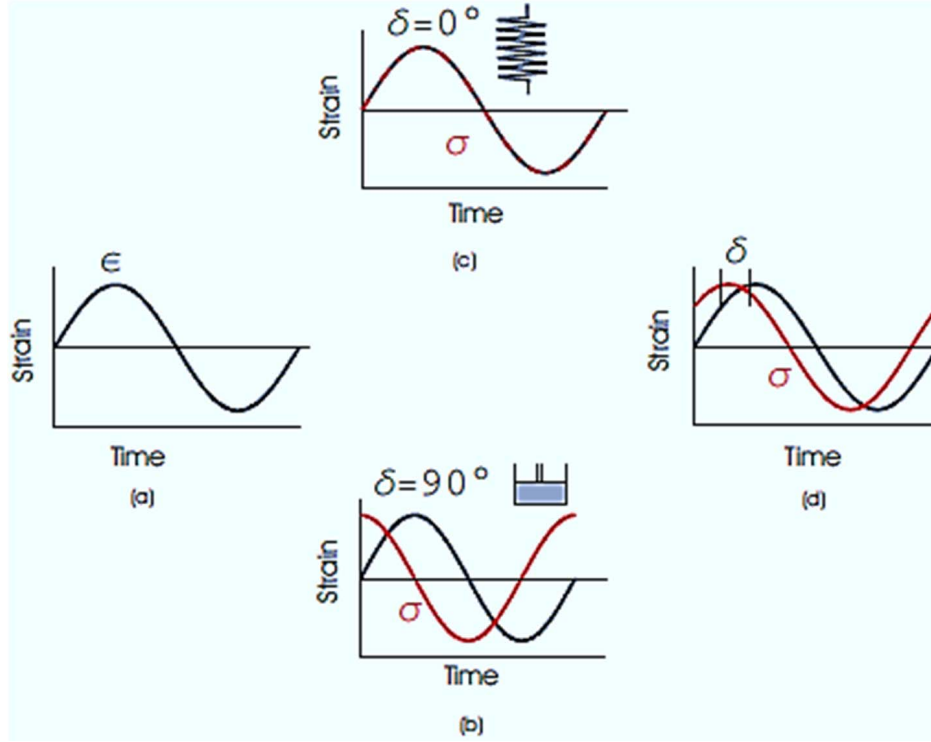


Figure 3.1: (a) Sinusoidal strain applied to the samples (black). Response to sinusoidal strain as sinusoidal stress (red) for perfectly viscous system (b), for elastic system (c) and for a viscoelastic system where it lies in between these two extremes (d). Adapted from [127].

(imaginary) moduli:

$$\sigma = \epsilon_0 G' \sin(\omega t) + \epsilon_0 G'' \cos(\omega t) \quad (3.4)$$

where $G' = \frac{\sigma_0}{\epsilon_0} \cos \delta$ and $G'' = \frac{\sigma_0}{\epsilon_0} \sin \delta$.

In complex notation, storage modulus G' and loss modulus G'' can be combined to a dynamic modulus G^* which can be written as

$$G^* = G' + iG'' \quad (3.5)$$

where G' , which is in phase with the strain, is called the storage modulus because it defines the energy stored in the specimen due to the applied strain and G'' , which is $\pi/2$ out of phase with strain, defines the loss of energy, and is called the loss modulus. The ratio G''/G' gives $\tan(\delta)$ which is termed as loss tangent or damping factor:

$$\tan \delta = G''/G' \quad (3.6)$$

The loss modulus, G'' , defines the energy dissipation because of the following calcula-

tions of the energy (ΔE) dissipated per cycle:

$$\Delta E = \oint \sigma d\epsilon = \int_0^{2\pi/\omega} \sigma \frac{d\epsilon}{dt} dt \quad (3.7)$$

Substituting for σ and ϵ values from the Eq 3.1 and 3.2 respectively, yields

$$\Delta E = \omega \epsilon_0^2 \int_0^{2\pi/\omega} (G' \sin \omega t \cos \omega t + G'' \cos^2 \omega t) dt \quad (3.8)$$

The integral is solved by using $\sin \omega t \cos \omega t = 1/2 \sin 2\omega t$ and $\cos^2 \omega t = 1/2(1 + \cos 2\omega t)$, resulting in

$$\Delta E = \pi G'' \epsilon_0^2 \quad (3.9)$$

3.1.1 Temperature-dependent Measurement (Temperature Sweeps)

Temperature-dependent dynamic shear mechanical measurements were performed on RDA-2 from TA Instrument. All the measurements were carried out in the linear response region (confirmed by strain sweeps) with an oscillation strain amplitude of 0.2%. Measurements were performed on as-prepared samples with rectangular geometry having average dimensions of 20 x 10 x 2 mm³ (Length x Width x thickness). In each test, sample was first cool down (within 10 minutes) with the help of liquid nitrogen to a temperature lower than the glass transition temperature of the specific sample, for instance, -75°C. A temperature equilibration time of 10 min was always necessary.

The temperature sweeps on RDA-2 started from a -70°C to 150°C with a temperature step of 3°C and a step soak time of 60s. In each step, data were evaluated at four different angular frequencies 0.1, 1, 10 and 100 rad/s, so as to see the effect of varying frequency on the viscoelastic behavior. During the measurement, the sample was kept oscillating, and data were obtained from regular intervals of time. No prestrain was applied to the sample and hence the normal force was kept zero through out the shear measurement.

3.1.2 Time-Temperature Superposition (Master Curves)

Frequency sweeps in the range of 0.1 - 100 rad/s with five points per decade were carried out at temperatures between -35 and 150°C to construct master curves. The soak time for each temperature was 600 s, and the temperature increment was 3 K.

After the measurements, master curves were constructed according to time-temperature superposition principle.

Time-temperature superposition implies that the effect of changing the temperature is the same as a rescaling of the time scale by a multiplication factor 'called horizontal shift factor' a_T . This means that the response frequency function of the modulus at a certain temperature resembles the shape of the same functions of adjacent temperatures. This principle is essential to study the viscoelastic nature of polymeric materials and is well established by Williams, Landel and Ferry [128].

Experimentally different isotherm curves in $\log G'$ or $\log G''$ vs. $\log \omega$ in limited frequency window are obtained, normally in 3 decades frequency window. For the construction of the master curve, an isothermal curve (α -transition) in $\log G'$ vs. $\log \omega$ is taken as reference at one temperature and considered as reference temperature T_0 . While the other isothermal curves are shifted according to the reference curve by a logarithmic shift parameters a_T . From this, the frequency window is expanded and the entire view of the effect of temperature at different frequency ranges in different regions of a polymer i.e., α -transition region, rubber plateau, and terminal flow region can be observed. This results in the formation of a master curve. As the shape of the of α -transition curve (and terminal flow curve) is independent of temperature, so any isotherm curve can be chosen as reference and shift other curves on it and from this one can get a very good idea about the plateau region at lower frequency range or α -transition region at higher frequency range. The distance of the shift is referred to as the time-temperature superposition shift factor a_T which is calculated by the following equations:

$$a_T = \omega(T)/\omega(T_0) \quad (3.10)$$

The shift factor, a_T , represents the magnitude of shifting along x-axis, necessary for a specific isotherm to superimpose on its neighbor in the final master curve with respect to a give reference temperature. The shift factor is usually described by Williams-Landel-Ferry equation (WLF) equation as

$$\log a_T = \frac{-C1(T - T_0)}{C2 + T - T_0} \quad (3.11)$$

and is associated with the transition, plateau, and terminal regions of the frequency scale. The constants C1 and C2 are material dependent parameters whose values are in the range of $C1 = 14-18$ and $C2 = 30-70$ K if $T_{ref} = T_g$ [128]. With the aid of a_T we can express response functions at any temperature in terms of the respective

response function at T_0 . Explicitly, for the dynamical shear modulus, the following relation holds:

$$G(T, \omega) = G(T_0, a_T \omega) \quad (3.12)$$

or for a logarithmic frequency scale

$$G(T, \log \omega) = G(T_0, \log \omega + \log a_T) \quad (3.13)$$

3.1.3 Strain-dependent Measurement (Payne Effect)

For nonlinear mechanical analysis, strain induced softening phenomena (Payne Effect) were studied on Anton Paar MCR501 because of its high accuracy at very low strains, and these experiments were performed at three different temperatures $25^\circ C$, $60^\circ C$ and $150^\circ C$. Isotherms were measured at an angular frequency of 10 rad/s after 600 s soak time over a strain amplitude range from 0.001 to 20%.

3.2 Low-field NMR

To achieve higher sensitivity in many industrially important elastomeric materials filled with various kinds of filler systems, magnetic fields of increasing strength are required. Currently, superconducting magnets with proton Larmor frequencies up to 1 GHz are available. [129] Yet, such magnets are heavy, bulky, immobile and expensive in purchase and maintenance. Moreover, the operation of high-field spectrometers is rather complex. However robust and cheap low-field proton NMR may provide valuable insights in structure and dynamics of filled elastomers. Low-field spectrometers are easy to handle since they use permanent magnets and comparably simple technology. An apparent drawback of this simple technique is that it has weak magnetic field i.e., 0.5 T. This problem results strong magnetic field inhomogeneity within the sample and hence the desired chemical resolution cannot be achieved here. Therefore, low-field devices are mainly used for standard relaxometry applications in industry. However, it is also possible to investigate proton-proton dipolar couplings qualitatively, the strength of which does not depend on the magnetic field strength. As the proton dipolar coupling strength is an indicator for segmental dynamics in polymers, low-field NMR is a suitable method for the investigation of chain dynamics, e. g., in rigid-crystallites and mobile-amorphous domains of semicrystalline polymers or in elastomer composites. Hence, differences in chain mobility between the individual phases of a filled polymer can be observed by low-field NMR, enabling the detection of mobile and immobile domains of polymer composites [130]. Additionally, based on the influence of the weaker dipolar couplings on the NMR signal, ^1H low-field solid-state NMR can also be used to study the structure of the network i.e., measurement of the network crosslink density.

3.2.1 Theoretical Concept

The basic principle behind the NMR approach is based on the time-dependent orientation of the polymer segments in a network which can be described by an orientation autocorrelation function. The relevant time-dependent autocorrelation function $C(t)$ is the one based on the second Legendre polynomial.

$$P_2 = \frac{1}{2}(3\cos^2\vartheta(t) - 1) \quad (3.14)$$

This function gives the probability for a chain segment in a certain orientation at a time t_1 to be again in the same orientation at another time t_2 , hence it reads as:

$$C(t) = \langle P_2(\cos \vartheta(t_1)) P_2(\cos \vartheta(t_2)) \rangle \quad (3.15)$$

The angle brackets $\langle \dots \rangle$ in above equation represents an elapsed time averaging over the whole Kuhn segments N of all the individual chains. Therefore, the autocorrelation function gives the information about the average orientation of all the polymer chain segments.

The mobility within the polymer chains arises due to thermal fluctuation. At short time differences $t_2 - t_1$, the polymer segments quickly lose their orientational memory $C(t)$ due to fast local fluctuations, and the autocorrelation function decreases rapidly (as shown in Figure 3.2). At some point, however, the long-range or slower motions of the segments are hindered by the presence of topological constraints such as entanglements and cross-links. This leads to a very slowly decaying component in the autocorrelation function, which can almost be seen as a plateau. In this case the height of the plateau of the autocorrelation function corresponds to the square of a dynamic order parameter of the polymer backbone S_b [29]. These long-time correlation (ms-s), which is expressed by an order parameter S_b , quantifies the crosslinked-induced average residual orientation of the polymer chain segments along the polymer backbone and will be discussed in detail in later section.

Relationship between Segmental orientation fluctuations and NMR observables

The relationship between polymer chain dynamics and NMR detected parameter is the orientation dependence of the spin-pair dipolar couplings. The spin interactions which are most important for low-field ^1H solid-state NMR is the direct pairwise dipole-dipole coupling of nuclear spins. A nuclear magnetic dipole moment μ associated with the nuclear spin I generates a small magnetic field B in its environment at a distance r . This field interacts with the dipole moments of surrounding spins, resulting in a direct dipolar coupling of spins through the space (see Figure 3.3). The strength of the dipolar coupling between two spins of the same species is given in the form of an angular frequency ω_D

$$\text{Dipolar Coupling} \approx \omega_D = -\frac{\mu_0 \hbar \gamma_j \gamma_k}{4\pi r_{jk}^3} \frac{1}{2} (3\cos^2\vartheta_{jk} - 1) \quad (3.16)$$

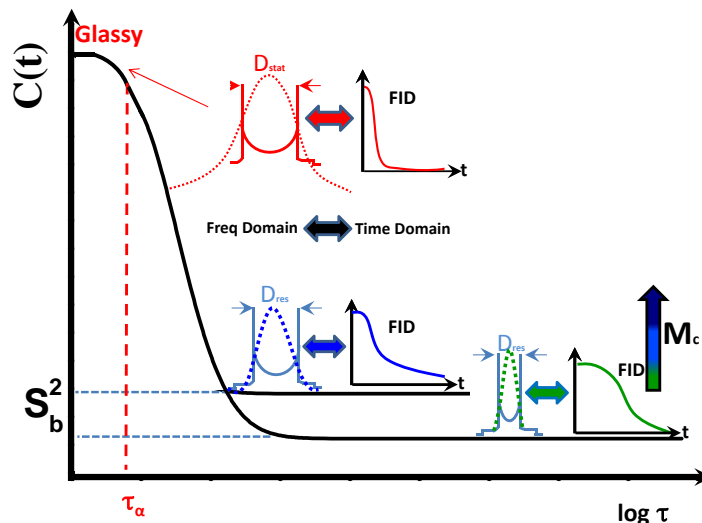


Figure 3.2: Schematics of orientation autocorrelation function vs segmental relaxation times with corresponding NMR observables motion-averaged Pake-doublets. Width of the doublets represents the coupling strength which is maximum in glassy state and decreases relatively with the chain mobility due to motioned narrowing of dipolar couplings.

The coupling strength depends on the distance r between the nuclei and the angle ϑ of the spin-spin interconnection with respect to the magnetic field B_0 as depicted. The orientational dependence is expressed by the second Legendre polynomial P_2 (as discussed above) and the quantity μ_0 represents the magnetic constant. Hence the apparent dipolar coupling strength and the autocorrelation function is directly proportional to each other.

$$\omega_D \propto \sqrt{C(t)} \quad (3.17)$$

In isotropic liquids, the fast Brownian motions change the molecular orientation. These motions are fast enough on the time scale of NMR experiment to detect the dipolar couplings as it is averaged out completely. However, in the polymer-filler nanocomposites, the mobility of the polymer chains is significantly reduced as a result of strong adsorption interactions on the filler surfaces. Due to such phenomenon, an immobile/rigid phase of the polymer develops where the polymer chains are densely packed and the relative chain mobility is restricted compare to the bulk regions. Due to restricted chain mobility, only minor orientational changes of the proton spin interconnection vectors is possible, hence leading to a static coupling constant, D_{stat} . The strong dipolar couplings in such a phase affects the NMR signal both in time and frequency domain. Instead of a single spectral line at $\omega = \omega_0$, a single pair of dipolar coupled spin produce

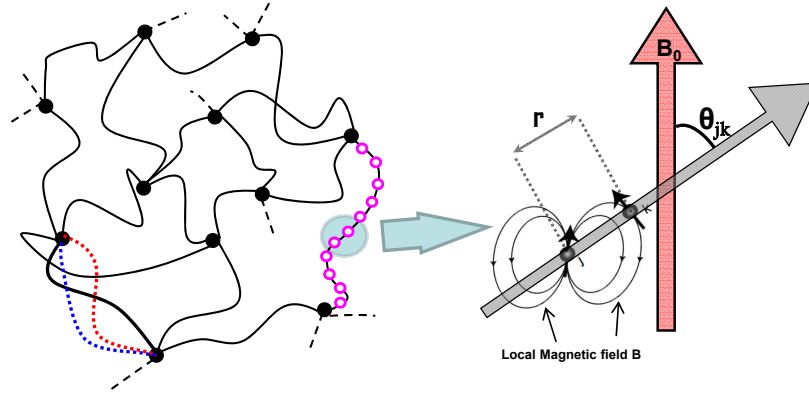


Figure 3.3: (left) Schematic illustration of fluctuating polymer chains between crosslinks. (right) The dipolar coupling between two nuclei (j and k) which depends on the distance between them r , and the angle ϑ_{jk} relative to the external magnetic field B_0 .

a doublet of the spectral lines appear at

$$\omega_D = \omega_0 \pm (3/2) \langle \omega_D \rangle_t \quad (3.18)$$

There are multiple possibilities of the spin-spin interconnection orientation in a rigid powder sample due to the presence of different coupling strengths. Consequently the final shape of the spectrum appears to be a superposition of spectral lines at different frequencies and forms a dipolar broadened spectral line with a characteristic shape, called as Pake doublet (as shown in Figure 3.2).

Surface Immobilized Component

In the time domain curves of the NMR, the superposition of the different frequency components (dipolar spin-spin couplings) causes an accelerated decay with a short T_2 values compared to the signals from non-coupled systems [129]. This means, the protons residing within the rigid-immobile domains are subject to strong dipolar couplings ($\omega_D/2\pi \approx 20$ kHz), resulting a rapidly decaying time-domain (FID) signal with a T_2 relaxation time $\tau_{rigid} \ll 20 \mu s$. Far above the glass transition temperature the chains in the mobile domains of a elastomeric composites exhibit fast mobility, resulting in an averaging of the dipolar couplings on the NMR time scale and leading to a significantly reduced residual coupling strength as opposed to the value of the immobile regions ($\tau_{rigid} \gg 20 \mu s$). Therefore, the time-domain signal decays slowly with a long T_2 time constant [57].

To quantify the contribution of immobile phase from the time-domain FID signal, we

use following two component fit in Eq 3.19.

$$M(t) = M_0 \left[a_g \exp \left(- \left(\frac{t}{\tau_g} \right)^2 \right) + (1 - a_g) \exp \left(- \left(\frac{t}{\tau_{mob}} \right)^b \right) \right] \quad (3.19)$$

Where a_g stands for the immobile fraction, exponent, b (≈ 1) which is less than gaussian exponent 2, describes the mobile behavior of elastomer, while τ_g and τ_{mob} represent decay times for the immobile and the mobile components respectively.

Estimation of the Network Crosslink density

In a chemically crosslinked networks, when the individual chains are chemically linked (covalently bonded) together, the reptation or the complete chain motion is not possible. Therefore, in terms of orientation autocorrelation function $C(t)$, a complete orientation correlation is never lost rather a certain correlation maintains in the long time limit. Consequently a resulting plateau appears in $C(t)$ as shown in Figure 3.2 which is define as the dynamic backbone order parameter S_b of the polymer chains in the network [29, 131].

$$S_b^2 = \lim_{t \rightarrow \infty} C(t) \quad (3.20)$$

Proton NMR spectroscopy can be used to study the structure of an elastomer also by exploiting the dipolar interactions within a polymer chain. Therefore to estimate the network crosslink density, τ_{mob} from Eq 3.19 is the parameter which is analyzed more closely in this section.

Polymer networks act partially solid-like. The existence of crosslinks and other topological constraints in rubber matrices lead to weakly nonisotropic, fast segmental fluctuations of the chain which is seen as a plateau of $C(t)$ [132] in Figure 3.2. This means that the internuclear vector of dipolar coupled nuclei at the backbone of the polymer chain cannot adopt all possible orientation with respect to static magnetic field. As a consequence, their dipolar couplings are not averaged out completely due to the partial alignment of molecules. Therefore, an average anisotropic dipolar coupling remain which is called “*Residual Dipolar Coupling*” (D_{res}) (NMR-determined parameter) and a reliable information on the absolute values as well as the distribution of residual couplings becomes accessible considering the fact that in crosslinked networks, large-scale chain dynamics is mostly absent. The large-scale chain dynamics would further reduce D_{res} .

$$S_b \propto D_{res} \propto \frac{1}{N} \propto \frac{1}{M_c} \quad (3.21)$$

The above correlation represents the connection between the experimentally accessible quantity by NMR i.e., residual dipolar coupling D_{res} and number of segments within a polymer chain between a crosslink i.e., N or the average molecular weight of a network chain, M_c [133]. In SBR, a more qualitative approach is adopted to correlate D_{res} with $1/M_c$. In order to convert D_{res} into a crosslink density, a model is needed to give the quantitative estimation of $1/M_c$. Based on the computer simulations of fluctuation (orientation) statistics, the value of prefactor has been determined for natural rubber (NR) and butadiene rubber (BR) [29].

$$M_c^{(NR)} = \frac{617\text{Hz}}{D_{res}/2\pi} \text{kg/mol} \quad (3.22)$$

and

$$M_c^{(BR)} = \frac{656\text{Hz}}{D_{res}/2\pi} \text{kg/mol} \quad (3.23)$$

However in SBR, the complex spin dynamics of the PS comonomer with its phenyl side group would still require a suitable model to explain the local molecular dynamics. Therefore, a crosslink density is qualitatively estimated as $D_{res} \propto 1/M_c$ [32].

3.2.2 Experimental Details

The following MSE and DQ-NMR experiments performed to quantify the phase composition and the average crosslink density of the composite materials mentioned in Table 5.1 respectively, were carried out on a Bruker minispec mq20 spectrometer operating at 0.5 T (20 MHz). The 90 and 180° pulses had a length of 1.7 μs and 3.5 μs , respectively. The dead time was 12 μs . For the DQ-buildup curve experiments to determine crosslink density, all the samples were measured at 120 °C.

Quantification of Mobile/Immobile Phase

The NMR sequences typically used to study polymer chain mobility in filled rubbers are the solid-echo pulse sequence to study the rigid polymer fraction (seen at short time scales) and the Hahn echo for the mobile fraction (at longer time scales). However, those methods are tend to produce artifacts related to over interpreted or inapplicable fitting models and parameter interdependencies [134]. Here we used magic-sandwich echo (MSE) to study the polymer relaxation at short time scales (less than 0.2ms). The MSE refocuses the initial part of the free-induction decay (FID) and thus avoids the dead time issue. Compared with solid echo, it enables a better refocusing of multispin

dipolar interactions and has been shown to be a robust method to investigate polymer mobility [28, 57, 134].

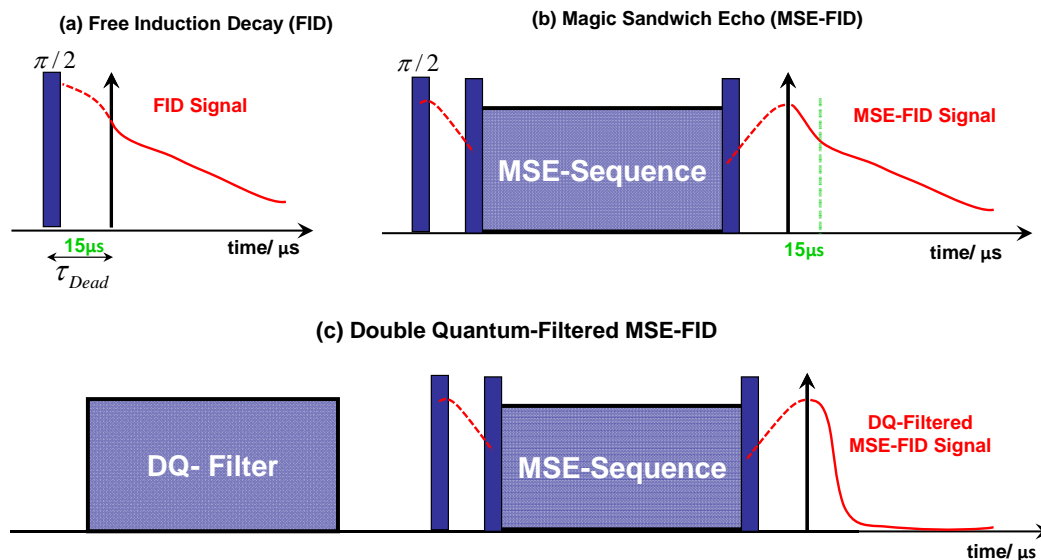


Figure 3.4: (a) Pulse sequences. Solid bars denote 90° pulses, and the blue-shaded areas represent group of pulses. (a) Initial part of the free-induction decay (FID) (dashed line) is missing due to the receiver dead time (τ_{Dead}). (b) MSE sequence is employed after τ_{Dead} to refocus the lost signal and thus measure the entire shape of the FID. (c) Double Quantum (DQ) sequence is used before the MSE sequence to filter out the contributions from the mobile phase i.e., $> 30 \mu\text{s}$.

However the FID cannot be directly exploited due to the rather long dead time of the receiver: the first $15 \mu\text{s}$ of the FID are missing and this part of the signal is very important since it contains the initial fast decay part and so the immobilized polymer response (see schematically in Figure 3.4a). The receiver dead time of the spectrometer is required to ensure the complete decay of the pulse intensity and hence it ranges between $11 \mu\text{s}$ and $15 \mu\text{s}$ for the low-field devices used here. To obtain information on the shape of the entire FID signal decay, we used a Magic-Sandwich echo coupled with double quantum (DQ) filter in order to refocus the signals entirely from the immobile part of the matrix. The Magic Sandwich Echo (MSE) sequence is a so-called time-reversing pulse sequence. It refocuses rapidly decaying NMR signals, which are governed by the action of strong multiple dipolar couplings between the nuclear spins of the sample, by reversing the dipolar dephasing [129] and it is schematically shown in Figure 3.4b. On the other hand Double quantum filter, with short DQ evolution time $\tau_{DQ} \approx 15\text{-}20 \mu\text{s}$, is used here for the selection of magnetization in the rigid polymer phase. Strong dipolar couplings between spins create a complex network of interacting spins in which multi-quantum coherences, involving orientation correlations

between interacting spins, can be excited by certain rf-pulse sequences [135]. These certain rf-pulse sequences are used here as DQ-filter. The DQ-filtered MSE-FID is schematically shown in Figure 3.4c and it can be qualitatively analyzed by the following single-component exponential fit

$$M(t) = M_0 \exp \left[- \left(\frac{t}{\tau_g} \right)^2 \right] \quad (3.24)$$

From above Eq 3.24, one can get the τ_g which is the shape parameter of the immobile phase and shows the decay time due to immobile part. Further τ_g can be used in Eq 3.19 to fit the entire shape of the initial FID. The fitting results of these Eq 3.19 and 3.24 are shown in Figure 6.7 in the Section 6.3 of the results Chapter 6.

Determination of Crosslink Density

Quantitative double-quantum (DQ) or, more generally, multiple quantum (MQ) NMR is a powerful method to measure the crosslink density of polymer networks by detecting weak residual dipolar coupling [29, 31]. DQ NMR spectroscopy generates two qualitatively different signal components. A buildup curve (I_{DQ}) dominated by spin-pair double-quantum coherences and a decay curve (I_{ref}). The sum of both components ($I_{DQ} + I_{ref}$) contains the full magnetization of the sample, i.e., contributions from dipolar coupled network segments and contributions from uncoupled units (isotropically mobile network defects, e.g. dangling ends, loops, oil content). Dipolar coupled segments (network) exhibit non-exponential faster relaxation while the signal from uncoupled parts appears in the form of slower exponential decay (Figure 3.5a) and regarded as the defect fractions of the network i.e., dangling chain ends, loops, oil content etc.

In order to correct the raw I_{DQ} build-up data shown in Figure 3.5a for the obvious long-time relaxation effects and enable a quantitative analysis, it is divided point-by-point by a suitable relaxation-only function, $I_{\Sigma MQ}$. This function is an additive part of the mentioned ($I_{DQ} + I_{ref}$) sum function, and in order to obtain it, the mentioned defect fraction has to be subtracted:

$$I_{\Sigma MQ} = I_{DQ} + I_{ref} - B \cdot \exp(-2\tau_{DQ}/T_2^*) \quad (3.25)$$

The defect fraction with relative amplitude B is easily identified by an exponential fit to the data range where I_{DQ} has essentially decayed to zero (i.e., beyond a DQ

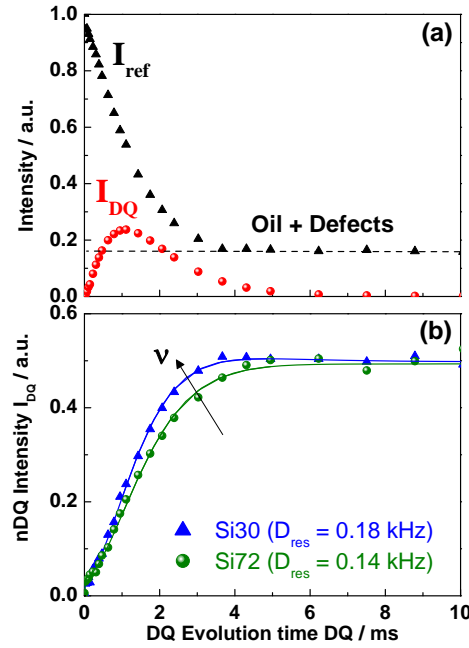


Figure 3.5: (a) DQ buildup (I_{DQ}) and reference decay (I_{ref}) data as a function of the double-quantum evolution time t_{DQ} . $I_{ref} - I_{DQ}$ can be used to highlight the non-elastic, slowly relaxing (isotropically mobile) defect fraction. (b) Normalized buildup curves (I_{nDQ}) as a function of t_{DQ} . The solid lines are fits based on Eq 3.26 assuming a Gaussian distribution of dipolar couplings.

evolution time of about 6 ms). Now, the DQ build-up data can be normalized, obtaining $I_{nDQ} = I_{DQ}/I_{\Sigma MQ}$. I_{nDQ} is independent of temperature-dependent relaxation (decay) effects and it is dominated by the dipolar interactions that are only related to the network structure. In the absence of relaxation effects of nonelastic network defects, I_{nDQ} (Figure 3.5b) can be evaluated under the assumption of a Gaussian distribution of dipolar couplings according to

$$I_{nDQ}(\tau_{DQ}) = \frac{1}{2} \left(1 - \frac{\exp \left\{ -\frac{\frac{2}{5} D_{res}^2 \tau_{DQ}^2}{1 + \frac{4}{5} \sigma^2 \tau_{DQ}^2} \right\}}{\sqrt{1 + \frac{4}{5} \sigma^2 \tau_{DQ}^2}} \right) \quad (3.26)$$

The values of residual dipolar coupling D_{res} (Table 5.1) are proportional to the crosslink density ν of the polymer network. The parameter σ represents the distribution width in an inhomogeneous sample, which for the case of SBR is dominated by “spin inhomogeneity” related to the copolymer character of SBR [31]. The ratio σ/D_{res} is found to be nearly constant at a value of around 0.35 ± 0.05 for all samples. Experimental D_{res} values are used to study the influence of filler content on the crosslink density of the rubber matrix in composite materials.

Chapter 4

Optimizing the Tire Tread

The tread of the tire fulfills an essential function in the transmission of force to the road. Therefore, tire tread is designed by considering several performance criteria. Out of these, two functional properties of the tire tread rubbers are given prime importance: low rolling resistance and high wet traction during braking. In connection with the fuel economy and the environmental concerns, low rolling resistance in the tread is demanded to minimize the fuel consumption. For a better road grip and safety concerns under wet or icy conditions, a tire must deliver high wet/skid resistance to ensure the predictable steering characteristics. Additionally a tire must also show low wear and good durability which means the resistance to abrasion should be as high as possible to create a high mileage [136–138]. However, improvements of the rolling resistance can only be achieved with a reduction of the wet grip. Hence the optimization of these interrelated but contradicting properties forms the so called “Magic Triangle” of tire properties as shown in Figure 4.1 [139, 140]. A compromise level between these characteristics is always necessary to maintain a balance among them.

Rubber friction differs in many ways from the frictional properties of most other solids. The reason for this fact is the low elastic modulus of rubber and the high internal losses due to friction exhibited by the rubber in a wide frequency range. A description of the viscoelastic behavior of tread rubber is usually presented as a general practice by the curve of $\tan \delta$ against temperature (as shown in Figure 4.2). This description is based on certain strong assumption and crude estimation. However still as an indication of skidding behavior (grip, traction) on wet or icy roads, the high values of the loss tangent around 0°C till $+30^{\circ}\text{C}$ are considered as an important parameter [137]. Since the peak in $\tan \delta$ correlates with the glass transition temperature T_g of the polymer, for the extensive screening this value became a tool for the selection of a suitable tyre

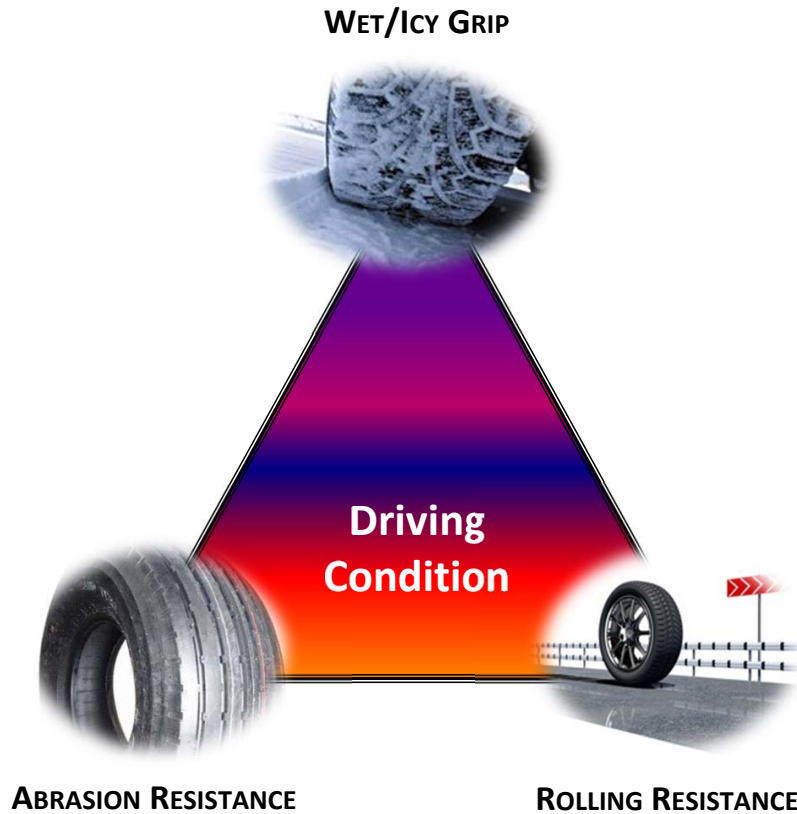


Figure 4.1: Schematic shows these three basic performances considered in modern tire production: traction, abrasion resistance and rolling resistance. The optimization of these three conflicting parameters is called “Magic Triangle” optimization because it is impossible to improve all three characteristics at the same time and a balance must be found between these properties [139].

rubber [141]. While for the rolling resistance optimization, the low values of the $\tan \delta$ around 60°C to 80°C are believed to be an appropriate parameter.

However, this viscoelastic description is basically translated on the basis of temperature-frequency equivalence of the viscoelastic material [137,141]. According to this equivalence principle, rolling resistance is predominantly related to loss tangent of the bulk polymer at comparatively low frequencies in the plateau region of the loss tangent (see Figure 4.2). While, the wet skid resistance (WSR) is appeared to be linked with dynamic losses in the glass-rubber transition zone of the bulk polymer i.e., typically in the range of 1 kHz - 1 MHz.

The aim of this chapter is to address few ambiguous questions concerning the two main tread properties i.e. Wet resistance and the rolling resistance. 1) Usually the friction properties of the tread rubber are characterized by dynamic mechanical analysis. It is very important to identify and to understand the potential relationship between the

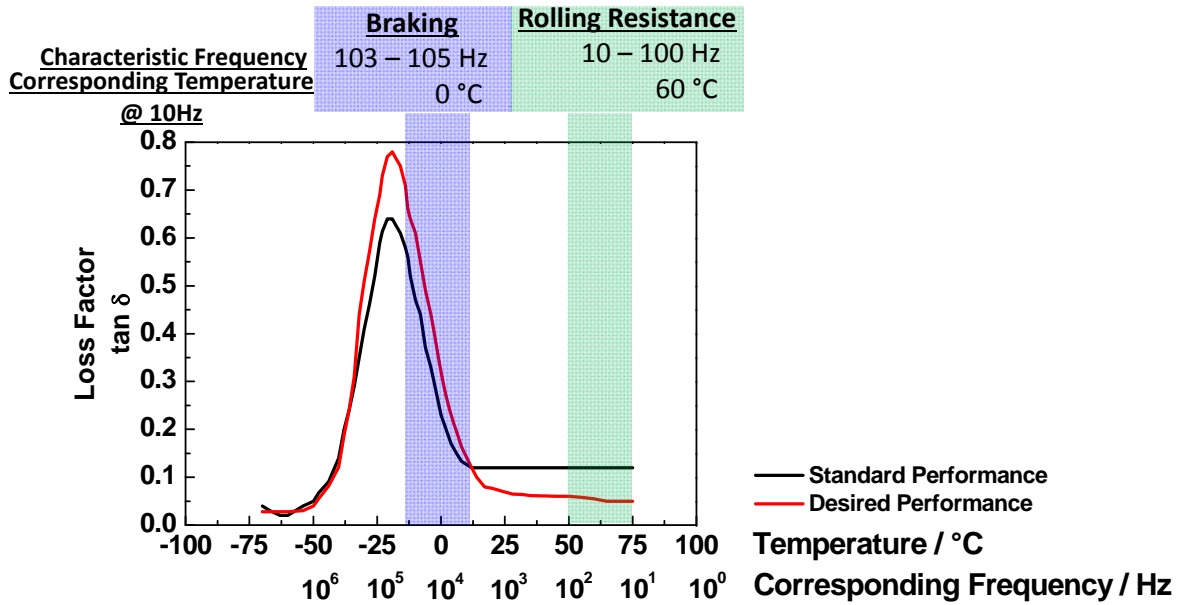


Figure 4.2: $\tan \delta$ as function of temperature and frequency of a standard and a target curve of tire tread material. Adapted from [142].

tread friction (either skid or rolling) and the experimentally observed dynamic mechanical quantity ($\tan \delta$). 2) Secondly the $\tan \delta$ is typically being used to quantify the loss mechanism of the tread rubber to optimize friction. A literature will be reviewed to find out the possible reasons for the relevance of the dynamic loss ($\tan \delta$) to the loss mechanism in tire tread instead of loss modulus G'' . 3) Finally in this chapter, physical basis of the typical frequency dependence of the wet and the rolling resistance of the tread component will be explored.

4.1 Relation Between Friction and the Mechanical Properties of Tire Rubbers

The generally accepted view is that the friction force (either sliding or rolling) between rubber and a rough (hard) surface has two contributions commonly described as the adhesion and the hysteretic component respectively [143,144]. The adhesion component is a surface effect which takes place within a thin layer at the sliding interface. The hysteretic component arises due to the internal friction of the rubber. During sliding, the asperities of the rough surface exert oscillating forces on the rubber surface [11]. These oscillating forces result in cyclic deformations of the rubber and energy loss via the internal damping of the rubber. Hence, this contribution to the friction force has also the temperature dependence as that of the complex elastic modulus $E^*(\omega)$ [145,146].

$$\text{Friction force } F = \text{Adhesion component} + \text{Hysteresis component}$$

The adhesion component of the friction was initially studied experimentally by Bulgin et al. [145]. They explained that the adhesion term of the total friction is a surface effect due to intermolecular forces between polymer and the contact surface, which takes place within a thin layer (few nm) of a sliding interface. This sliding process leads to a local drag force which acts as a retarding force on the system. An associated strain also develops in the material, causing energy to be stored elastically in the adhering element of the polymer. When the elastic stress exceeds the adhesive force, failure of the adhesion occurs and the element relaxes. The elastic stored energy is partially returned to the moving system as an accelerating force. However the proportion of energy returned will depend on the hysteresis loss in the material. Hence group of molecules near to the contact surface experience alternating retarding and accelerating forces of different magnitude and the difference is the net retarding force corresponding to the external friction force. A simplistic model was presented where they showed that the frictional force developed between a polymer and a solid surface arises from the adhesion release processes at the interface. The model concluded that the coefficient of friction μ at the adhering area is

$$\mu \approx \left(\frac{1}{H} \right) \left(\frac{E''}{E'} \right) \quad (4.1)$$

where H is hardness of the material and $\frac{E''}{E'}$ is the hysteresis loss in the material.

The existence of hysteresis friction is a result of energy loss associated with internal

damping effects within a viscoelastic body, and it normally appears in the form of heat. When tread rubber slides or rolls on an asperity of a harder surface (road), a certain amount of work is performed in deforming the rubber in front of the asperity. Partial amount of this work is recovered from the rear side of the rubber-surface contact. However, since the filled rubber shows the hysteresis due to the internal friction, energy is lost. In rolling this is the primary source of the frictional work. In sliding, there is additional energy dissipation due to the shearing of junctions formed as a result of adhesion at the interface. Under dry conditions, the adhesional contribution to the total friction is large enough that the hysteretic part of friction is almost negligible. However for wet conditions, the adhesional component of the friction is substantially reduced, and the remaining sliding friction is due to the work expended in deforming the surface, causing a hysteretic energy loss [143]. A comprehensive study of the friction was done by Grosch [146] on several types of rubber against different kinds of hard surfaces over a wide range of temperatures and sliding velocities. The results show that the friction increases with the sliding velocity to a maximum value and then falls (shown in Figure 4.3b). The dependence of the coefficient of friction on velocity and temperature has been shown by a master curve describing the velocity dependence at a constant temperature, T_s , which is related to the glass transition temperature of the material. This transform agrees closely with the W.L.F. transform and thus shows that both friction mechanisms are visco-elastic in nature (The isotherms of the friction coefficient as function of sliding velocity are shown in Figure 4.3a for natural rubber).

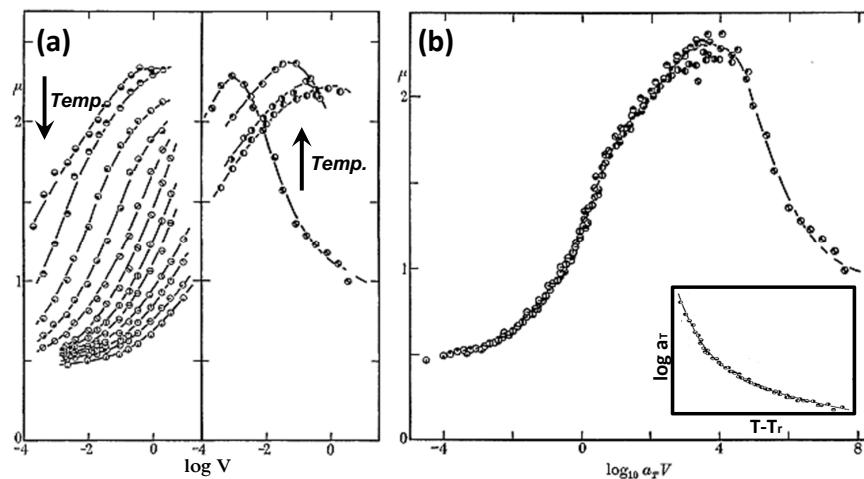


Figure 4.3: (a) Coefficient of friction as a function of sliding velocity on smooth surface at various temperatures of natural rubber. (b) Master curve for the coefficient of friction obtained using horizontal shift factors (inset) which follows WLF function. Adapted from [146].

From the discussion above, it is clear that the friction, along with the factors like load, hardness etc, depends also on temperature and frequency. Bulgin et al. [145] shows that when a hystereis loss, transformed apparently to the temperature and frequency appropriate to the friction, is plotted against the friction (experimental values) for different tread rubbers, a linear relationship is observed which passes through the origin of the graph (as shown in Figure 4.4).

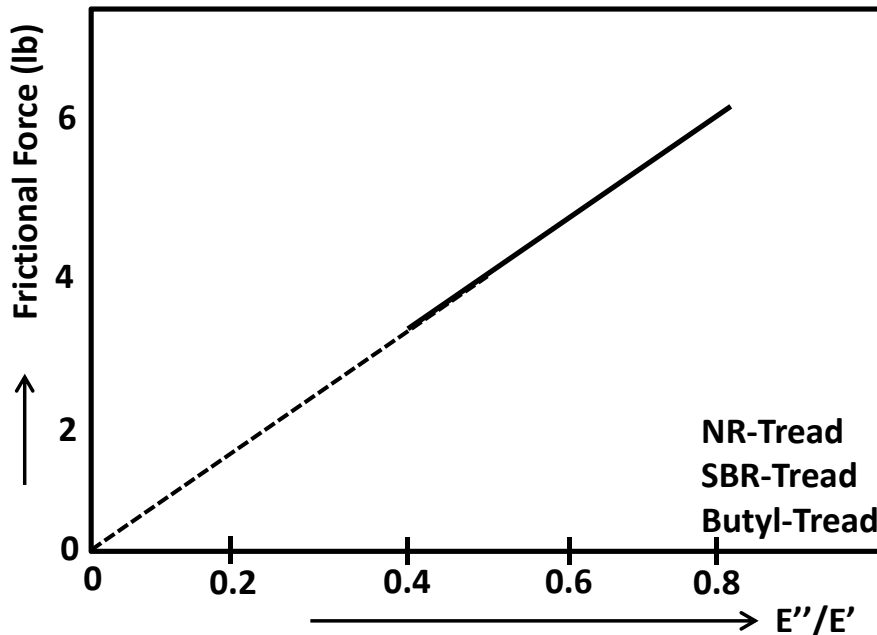


Figure 4.4: Friction force as a function of damping factor. Taken from [145].

Hence the the general relationship justifies the view that the friction as a phenomenon of polymers is controlled by the viscoelastic character of the tread material.

4.2 Usage of $\tan \delta$ As Loss Parameter

Generally in literature $\tan \delta$ has been used to optimize different properties of the tire. The objective to use this parameter is to monitor the energy loss at particular temperature and frequency. There are some indications in literature for that the loss modulus G'' alone does not give the appropriate quantitative information to understand that how much fraction of the energy is used for the deformation of the tread rubber and accordingly how much energy is dissipated [75, 146, 147]. However, Robertson et al. [148] shows that large differences in shape and magnitude of the peak in the loss tangent vs temperature are observed simply by varying the filler surface area and also

the filler quantity in the same type of the elastomer. The loss modulus (G'') peak, however, corresponding to the segmental relaxation process (glass transition) is not significantly affected of these investigated materials. The reason of the variation in $\tan \delta$ peak is due to the variations in the storage modulus in the rubbery states, which is influenced by the strength of filler network.

In this section, we review those indication through the relevant literature concerning the physical basis of the loss factor.

4.2.1 Theoretical Approach

The earlier concept of hysteresis applied elasticity theory to the sliding of spheres and cylinders on an elastomeric plane surface [149]. It was hypothesized that a small fraction of the input elastic energy to the deformed elastomer must be dissipated in the form of hysteretic friction. They considered a rigid cylinder or sphere of radius R (as shown schematically in Figure 4.5-left) pressed on to an elastomer by a load W per unit width of cylinder/sphere. If the elastic medium possessed ideal elastic properties, the part behind the rolling cylinder would yield the same amount of work. The elastomer would then effectively restore the work done to the object in the initial compressive stage, and no net energy would be expended. However, a constant fraction α of the input elastic energy is assumed to be lost as a consequence of hysteresis within the elastomer, and this gives rise to a friction force F . The coefficient of friction for the rolling cylinder can be written as

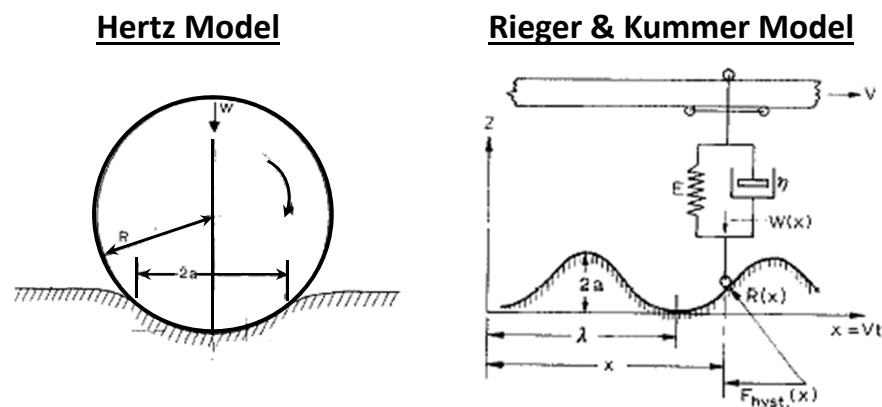


Figure 4.5: (Left) Rolling of rigid cylinder on an elastic medium. (Right) Sinusoidal asperity model for track roughness. Adapted from [149].

$$f_{rolling} = \frac{F}{W} \approx \left[\frac{\alpha W}{R} \left(\frac{1 - \nu^2}{E} \right) \right]^{1/2} \quad (4.2)$$

where ν and E is the poisson's ratio and the Young's modulus respectively for the elastomer.

The review [143] about these calculations mentioned that the above analysis for sphere and cylinder has very limited application, and it is valid for very low speeds of sliding. As speed increases to finite values, a complete elastic recovery becomes a necessity to sustain the rolling mode. The theory inherently contradicts itself, since if elasticity is assumed there will be complete recovery behind sphere/cylinder and hence no coefficient of rolling friction. To explain this contradiction, the authors have used the term "elastic hysteresis" which is a further contradiction.

The theoretical work by Tabor [143] assumed viscoelastic behaviour in the elastomer, usually by making use of some form of energy dissipative mechanical model. These various mechanical model theories were distinguished on the basis of the shape of asperities in the rigid base surface (i.e. sinusoidal, cylindrical or spherical). In the case of sinusoidal asperities, it is convenient to consider a multiple asperity model, since the mathematical definition of the surface is a continuous function of position. Rieger and Kummer [149], for instance, offer a similar simple Voigt model simulation of rubber sliding on a sinusoidal track, as shown in Figure 4.5-right. The amplitude of the track may be described by the equation

$$z = a(1 - \cos \omega t) \quad (4.3)$$

where $\omega = 2\pi V/\lambda$. The mean hysteretic friction force F_{hyst} was then calculated as on basis of Voigt model ($\tan \delta = \omega\eta/E'$)

$$F_{hyst} = E_d/\lambda = \pi a^2(L/\lambda)\eta\omega \quad (4.4)$$

E_d is total energy dissipated as hysteretic friction, λ wavelength of the sinusoidal roughness and L is the total characteristic length. Rieger and Kummer obtained two different forms of equation from Eq 4.4. If ω is replaced by $\omega = 2\pi V/\lambda$, the F_{hyst} is proportional to velocity

$$F_{hyst} = 2\pi^2 L(a/\lambda)^2 \eta V \quad (4.5)$$

and if $\eta\omega$ is replaced by $\tan \delta = \omega\eta/E'$, then F_{hyst} is proportional to $E' \tan \delta$

$$F_{hyst} = 2\pi^2 a^2 (L/\lambda) E' \cdot \tan \delta \quad (4.6)$$

This calculation was the first theoretical indication pointing that the deformation hysteresis is proportional to the loss factor. However, as the $\tan \delta$ is the ratio of E''/E' , one can also conclude from this equation that the F_{hyst} is also proportional to the E'' . Additionally, both Kummer and Rieger [149] have indicated that the above form of equation shows a constantly increasing hysteretic force F_{hyst} , as the sliding speed V is raised. Indeed this is the case as the viscosity term η is assumed constant in the Voigt model representation of Figure 4.5-right. This reasoning can be valid, however, only within a limited velocity range. At higher velocities, they fails to show any mathematical reasoning to account for a drop in hysteresis value, exhibiting the characteristic viscoelastic peak which one should expect (see Figure 4.3b). Similar result is obtained by Moore [150] where he relates the contact asymmetry to the loss tangent ($\tan \delta$) of the viscoelastic material. He also assumed the Voigt model and considered again the case of a rigid cylinder sliding on a viscoelastic plane.

Medalia [100] calculated of the energy (ΔE) dissipated per cycle:

$$\Delta E = \oint \sigma d\epsilon = \int_0^{2\pi/\omega} \sigma \frac{d\epsilon}{dt} dt \quad (4.7)$$

Substituting for σ and ϵ values from the Eq 3.1 and 3.2 respectively,

$$\Delta E = \omega \epsilon_0^2 \int_0^{2\pi/\omega} (G' \sin \omega t \cos \omega t + G'' \cos^2 \omega t) dt \quad (4.8)$$

The integral is solved by using $\sin \omega t \cos \omega t = 1/2 \sin 2\omega t$ and $\cos^2 \omega t = 1/2(1 + \cos 2\omega t)$, we have

$$\Delta E = \pi G'' \epsilon_0^2 \quad (4.9)$$

By the definition of the G'' and G^* from the Eq. 3.4 and 3.5 respectively,

$$\Delta E = \pi \sigma_0 \epsilon_0 \sin \delta \approx \pi \sigma_0 \epsilon_0 \tan \delta \quad (4.10)$$

Therefore, depending on whether σ_0 , ϵ_0 or $\sigma_0 \epsilon_0$ is kept constant during dynamic deformation (corresponding to constant strain, constant stress, or constant energy input), the energy loss or dynamic hysteresis is proportional to G'' or $\tan \delta$, respectively. However this relation is only valid when δ values are much smaller (then $\sin \delta \approx \tan \delta$).

Therefore in terms of viscoelastic properties of the elastomer, this relation of energy dissipation per deformation cycle is only valid for the $\tan \delta$ if the plateau region is considered, and not the glass-rubber transition region, where δ values are significantly smaller than the transition region. In the later section, the practical relevance of the transition region will be discussed in terms of wet skid resistance.

4.2.2 Experimental Indication

The extensive experimental studies on friction was done by Grosch [146]. He studied the friction of several types of rubber against hard surfaces over a wide range of temperatures and sliding velocities. For sliding the rubber, different types of hard surfaces i.e. rough and smooth surfaces, were used to analyze the friction behavior. The master curve on a rough abrasive track shows two peaks as shown in Figure 4.6a. According to his interpretation, i) one of these peak occurs at a velocity related to the frequency with which the track asperities deform the rubber surface. This statement was concluded on the basis of friction studies on the smooth surfaces where one maximum is absent. Thus the high frequency peak appeared on rough surfaces reflects the deformation losses produced by the passage of the asperities or roughness over the rubber surface.

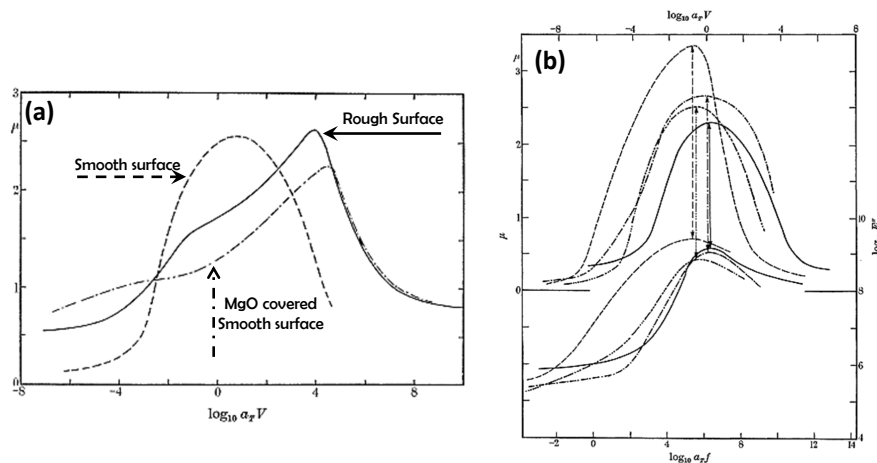


Figure 4.6: (a) Master curve of the coefficient of friction for SBR on three different surfaces. (b) Above: Master curve of the coefficient of friction for four different rubbers on smooth surface. (Below) Loss modulus curves E'' as a function of frequency for the same four rubbers. Adapted from [146].

ii) The other peak occurs in general at much lower velocities. This peak coincides in position with the single maximum obtained on a smooth surface. Hence they concluded that this peak, appearing on smooth surface at lower sliding velocities, originates due

to molecular adhesion between two sliding surfaces. To confirm this conclusion, fine powder (MgO) was introduced to the interface between the rubber and track. This method eliminates the friction peak appearing due to adhesion and only the hysteresis component of the friction left as a single peak (Figure 4.6a). Comparison (shown in Figure 4.6b) of the maximum of friction coefficient of the adhesion-peak with the dynamic loss modulus (E'') indicates the correlation of both quantities. It is finally concluded that the adhesional component of friction correlates with the loss modulus curve (E'') of the rubber. Hence the deformation friction, where the operative frequency is determined by the scale of the surface asperities and the sliding velocity, is assumed to be correlated with the loss factor or $\tan \delta$ without giving any experimental evidences. So far the review of the literature is done to find the appropriate reasons for using $\tan \delta$ as a viscoelastic loss parameter. However no concrete theoretical or experimental evidence has been found which clearly indicates that the $\tan \delta$ is more reliable parameter to quantify the loss as compared to the loss modulus G'' . The study in this thesis and the study by Robertson et al. (as discussed earlier) shows that the peak of the $\tan \delta$ and the corresponding glass-rubber transition region (which is currently regarded as the influential frequency region to the Wet Skid Resistance) are largely influenced by the addition of fillers. The variations in $\tan \delta$ primarily originates from the increasing storage modulus G' due to the filler addition ($\tan \delta = \frac{G''}{G'}$). G'' peak however, is not affected by the filler addition. Therefore the $\tan \delta$ might be a misleading parameter for the quantification of the dissipative mechanisms in the viscoelastic materials and an extensive comparative study for both parameters ($\tan \delta$) is needed to understand the overall picture.

4.3 Tire Optimizing Parameters and their Relation to Viscoelastic Behavior and Friction

The ultimate problem encountered by the tire designers is to achieve an optimal balance between three major tire properties i.e., obtaining a low rolling resistance, high wet traction and high wear resistance. These properties are physically interrelated with each other but their optimization trends are in opposite direction. In order to obtain the road grip/traction during braking under wet or icy conditions, a tire tread can be improved by making the rubber softer. In this way, one can get high friction under such conditions, resulting in high traction. However, if the same tread is used under normal rolling conditions at high temperatures, a high amount of the applied energy is dissipated in terms of heat due to high rolling friction. Thus the vehicle consumes more fuel. Additionally soft rubbers usually wear more quickly, resulting in frequent tire replacement. As a consequence, if tire manufacturers improve one of these parameters, they have no choice but to compromise on the other two tire properties. In this section, a typical frequency dependence of the Wet skid resistance and the rolling resistance will be discussed. Moreover we examine a relation between dynamic viscoelastic response of rubber and the corresponding frequency-dependent friction.

4.3.1 Wet Traction

Wet skid resistance is defined as the retarding force generated by the interaction between a tire and a road under a locked, or non-rotating, wheel (Standards-ASTM E 867). It is a measure of the ability of a material under wet conditions to resist the skidding of a tire material on a road surface. Skidding occurs when the frictional demand exceeds the available friction force at the interface between a tire and pavement [151]. Wet traction is the most important parameter for the optimization of the tire tread rubber. Some statistics indicate that the number of accidents increases by up to two folds during rainy conditions [152]. This happens due to the fact that skidding will occur easily when the water film covering the road surface act as lubricant and reduce the friction between the tire and pavement. The loss of skid resistance affects driver's ability to control vehicle. In addition to increasing the stopping distance while braking, lower skid resistance reduces steering controllability since both braking and steering depend on tire-pavement friction. Therefore the emphasis generally in tire development is placed dominantly on the improvement of skid properties with the least possible trade-off in rolling resistance and abrasion [153].

In literature, the wet skid resistance of elastomers is generally recognized as a high-frequency phenomenon [136, 138]. Figure 4.7 shows a rolling elastomeric object on a road surface. The road surface is composed of many irregularities or asperities (as discussed earlier). When braking force is applied, the tire is pressed against the road surface due to the weight of the car and comes into contact with most of the asperities [141]. Since there are large number of asperities located close together (schematically shown in Figure 4.7), the frequency of deformation experienced by the tires is also very high when tire slides over such surface. The deformation frequency is difficult to calculate accurately. It depends upon the speed of the sliding tire, the spacing of the asperities, surface contamination etc. The spacing between asperities is estimated to be 0.1 to 0.01 mm [10]. Assuming an average speed of slide of 8 kmh^{-1} , the deformation frequency encountered by the tire must be between 1 kHz to 1 MHz [136, 138].

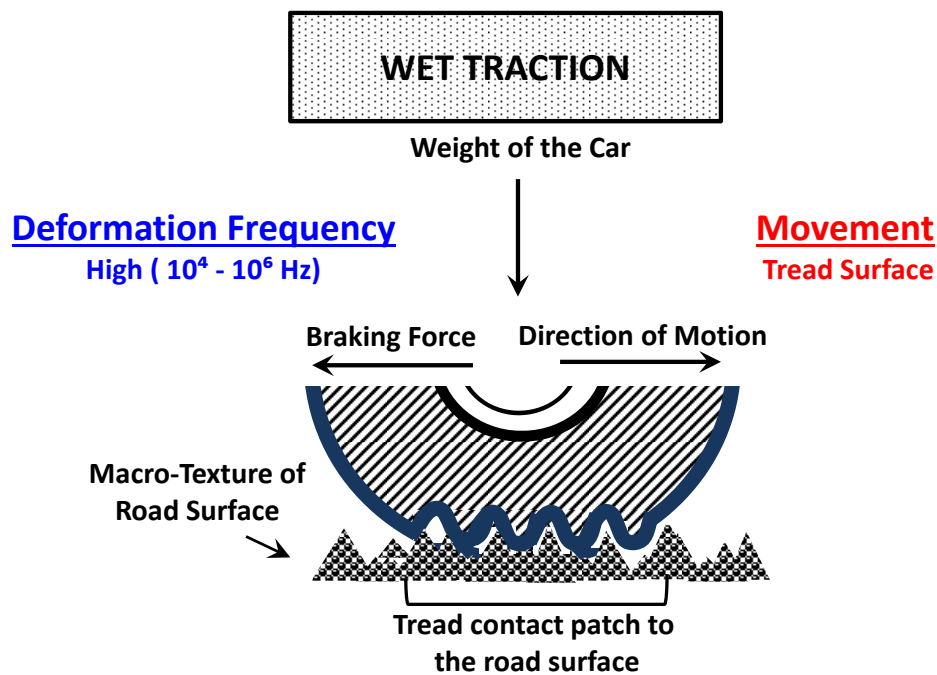


Figure 4.7: Schematic diagram of a tire encountering wet skid conditions. When the brakes are applied, the tire comes in contact with most of the asperities on the road surface and as result, the deformation frequency encountered by the tire during the wet skid process is quite high i.e., 1 KHz to 1 MHz.

4.3.2 Rolling Resistance

Rolling resistance is the force that resists the rolling of a wheel or other circular object along a surface caused by the deformations in the object and/or surface. Consider soft

wheels rolling on and deforming a hard surface (as shown schematically in Figure 4.8) with W as a vertical load on the rolling object. The resultant reaction force F_r from the surface opposes the motion can be expressed as

$$F_r = c \cdot W \quad (4.11)$$

where c is the coefficient of rolling resistance that characterizes the material property to resist the pulling force.

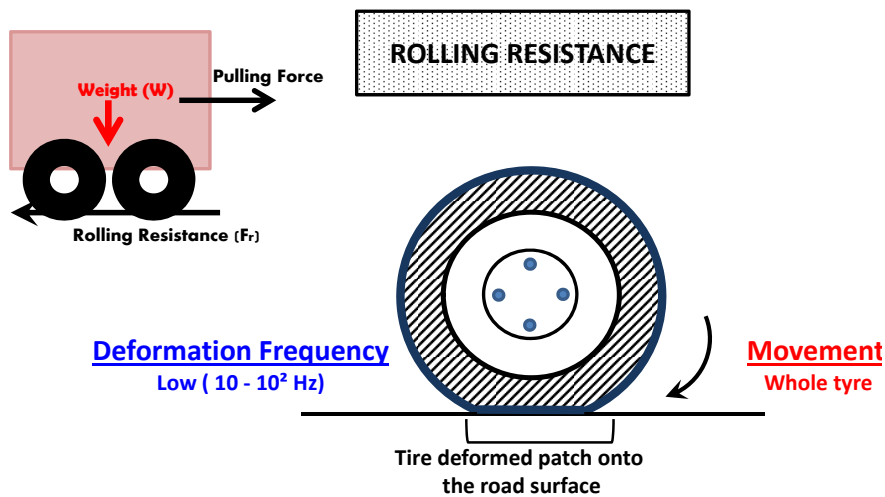


Figure 4.8: Schematic illustration of the rolling objects and the rolling resistance. Deformation frequency encountered by a tread during a complete rotation of a wheel is low $\approx 100\text{Hz}$ compared to wet skid resistance.

Concerning the tire tread, rolling resistance is a result of repeated movement of rubber caused by the tire rotation. These repeated movements lead to the constant deformations in the viscoelastic material in the form of bending, stretching and recovering as the viscoelastic material cycles between loaded (where the tread footprint flattens against the road) and unloaded states. The final contributor to tire rolling resistance is the tread's interaction with the road in the form of adhesion.

Consider the deformation versus time of a footprint section of a typical tire rolling at about 80 km/h (schematically shown in Figure 4.8). The footprint print of such a tire is approximately $1/10^{\text{th}}$ of the circumference of the tire. The rotational frequency (ω_{roll}) corresponding to 80 km/hr speed can be estimated around 10 - 12 Hz. Hence the tread rubber, during the contact, will be deformed at an effective frequency ω_{eff} equal [141]

$$\omega_{eff} = \omega_{roll} \left(\frac{\text{Tire Circumference}}{\text{Footprint Length}} \right) \quad (4.12)$$

According to the estimation based on equation above, the deformation frequencies of the tread rubber are in the range of 100 - 120 Hz.

4.3.3 Summary

The optimization of the tire related properties is often done based on strong assumptions and crude approximations. Based on the deformation frequencies corresponding to wet skid resistance and rolling resistance, optimizing temperature-dependent dissipation of both of these quantities is actually based on a linear viscoelastic spectrum. The linear viscoelastic spectrum of a pure polymer or rubber can be experimentally obtained from oscillatory shear measurements at suitable temperature on a mechanical spectrometer (cf. Figure 4.9).

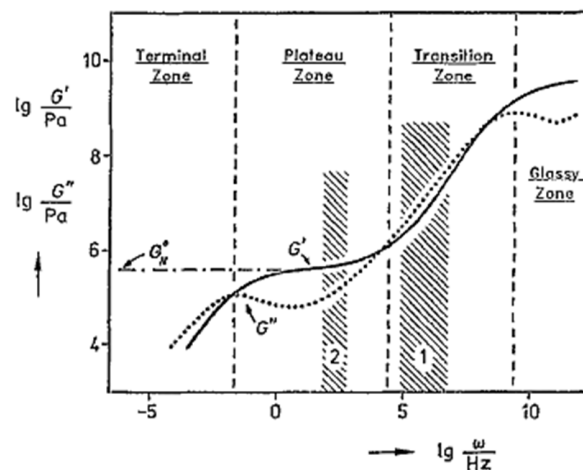


Figure 4.9: Schematically illustrated frequency-dependent storage (G') and loss (G'') shear moduli of an uncrosslinked polymer. Region-1 correlates with the wet skid behavior of a tread material; and Region-2 correlates with the rolling resistance of a tire. In case of crosslinked rubber, there is no transition zone instead the rubber plateau of G' is extended to lower frequencies (dash-dot line (G_N^0)). Adapted from [153].

The storage and loss moduli are measured as a function of frequency in a linear viscoelastic region [154]. Rolling resistance is related to the energy loss of the bulk polymer at comparatively low frequencies (as shown Region-2 in Figure 4.9). This radian low-frequency is in the order of the angular velocity of the rolling tire. The wet skid resistance is linked with dynamic losses in glass-rubber transition zone of the bulk polymer at high frequencies (shown as Region-1 in Figure 4.9) [153]. The viscoelastic properties of rubbers at such high frequencies are difficult to measure. Hence the master curve construction is considered as a useful tool to estimate high frequency behavior.

The linear viscoelastic spectrum (mentioned in Figure 4.9) is typical result for the unfilled/pure polymer and hence the construction of the viscoelastic master curve using time-temperature superposition principle (TTS) on a broad frequency scale is easily possible. However with the addition of fillers as reinforcing agents, the complex interaction between the filler and the polymer network leads to a failure of the TTS principle [55]. The typical discontinuous master curves of G' and G'' of the filled rubber after using the WLF horizontal shift factors of the pure rubber are shown in Figure 4.10.

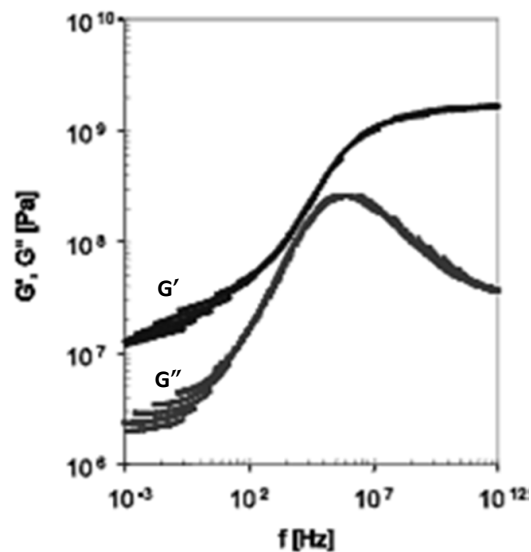


Figure 4.10: Discontinuous master curve of G' and G'' of the SBR filled with 60 phr carbon black after horizontal shifting with shift factors from the pure/unfilled SBR. Adapted from [55].

In literature, based on the temperature-frequency shifting principle, $\tan \delta$ at high frequencies and ambient temperature can be related to $\tan \delta$ at low frequencies and low temperatures. Thus $\tan \delta$ at 0 °C and low frequency (≈ 10 Hz) is widely accepted as an indicator of the wet skid resistance. While the $\tan \delta$ determined in the vicinity of 100 - 120 Hz is translated in the temperature range of 60-75 °C and considered as an appropriate material property that relates to the rolling resistance of the tire [136, 138]. These estimations are based on a strong assumption that the linear viscoelastic spectrum of the investigated filled composite follows time-temperature superposition principle. This assumption is rather an idealistic approach as it is observed that it is difficult to construct smooth master curve for the filled system. Therefore a method needs to be developed which gives a smooth and a continuous master curve for filled composites. By using that method, one can optimize directly the frequency-dependent viscoelastic properties of a tire.

Chapter 5

Sample Mixing and Processing

Solution styrene-butadiene rubber (Sprintan[®] SLR-4602 - Schkopau from Styron Deutschland GmbH) filled with nano-sized silica particles were investigated. Sprintan[®] SLR-4602 - Schkopau contains 21wt% styrene, 63% vinyl content (butadiene component) and its T_g is -25°C . [155]. Unfilled rubbers are used as a reference to determine crosslink densities in absolute units. The sample series of filled composites contain 0 to 80 phr (parts per hundred rubber) of silica (Ultrasil[®] U7000GR from Evonik Industries AG with a BET surface area of $175\text{ m}^2\text{ g}^{-1}$). [156] The filler volume fraction in the series ranges from $\Phi \approx 0$ to 0.21. The sample formulations are summarized in Table 5.1. 3-octanoylthio-1-propyltriethoxysilane (NXT Silane from Momentive Inc.) is used as a rubber-filler coupling agent to reduce the filler-filler interaction and to get well dispersed silica. By varying the silica content, the content of silane and oil were varied accordingly in order to obtain better filler dispersion in the rubber. Vulcanization additives, stearic acid (1 phr), zinc oxide (2.5 phr) and sulfur, were obtained from Roth, while CBS (N-cyclohexyl-2-benzothiazylsulfenamide) and DPG (Diphenylguanidine) were from Rhein-Chemie. Both CBS and DPG were employed as vulcanization accelerator. The use of two types of accelerators is due to the positive synergistic effect that could be achieved by combining different types of accelerators. [74] Zinc oxide is applied as accelerator activator and the activation would be further promoted by the addition of stearic acid which reacts with zinc oxide, forming hydrocarbon-soluble zinc stearate. On the other hand, the presence of fatty acid salts (zinc stearate) also lead to better processing and improved dispersion of fillers and chemicals. [74]

	Label	Sulfur phr	U7000GR phr	$\phi_{U7000GR}$ vol%	D_{res} kHz	Defects %	ν $10^{26} \cdot m^{-3}$
Unfilled reference samples	X0.9	1.26	–	–	0.2258	5.8	2.32
	X1.0	1.4	–	–	0.2465	4.2	2.53
	X1.1	1.54	–	–	0.2598	4.8	2.67
	X1.2	1.68	–	–	0.2683	5.9	2.76
Composites filled with silica U7000GR	Si20	1.4	20	0.075	0.2067	10.1	2.12
	Si30	1.4	30	0.105	0.1831	12.2	1.88
	Si40	1.4	40	0.132	0.1757	13.0	1.81
	Si60	1.4	60	0.173	0.1570	26.9	1.61
	Si64	1.4	64	0.18	0.1455	27.0	1.50
	Si68	1.4	68	0.189	0.1445	27.6	1.48
	Si72	1.4	72	0.197	0.1436	27.9	1.47
	Si80	1.4	80	0.213	0.1253	27.4	1.29

Table 5.1: Sample formulations and network properties

5.1 Rubber Mixing and Processing

Mixing was done in an internal mixer (Plasticorder PL2000, Brabender) for all kinds of filled and unfilled samples. In case of unfilled compounds with different vulcanization systems a single step mixing process with an initial temperature of 50°C and 60 rpm rotor speed is used for 10 min. This low temperature was chosen to avoid vulcanization reaction during the mixing process. For each sample, the polymers were placed in the chamber and masticate for 1 min, followed by the addition of all the additives and further mixing for 9 min. The mixed compound was then placed in a two-roll-mill at room temperature, passing through the gap for 5 times in order to obtain sheet-like shape which is favorable for the further processing. All the unfilled compounds were then vulcanized according to the procedure mentioned in Section 5.2. Please note that these reference unfilled samples with different degree of crosslinking were used to determine crosslink densities in absolute units based on mechanical and NMR spectroscopy. A Mixing recipe for unfilled system is shown in Table 5.2 which is schematically presented in Figure 5.1.

However compounds containing filler were processed by using two step mixing process (recipe is given in Table 5.3). In the first mixing step, a starting temperature of 125°C was chosen in order to guarantee that silanization can take place at a temperature higher than 140°C for 4 min. The rotor speed during that mixing step was 60 rpm and the mixing time was 15 min. In the second mixing step, the vulcanization system was added at an initial kneader temperature of 50°C, a rotor speed of 50 rpm

Component	Quantity (phr)	Density (gcm ⁻³)	Weight (g)	Volume cm ³	Mixing time (min)	Remarks
Rubber	100	0.93	48.1346	51.7576	00 : 00	$T_{initial} = 50^{\circ}\text{C}$
Stearic Acid	1	0.92	0.4813	0.5232	00 : 30	Mixing speed = 60 rpm
ZnO	2.5	5.4	1.2034	0.2228	00 : 30	—
Sulfur	1.4	2.07	0.6739	0.3255	00 : 30	—
CBS	1.5	1.28	0.7220	0.5641	00 : 30	—
DPG	1.5	1.19	0.7220	0.5641	00 : 30	—
Total	107.9	0.962	51.9372	54	10 : 00	—

Table 5.2: Compound recipe for unfilled SBR

and 5 min mixing time.

Component	Quantity (phr)	Density (gcm ⁻³)	Weight (g)	Volume cm ³	Mixing time (min)	Remarks
Rubber	100	0.93	28.78	30.9463	00 : 00	$T_i=130^{\circ}\text{C}$
2/3 Silica	53	2	15.2534	7.6267	01 : 00	n=60 rpm
Silane	9.7	0.97	2.7917	2.8780	01 : 00	$t_{mix} = 10 \text{ min}$
1/3 Silica	27	2	7.7706	3.8853	02 : 30	—
ZnO	2.5	5.4	0.7195	0.1332	02 : 30	—
Oil Distillate	20	0.91	5.7560	6.3253	02 : 30	—
Microcrystalline Wax	1.5	0.91	0.4317	0.4744	02 : 30	—
Antioxidant	2	1.1	0.5756	0.5233	02 : 30	—
Stearic Acid	1	0.92	0.4813	0.5232	02 : 30	—
2nd Batch					10 : 00	
Sulfur	1.4	2.07	0.4029	0.1946	01 : 00	$T_i=50^{\circ}\text{C}$
CBS	1.5	1.28	0.4317	0.3373	01 : 00	$n = 50rpm$
DPG	1.5	1.19	0.4317	0.3628	01 : 00	$t_{mix}=5 \text{ min}$
Total	221.1	1.165	62.9132	54	15 : 00	—

Table 5.3: Compound recipe for 80 phr silica filled SBR composite

All rubber compounds (unfilled and filled) are finally vulcanized at 160 °C in a compression molding machine. The pressing time was chosen in accordance with vulcanization times t_{90} determined from dynamic vulcameter measurements [157] and the procedure is discussed in detail in the following section.

5.2 Vulcanization

The characterization of the vulcanization process to obtain the optimum cure time t_{90} was carried out on a moving die rheometer at 160°C with an arc of oscillation of

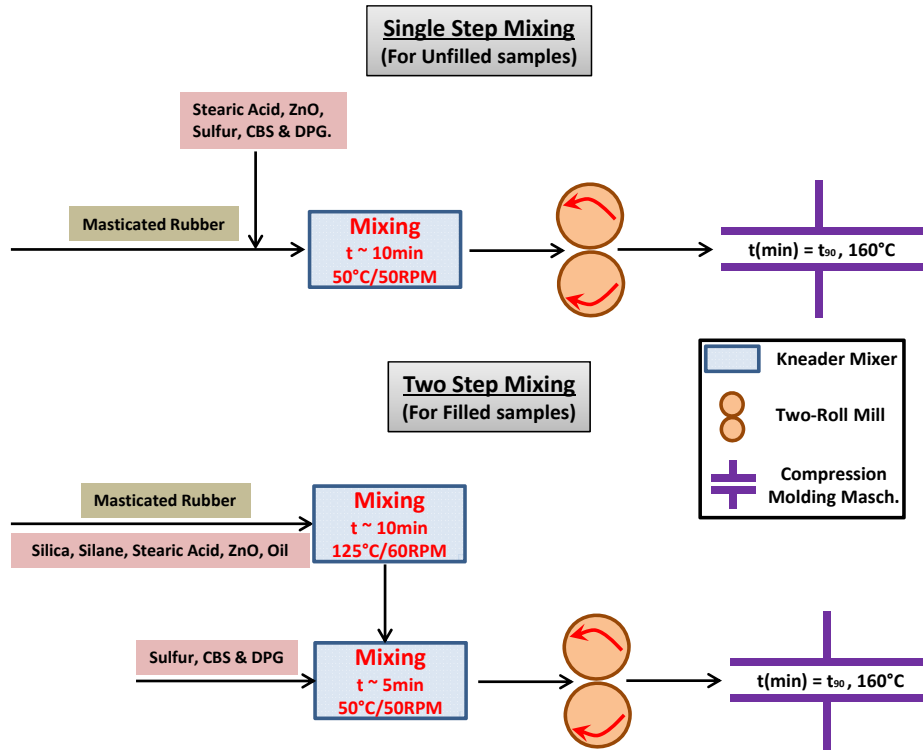


Figure 5.1: Schematic illustration of the mixing procedure for both unfilled (top) and filled (bottom) elastomer samples.

$\pm 0.5^\circ$. For each sample, a small portion was used for the test. After a scorch time, the measured torque increases as vulcanization reaction takes place, and reaches a maximum. t_{90} is the time required to reach 90% of the maximum torque increment and this torque can be evaluated from the following equation [158]:

$$M_{90} = 0.9 (M_H - M_L) + M_L \quad (5.1)$$

where:

M_{90} = 90% of the maximum torque increment

M_H = maximum torque

M_L = minimum torque

t_{90} was then read from the cure curve (see Figure 5.2). This t_{90} time was recorded for each sample and used for the next vulcanization step.

Vulcanization was carried out by compression molding, in which the mixed compounds (stored in the refrigerator for 2-4 days) were molded at 160°C under a pressure of 100 bar to the optimum cure time t_{90} . Afterwards, the vulcanized samples were cooled down with cooling water. Rubber sheets with a size of $(15\text{cm} \times 15\text{cm} \times 2\text{mm})$ were

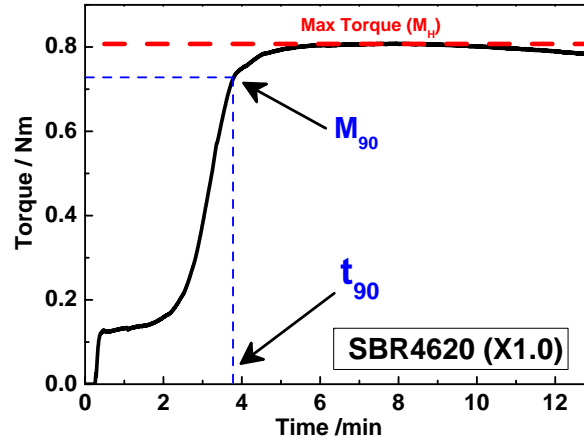


Figure 5.2: Vulcanization isotherm of unfilled SBR (X1.0) where torque is measured as a function of cure time.

obtained.

The sample formulation, mixing and processing were done in collaboration with the group of Prof. H.-J. Radusch. Special thanks to Dr. S. Illisch and Miss M. Keller who prepared the samples.

5.3 Morphological Analysis by TEM

The morphology of the nanocomposites was studied by Transmission electron microscope (TEM). A JSM 2100 transmission electron microscope from JEOL was employed for the investigations, and a voltage of 200 KV was used. Four silica-filled composite, Si20, Si40, Si60 and Si80 were selected for the TEM investigations. Specimens for TEM investigations were prepared by microtome on the frozen samples, with a thickness of approximately 80-100 nm.

In Figure 5.3, representative micrographs for two samples ($\phi_{Si} = 7.5\%$ vol. (top) and $\phi_{Si} = 21.3\%$ vol (bottom)) are shown with two different length scales i.e., large scale images with 1 μm scalebar (on left) and small scale images with 100 nm scalebar (on right). TEM pictures of both the samples show nice structural features with bright-grey contrast represents matrix and the dark-grey spots highlight the fillers. The less magnified TEM image (1 micron scalebar) of 7.5% vol.-sample shows nice homogeneously distributed filler structure. The majority of the filler aggregates are found below 1-micron size. Few micron-sized filler agglomerates are present in the other investigated figures presented in the Appendix. Filler aggregates are found to be spatially distributed in the sample with no connectivity among each other. High

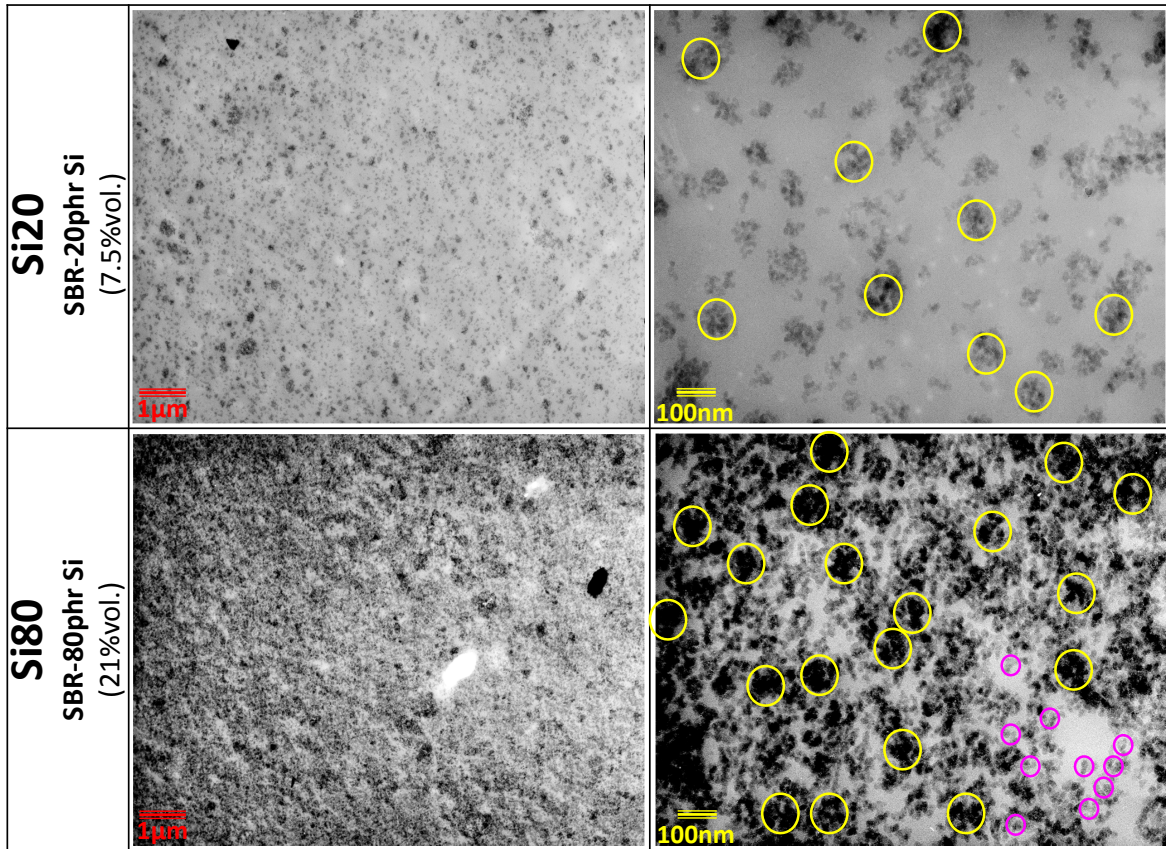


Figure 5.3: TEM pictures of nanocomposite samples: (top) $\phi_{Si} = 7.5\%vol.$ (bottom) $\phi_{Si} = 21.3\%vol.$

magnified image demonstrates the presence of average aggregates size in the range of 50 - 200 nm. Yellow circles have a diameter of 100 nm and these are simply a guide to an eye for the size estimation. The TEM micrographs of 21.3% vol.-samples, on the other hand, show dense structure of filler aggregates. These filler aggregates are connected to each other resulting a significantly less number of voids compare to the 7.5% vol.-sample. Few micron-sized filler agglomerates are visible. However high magnified image reveals that even at high filler fractions, composite contains several 50 - 200 nm size aggregates. This observation indicates that the investigated sample series contain an average aggregate size around 100-200 nm and the size does not change with increasing filler fraction. Moreover this observation is also in accordance with recent literature reported based on SAXS measurements. [159]

Chapter 6

Results

6.1 Filler Reinforcement

Polymer nanocomposites, produced by adding nanofillers to polymer melts, frequently display significantly improved thermomechanical properties relative to the pure polymer. Particularly it is well known that the addition of fillers in rubbers increases the high temperature plateau modulus (G'_p) of the composite materials [92, 94, 95] and hence it enhances the overall reinforcement. Not only that, particulate fillers also influence the overall temperature-dependent mechanical response of composites [34]. This effect can be observed as the decreasing behaviour of the plateau modulus over the whole investigated temperature range. Limited focus has been given to the fundamental physical understanding of such viscoelastic properties of heterogeneous elastomer materials and, the underlying physical basis of temperature-dependent large reinforcement effects due to fillers. In this chapter, we explore the molecular origin of the temperature-dependent mechanical properties and the large reinforcement observed for the SBR composites containing nanosized silica particles.

Shown in Figure 6.1 are G' and G'' as a function of temperature, for silica-filled SBR composite over a loading range from 0 to 80 phr. Temperature sweeps for different silica-filled composites were measured from -75°C to 150°C at 100 rad s^{-1} with a strain amplitude of 0.2%. Initial strain sweeps showed that the given strain amplitude was quite in the linear range. The glass to rubber temperature of the main transition α of the SBR matrix is same for all the samples. The peak position of G'' displays the glass transition of all the samples and it appears around -25°C (see Figure 6.1b). The plateau modulus (G'_p) in Figure 6.1a of the unfilled SBR shows a constant increase with the temperature. This peculiar effect of temperature on G'_p is due to the rubber elasticity

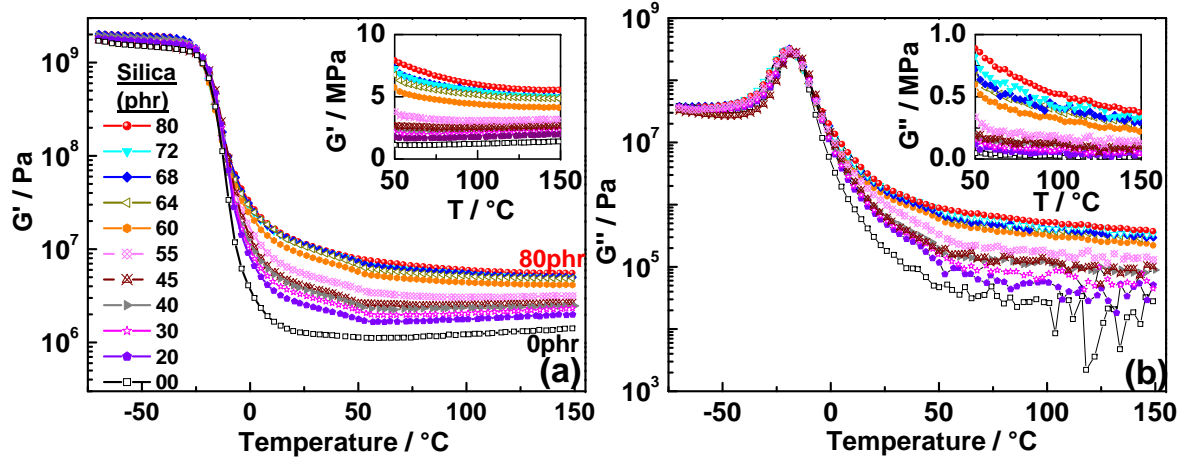


Figure 6.1: Temperature-dependent shear (a) storage and (b) loss modulus of composites filled with 0 to 80 phr silica. Measurements were done at 0.2% strain amplitude and at an angular frequency of 100 rad/s. Insets show a linear representation of G' and G'' in the temperature range 50°C to 150°C.

(details of rubber elasticity can be found in Section 2). Both the storage and the loss moduli increase with filler loading over the whole temperature range. Interestingly the feature of rubber elasticity can still be observed in the filled composites containing fillers up to 55 phr. However the reinforcement suddenly increases for the composites 60 phr or higher (see Figure 6.1a-inset, a linear representation of G'_p). Unlike the composites containing $\text{Si} < 60$ phr, a trend of a decreasing plateau modulus (G'_p) with T is observed for high silica-filled systems ($\text{Si} > 60$ phr). The loss modulus (G''_p) in the plateau range (Figure 6.1b) is affected in the same way as reinforcement by the addition of silica content. G''_p increases with the silica loading and a small jump in loss modulus is seen around 55 phr to 60 phr composite (see Figure 6.1b-inset, a linear scale of G'').

A jump observed in G' and G'' can be explained by assuming the formation of a filler network in 60 phr or higher silica-filled composites. The filler network is a three dimensional percolating path of a solid phase incorporating filler particles which spans over the whole rubber network. Below the formation of a filler network, the dynamics (mechanical response) of the rubber network is dominant in low silica-filled composites and hence those composites show rubber like elasticity from $T > 50^\circ\text{C}$ onwards.

Another interesting feature revealed in Figure 6.1a is the negative slope of G'_p with temperature for the composites having $\text{Si} > 60$ phr. This behavior can be interpreted by assuming a relaxation of the filler network due to the softening of a presumably overlapping glassy layer on the filler particles from $T > 50^\circ\text{C}$. This explanation can also hold for the amplified loss modulus in the plateau range for highly-filled samples as compared to less-filled samples. A constant relaxation of the composites ($\text{Si} > 60$ phr)

leads to a constant amplified dissipation through the complete investigated temperature range.

To understand the relaxation dynamics of the composites and to verify the hypothesis of filler network relaxation based on the existence of a glassy layer, we need to look at the time-dependent response of the composite material at a given temperature.

6.2 Frequency-Dependent Mechanical Response of the Composite

As we have seen earlier that the measurement of the viscoelastic modulus as a function of temperature at a given frequency can be realized on a broad temperature scale. However, the same mechanical characterization carried out at one temperature by varying the frequency scale can practically be applied only from 0.1 to 100 rads^{-1} . The issue of estimating of the high frequency moduli is accessible via the time-temperature superposition principle. For different elastomer systems, this concept works well for unfilled rubbers and allows for the construction of master curves of the complex modulus on a broad frequency scale.

To construct a master curve of the unfilled SBR, frequency sweeps were performed at temperatures from -35°C to 150°C with a given strain amplitude 0.2%, and the respective modulus is plotted against the given frequency window in Figure 6.2.

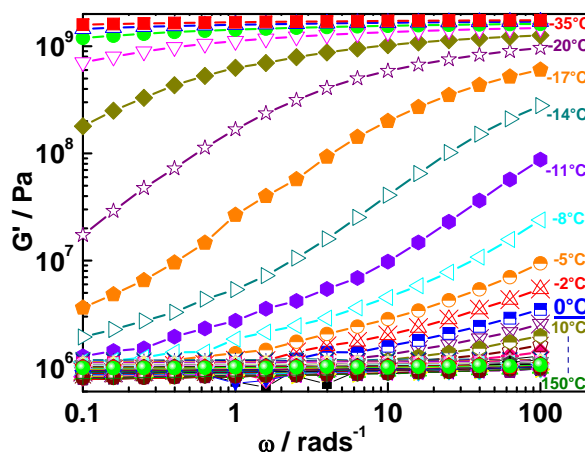


Figure 6.2: Isothermal storage modulus curves of SBR in the region of glass transition to rubber plateau plotted against frequency at temperatures from -35°C to 150°C (as indicated few of them).

To obtain master curves of G' and G'' , the isothermal frequency curves shown in Figure 6.2 were shifted horizontally along the frequency scale with the reference curve of 0°C . The resultant viscoelastic master curves $G^*(\omega)$ are shown in Figure 6.3. The obtained temperature-dependent horizontal shift factors a_T (see inset) behaves like WLF and will be discussed more closely in the following sections.

$G'(\omega)$ in Figure 6.3 as a function of frequency for the unfilled SBR displays only a single relaxation process namely the α relaxation process and the $G''(\omega)$ exhibits a maximum corresponding to this relaxation. A constant elastic plateau modulus sug-

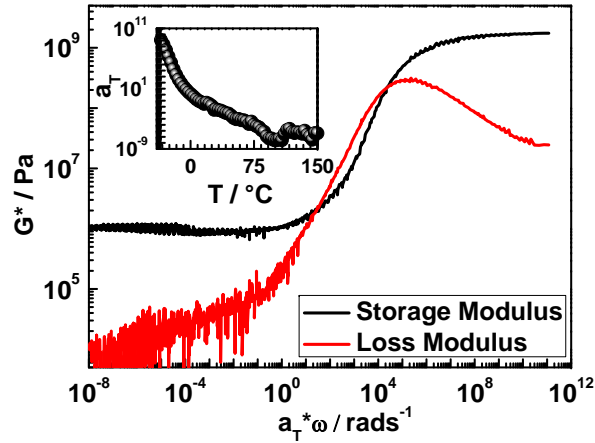


Figure 6.3: Master curves G' (black) and G'' (red) of pure SBR obtained by shifting the data of Figure 6.2 horizontally using the shift factors (as shown in inset), giving the viscoelastic behaviour over an extended frequency scale at reference temperature $T_0 \approx 0^\circ\text{C}$. A dip in a_T appeared around 80°C (in inset) is due to manual switching of the high-range transducer to the low-range transducer.

gests the absence of any other relaxations at frequencies lower than the main relaxation. Ideally an unfilled elastomer having a constant plateau modulus below the frequencies of the α -relaxation step does not display a corresponding loss modulus which appear here in Figure 6.3 as a tail of the α -dissipation peak. The origin of the plateau modulus is the crosslinked rubber matrix which acts as a spring through the whole ω -range of the plateau and hence does not contain any time-dependent element. The loss-tail might appeared due to some network defects in the form of dangling chains or dilated loops etc present in the rubber matrix.

6.2.1 Master Curve Construction of the Filled Composite Following WLF Procedure

As discussed before (Section 2.3), Klüppel [55, 65] shows that a smooth viscoelastic master curve ($G^*(\omega)$) for the carbon black filled composites can be constructed by first shifting the isothermal frequency curves horizontally on the frequency scale and then vertically on the modulus scale. By this method, he assumed that the significant decrease of the storage modulus with increasing temperature is due to the loss of filler-filler bonds or glassy bridges. Hence this model takes into account the changes in the structure of a filler network by vertically shifting of the isotherms. We applied the same method on silica-filled SBR composites to verify the validity of this mastering procedure for both $G'(\omega)$ and $G''(\omega)$ by first shifting the isotherms horizontally on ω -scale and then vertically on G' -scale.

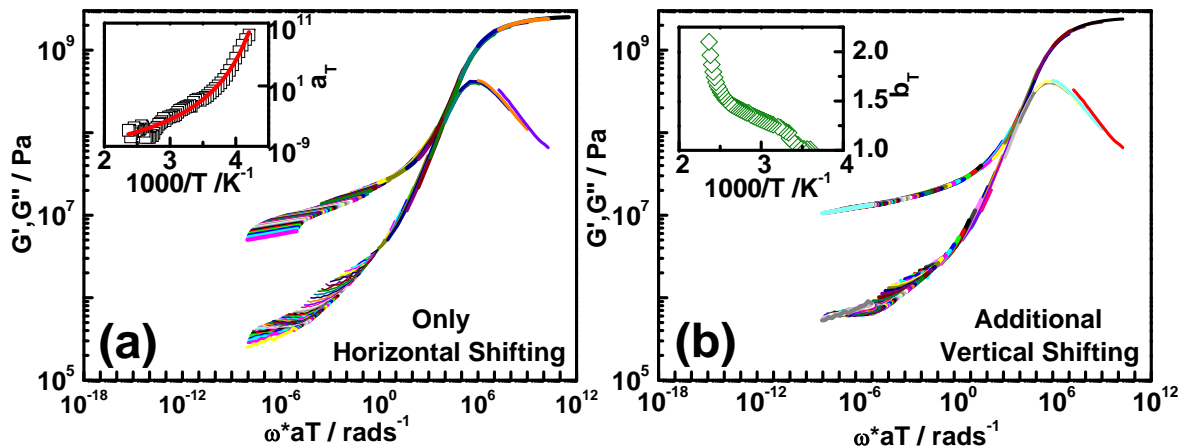


Figure 6.4: (a) Master curves constructed from the isothermal frequency sweeps of 80 phr silica-filled composite by using horizontal shift factors of pure SBR (inset as empty squares). (b) Master curves as in (a) with additional vertical shifts. The vertical shift factors (empty diamonds) are shown in the inset.

Isothermal frequency sweeps of 80 phr ($\phi_{silica}=0.213$) silica-filled composite were measured in the temperature range -35°C to 150°C with a strain amplitude of 0.2% (shown in Figure A.1 in appendix). Figure 6.4a shows the horizontally shifted isothermal frequency sweeps of this silica-filled composite based on the shift factors determined for a pure SBR (see inset Figure 6.4a). The shift factors obtained for pure SBR were fitted with the WLF function (Eq 3.11) with $T_{ref}=0^{\circ}\text{C}$ and the values of C_1 and C_2 are found to be 17.1 and 52.2°C respectively which are typical values for the diene unfilled rubbers [128].

In Figure 6.4a, high frequency isotherms ($\omega_T > 10^0 \text{ rads}^{-1}$) nicely overlap corresponding

to a temperature range of 5°C to -35°C. For the frequencies lower than 10^0 rads^{-1} , isotherms of G' and G'' in the range of 5°C to 150°C do not overlap. This result is a typical behavior for filled elastomers and as recommended earlier that an additional vertical shifts has to be applied to construct a smooth and continuous master curve. The result of this procedure is shown in Figure 6.4b. The nonoverlapping G' isotherms were shifted vertically on the modulus scale with a reference temperature of 5°C and the respective vertical shift factors were recorded accordingly in the inset Figure 6.4b. A similar procedure was applied for the G'' isotherms using the vertical shifts obtained in the previous case. From the plot, we can see that while a smooth master curve can be obtained for $G'(\omega)$, the procedure does not give simultaneously a smooth master curve for $G''(\omega)$.

6.2.2 Master Curve Construction of Nanocomposites for $G^*(\omega)$ With Single Set of Shift Factors

In the previous section we saw that the time-temperature superposition principle does not hold for $G''(\omega)$ even if we use additional vertical shift factors obtained from $G'(\omega)$. Therefore, the Kramers-Kronig relation is not fulfilled and it appears that both components of the dynamic modulus transform to master curves independently. To solve this issue, we propose here a method to construct master curves of $G'(\omega)$ and $G''(\omega)$ with a single set of horizontal shift factors assuming that the filled composite behaves as a relaxing object.

Figure 6.5 shows the master curves for both storage and loss modulus for different degree of silica filling by shifting each frequency isotherm of the composite horizontally along the frequency scale only. The shift factors necessary to obtain a smooth, overlapping master curve are different from shift factors determined for the pure SBR. (cf. Figure 6.6). The shift factors for low-silica composites (Si<60 phr) shown in Figure 6.6 follow the WLF-trend of a pure SBR. However, shift factors obtained from high silica-filled composites (Si>60 phr) show strong deviations from the WLF trend particularly at high temperatures ($T > T_g$). The underlying physical interpretation for such deviations is yet an open question and will be discussed later in this section. However, systematic trends of the plateau region for both $G'(\omega)$ and $G''(\omega)$ with different degree of silica loadings nicely confirm the systematic trends observed in the temperature sweeps (Figure 6.1). The resulting complex shear modulus $G^*(\omega)$ contains an α -relaxation at high frequencies which is basically identical with pure SBR. A constant rubber plateau down to lower frequencies for composites containing less

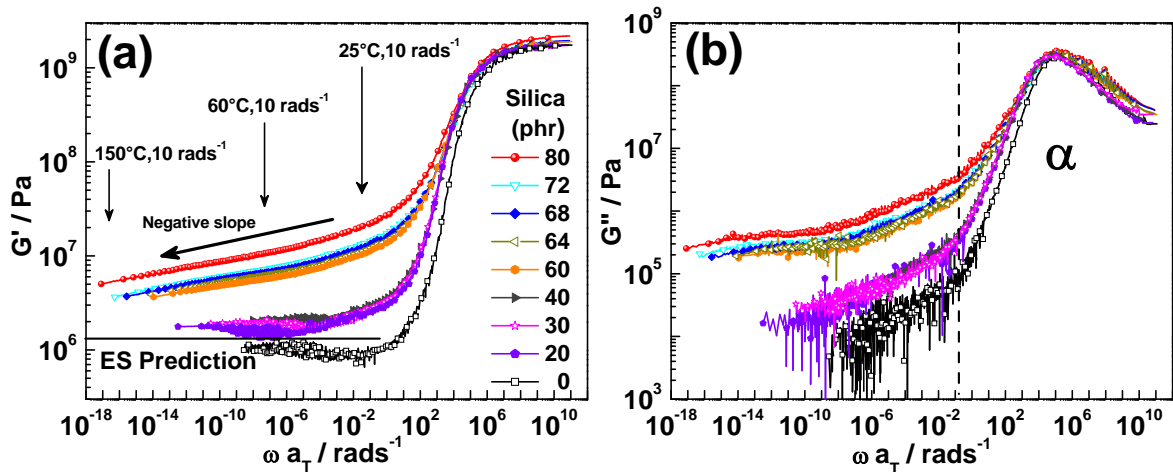


Figure 6.5: Master curves of (a) storage and (b) loss modulus for composites containing different amounts (0 to 80 phr) of silica U7000GR. The original isotherms are only horizontally shifted. The horizontal line represents the maximum limit (for $\phi_{silica} = 0.213$) of Einstein-Smallwood hydrodynamic reinforcement due to fillers. A dissipation regime in the loss modulus at high frequencies is indicated as α peak regime. Reference temperature is 0°C.

than 60 phr silica indicates the absence of any relaxation processes. An abrupt increase in the plateau modulus is found for 60 phr silica-filled composite which we, in the previous section of temperature scans, attributed to the formation of a filler network. For the composites containing filler 60 phr or higher, $G'(\omega)$ increases with ω over the full frequency range indicating relaxations even in the temperature range in which a polymer network shows approximately elastic properties. As this relaxatory behaviour appears only for the composites containing filler 60 phr silica or higher, we concluded that this phenomenon originates from the filler network and for the slow relaxations the modulus is dominated by the filler network contributions. One possible reason for this relaxatory nature of highly-filled nanocomposites is the immobilized polymeric layer associated with fillers/filler aggregates surfaces as suggested by several researchers in literature [28, 34, 54–57]. Upon increasing the temperature, the glassy component over the filler network softens and hence the composite relaxes. Following this interpretation, it is important to note that the filler network has a homogeneous structure through the whole extended frequency range of the master curves, and that the temperature does not change the assembly of the filler network. Up to this point, the whole argument is based on the hypothesis of the formation of a filler network and the immobilized fraction of the matrix associated with the fillers. To characterize the rigid/immobilized fraction, we used a low-field NMR technique and the results will be shown in the next section.

An obvious question which comes to mind is that how the horizontal shift factors, which do not follow WLF, work well for constructing a master curve? In the light of the hypothesis of the formation of the filler network at certain critical filler loading, one can also explain this question and the subsequent unusual behavior of the shift factors of highly filled composite which deviates from the shift factors of the pure polymer at high temperatures.

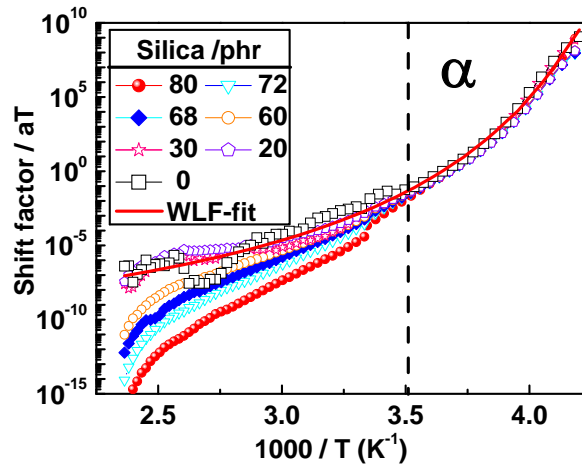


Figure 6.6: Horizontal shift factors a_T as a function of $1/T$ for composites containing different amount of silica U7000GR particles. The reference temperature is 0°C . The dashed line indicates the lower limit of the α relaxation region at $T \approx 10^\circ\text{C}$.

From Figure 6.6 we can see that the low silica-filled composites follow WLF trend (20 phr/30 phr composites). Fitting of the WLF function to the measured curves of unfilled and low silica-filled composites confirms that the dominant contribution to the shift factors is the pure elastomer matrix. Addition of nanofillers (<60 phr) barely affects the Vogel-Fulcher behavior of those composites. On the other hand, shift factors for the high silica-filled SBR composites ($\text{Si} > 60$ phr) follow the WLF trend at low temperatures (up to T_g). However shift factors then deviate from this trend at high temperatures. Figure 6.6 shows a decade difference in the horizontal shifting of the unfilled and 80 phr silica-filled composite at maximum measured temperature. We interpret this deviation due to the dominant dynamics of the interpenetrating hard filler network within the soft elastomer matrix at $T > T_g$. At $T < T_g$, both the unfilled and filled SBR composite are in the glassy state. Therefore the shifting of the isothermal curves for both the systems is same and hence follows the WLF trend. At $T > T_g$, horizontal shifting of the isotherms for composite containing $\text{Si} > 60$ phr is possible due to the fact that the filler network dominates over the elastomer matrix and the shifting procedure no longer follows the WLF of a pure polymer. Systematic trends of $a_T(T)$

observed in Figure 6.6 indicate that further addition of the nanofillers in the composites over $\text{Si} = 60$ phr, horizontal shifting varies accordingly with respect to the strength of the filler network formed.

Another important information obtained from Figure 6.5a is that the reinforcement (G'_p) observed in nanocomposites is nearly a decade higher than the hydrodynamic limit proposed by Einstein and Smallwood (ES) (as indicated by the horizontal line predicting ES limit for $\phi_{max} = 0.213$). To understand the significant reinforcement beyond the hydrodynamic limits, we need to quantify different factors contributing to the reinforcement. For this purpose we use in the later sections the dynamic strain sweep measurements to quantify different contributions to the reinforcement in particular the filler network.

6.3 Evaluation of Immobilized Fractions in Composites

To prove the existence of an immobilized fraction within the given matrix, a proton low-field NMR was used to characterize the polymer chain dynamics of the matrix at different temperatures and different degree of silica fillings. Low-field ^1H NMR, being sensitive to the segmental mobility in polymers, detects the phase composition based on heterogeneities in molecular mobility. In a filled elastomer, the parts of the polymer chains are densely packed and confined onto the filler surfaces due to strong adsorption phenomenon. Considerable effort has been done on defining the role of confinement on the glass transition temperature, T_g , of thin planar polymer films [160, 161]. Primarily two of the experimental observations are now regarded as being universal i.e., (i) T_g is a function of the film thickness, and (ii) the magnitude of the T_g shift depends upon polymer-substrate interactions. An interesting experimental study by Bansal et al. [161] has already established a quantitative equivalence between polymer nanocomposites and thin polymer films indicating the presence of high T_g -rigid/amorphous materials at filler interfaces. In confined spaces between filler particles, the rigid polymer consists of restricted chains mobility which allows only minor orientational changes of the proton spins. Hence, the protons residing within the polymer chains at confined interfaces of the filled composites experience a strong dipolar couplings and influence a free induction decay (FID) of the NMR. The FID shows a rapidly decaying time-domain signal consisting of a short T_2 relaxation time of about 20-30 μs (as shown schematically in Figure 3.4a and b of the Section 3.2). On the other hand, the polymer chains within the bulk elastomer exhibit fast and isotropic mobility, resulting in an averaging of the dipolar couplings on the NMR time scale. The averaging of the dipolar couplings leads to a significantly reduced residual dipolar coupling strength and time-domain signal of the FID decays slowly with a long T_2 time ($T_2 > 30 \mu\text{s}$). Details of this method can found in Section 3.2.

Figure 6.7a shows the NMR results on the unfilled SBR with 80 phr silica-filled composite. Slow decay of the FID signal from the unfilled SBR (open circles-black) corresponds to the response from a mobile component within the matrix. The nonexistence of a fast decaying signal at short time-scales indicate the absence of any immobilized component. Comparing the unfilled with a filled composite (open triangles-blue), a relatively fast decay (see initial 50 μs of the FID signal in inset graph) signal, appearing due to the stronger dipolar couplings, indicates the presence of the immobile fraction within the matrix. However it is not possible to measure a FID for very short

time-scales due to the dead time issue of a NMR receiver. The receiver dead time τ_{rec} of the spectrometer is technically required to ensure the complete decay of the pulse intensity and ranges between 11 μs and 15 μs for the low-field devices. To obtain the entire shape of the FID, a Magic-Sandwich-Echo (MSE) coupled with double quantum (DQ) filter was used. This approach helps us to refocus the fast decay signal from an immobilized fraction and to filter out the remaining slowly decaying signals due to the mobile contributions. The DQ-filtered MSE-FID shows fast decay signals up to 0.0254 ms for the filled composite (closed triangles-blue) and the $\tau_{immobilized}$ was estimated based on 1-component fitting function (Eq 3.24) [28]. This $\tau_{immobilized}$ was later used to obtain the initial shape of the missing FID of the filled system (see Figure 6.7a). The MSE-FID obtained from the unfilled sample (closed circles-black), however does not show any peculiar decay at short time scales indicating the absence of an immobilized component.

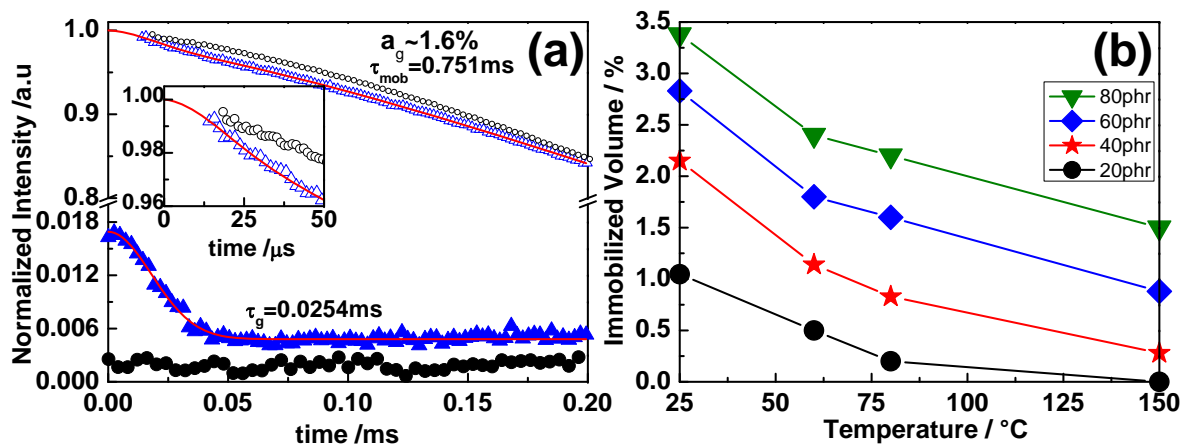


Figure 6.7: (a) FID (open symbols) and DQ-filtered MSE-FID (closed symbols) signals as a function of the acquisition time for the unfilled (circles) and filled (triangles) SBR with 60 phr silica at 80 $^{\circ}\text{C}$. Solid overlapping lines are 1-component Gaussian exponential and 2-components exponential fits of DQ-filtered and FID signals respectively for filled composite based on Eq 3.24 and 3.19. (b) Evolution of immobilized fraction as a function of temperature for 80 phr (triangles), 60 phr (diamonds), 40 phr (stars) and 20 phr (circles) silica-filled SBR.

The result of the above mentioned NMR investigations on different silica-filled composites measured at different temperatures is shown in Figure 6.7b. From the plot, it is evident that the rigid-immobilized fraction of the SBR matrix depends on the filler content and the temperature. At constant temperature, the immobilized component increases with the addition of silica nanoparticles. From this observation, we can safely assume that this immobilized component is associated with the internal surface of the filler particles. Upon increasing the internal surface of the nanofillers, the immobilized

component increases as an overlapping rigid layer around the filler aggregates. An increase in temperature, however, reduces the amount of the immobilized part of the matrix which indicates the softening of the overlapping-immobilized layer around the aggregates. Please note that, as discussed earlier in this section, based on T_2 relaxation times of polymer chains i.e., max. 30 μs , NMR differentiates the immobile and the mobile component of a matrix below and above this timescale. Therefore absence of a certain fraction of the immobile part means that the FID decays slower than 30 μs . Hence this fraction is no longer considered as a rigid component, rather a mobile component like a matrix. From NMR-determined volume fraction of the immobile component for the 80 phr composite, the maximum thickness of an overlapping layer, assuming a continuous rigid layer, was calculated around 2.5 nm. This thickness (d) estimation is based on assuming spherical filler aggregates, each having the average size (R) of 100 nm, distributed homogeneously within the matrix. The glassy layer thickness was estimated according to following calculations

$$\phi_{glassy} = \frac{Volume_{glassy}}{Volume_{glassy} + Volume_{polymer}} \quad (6.1)$$

$$Volume_{glassy} = \frac{4}{3}\pi ((R + d)^3 - R^3) \quad (6.2)$$

Volume of polymer is assumed to be 5 times to the volume of fillers i.e., 20% maximum, R is the average size of the filler aggregates and d is the thickness of the presumable immobilized layer over the filler aggregates.

The size of the aggregates ≈ 100 nm is a realistic estimation based on the findings from TEM images (see Section 3). However the existence of homogeneously distributed spherical aggregates is more an idealistic approach.

Thus NMR detects an apparent minimum fraction of immobilized material with a modulus that is considerably higher than that of matrix. Several authors [45, 54] propose that a rigid/glassy/immobilized layer forms glassy bridge between the filler aggregates. At certain high filler fraction, these glassy bridges (having a glassy modulus 10^9 Pa) act as a glue between the filler aggregates, resulting in a percolating filler network. Therefore, the temperature-dependent high reinforcement, in such models, has been interpreted with the help of these glassy bridges. The NMR results presented above support the hypothesis (stated in Section 6.1 and Section 6.2) that a highly filled elastomeric system acts as a relaxing object, mainly due to the softening of the filler network at high temperatures. However, it is still a question that an immobilized fraction of the matrix forms a continuous layer (or a bridges) over the filler/aggregates

or not?

In the following section, contributing factors, in particular temperature-dependent filler network, to the reinforcement will be studied. The filler network needs to be defined quantitatively to evaluate its contribution to the all overall G'_p . Hence based on the absolute values of the filler network, it is then possible to analyze the temperature and the frequency dependence of the filler network.

6.4 Factors Contributing to Reinforcement

As shown previously in Section 6.2 that a reinforcement, defined as plateau modulus G'_p , increases nearly half of a decade above the ES theoretical limits. Moreover, we found that the long time relaxation (shown as a continuously decreasing rubber plateau with frequency in Figure 6.5) of highly filled composites is due to the presence of a filler network. The following sections deal with the factors contributing to the reinforcement. For this purpose, first it is important to discuss the role of matrix crosslink density of the composites to the reinforcement, the formation of the filler network and the gain in reinforcement $\Delta G'$ due to the filler network.

6.4.1 Quantification of Crosslink Density of Nanocomposites in Absolute Units

The aim of this section is to study the variation in crosslink density of the matrix with the addition of fillers. Furthermore, to what extent the crosslink density of the pure matrix affects the reinforcement of the composite material. Several authors [4, 52, 53] have proposed that the fillers act as additional crosslinkers and hence changes in the crosslink density due to the addition of nano-sized fillers have a considerable influence on the mechanical properties. The crosslink density of a pure-unfilled matrix can be determined by the mechanical response experiments based on the classical theories describing the rubber elasticity. The crosslink density ν can be estimated in absolute units (m^{-3}) from the plateau modulus G_p^0 of the unfilled elastomer systems ($G' \propto T$). Details of this theory can be found in Section 2.1.

$$G_p^0 = \nu kT \quad (6.3)$$

However, the behavior of the G'_p gets complicated in the composite systems as the plateau modulus becomes no longer proportional to the temperature. Hence the classical theories fail in filled composites to calculate the crosslink density. NMR is a technique which is sensitive to the polymer chain dynamics between crosslinks, irrespective to the presence of the fillers inside the matrix, can be used to overcome this problem. Hence a qualitative information can be extracted from the DQ-NMR method to estimate the average crosslink density of the composite system [29]. Although one can estimate the average crosslink density of the composite by NMR, nonetheless, the units of this crosslink density will be in NMR units i.e., kHz. Therefore in this section, for the composites the absolute units of the crosslink density are estimated based on

the combination of mechanical and NMR experiments .

In literature for different vulcanization agents (sulfur/peroxide), it has already been systematically studied by NMR and swelling experiments that the crosslink density is proportionally affected with the additions of the vulcanization agent [30–32]. Hence we used four different pure SBR, as reference samples (without fillers), with different degree of crosslinking to estimate the crosslink densities of the nanocomposites in absolute units. The crosslink densities of the samples were varied based on their sulfur content. The 100% crosslinked sample contains 1.4 phr sulfur (a standard recipe) and, 90%, 110% and 120% samples contain sulfur accordingly (see table 5.1).

Based on the DQ-NMR measurements, crosslink densities (D_{res}) of these reference samples were estimated from the slope of the normalized DQ-buildup curves. Details of this method and the data treatment to obtain the normalized buildup curve (I_{nDQ}) can be found in the Section 3.2 and Section 3.2.2 respectively. The DQ-buildup curve fittings were carried out on four different reference samples by using Eq 3.26 and the results are shown in Figure 6.8. The systematic increase of the slope of the buildup curves show a systematic increase in NMR-determined crosslink densities (D_{res} in kHz-units). This observation indicates the fact that the addition of the sulfur proportionally affects the degree of the vulcanization of the matrix.

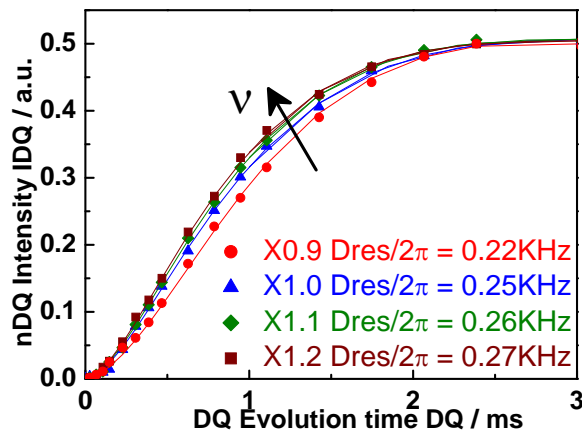


Figure 6.8: Normalized buildup curves (I_{nDQ}) as a function of t_{DQ} . The solid lines are fits based on Eq 3.26 assuming a Gaussian distribution of dipolar couplings.

Figure 6.9a shows the temperature-dependent mechanical response measurements performed on the different crosslinked samples. A systematic increase in the plateau modulus G_p^0 is observed with the relative increase of the sulfur content of the unfilled reference samples. A plateau modulus from 50°C to 150°C of a particular reference sample in Figure 6.9a was linearly fitted using Eq 6.3 with a zero intercept. The slope

of the linear fit contains the information about the crosslink density ν . Therefore one can conclude from the mechanical experiments that the crosslink density of the unfilled reference samples increases linearly with the addition of sulfur.

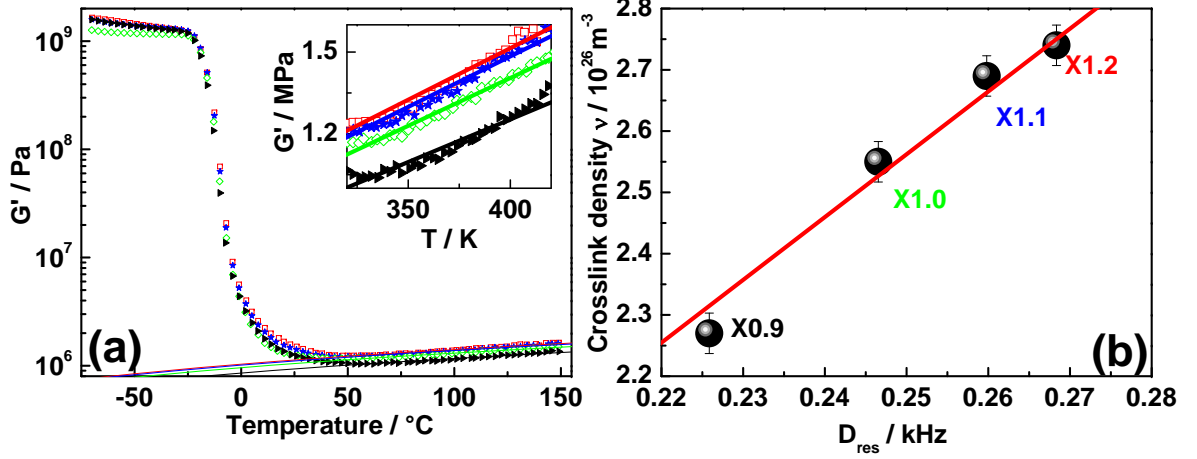


Figure 6.9: (a) Temperature dependence of storage (G') and loss (G'') part of the dynamic modulus of reference samples (unfilled and differently crosslinked). The 100% crosslinked sample (Red open-squares) contains 1.4 phr sulfur (standard recipe) and accordingly 90% (Black full-triangles), 110% (Green open-diamonds) and 120% (Green full-stars) samples are crosslinked with respective sulfur content. The lines are linear fits to the rubber plateau modulus based on Eq.(6.3). (b) Crosslink densities ν obtained by dynamic shear measurements as function of D_{res} from DQ NMR measurements. The red line is a linear fit to the data with zero intercept and the slope is $A_{NMR} = 1.027 \times 10^{27} \text{ m}^{-3}/\text{kHz}$.

The estimated values of the crosslink densities in absolute units (m^{-3}) based on mechanical measurements for four different samples are plotted as a function of NMR determined crosslink densities (D_{res}) in Figure 6.9b. The comparison between the values from both experimental methods shows a linear relationship (Figure 6.9b) having a zero intercept. The emphasis on the zero intercept is important concerning the fact that some entangled chains within the matrix act as physical crosslinks during shearing. These physical crosslinks are also detected by NMR as a restricted chain mobility. Therefore NMR also detects these entangled chains as crosslinks. The slope $A_{NMR} = 1.027 \times 10^{27} \text{ m}^{-3}/\text{kHz}$ obtained from this linear relation allows us to determine the crosslink density of the composite material ν containing the same rubber matrix in absolute units by multiplying the slope with D_{res} measured by DQ-NMR measurements.

$$\nu [\text{m}^{-3}] = A_{NMR} \left[\frac{\text{m}^{-3}}{\text{kHz}} \right] \cdot D_{res} / 2\pi [\text{kHz}] \quad (6.4)$$

This factor A_{NMR} is valid only for the particular Sprintan-4602 SBR samples with a

specific microstructure (21 wt % styrene and 63% vinyl content).

Now to address our basic question that is there any change in crosslink density with the addition of fillers? Figure 6.10 shows NMR determined crosslink densities for the silica filled nanocomposites and the crosslink density ν (in absolute units) was calculated by multiplying the NMR-determined crosslink density D_{res} and the factor A_{NMR} .

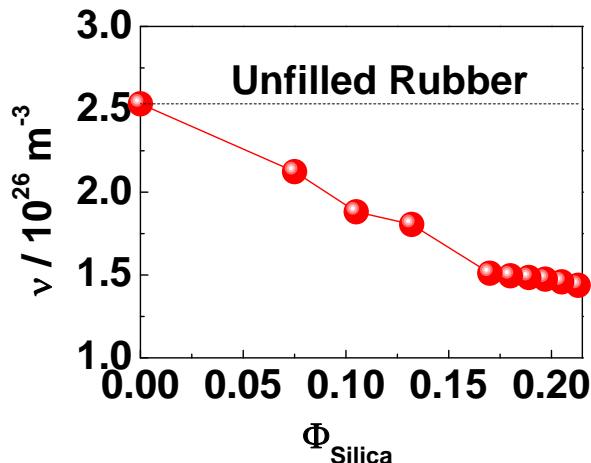


Figure 6.10: Crosslink densities in absolute units as function of silica U7000GR content.

The crosslink density of the rubber matrix depends systematically on the filler content and gradually decreases with increasing silica content. This observation shows that there is indeed a systematic effect of the filler on the average crosslink density of the matrix. However, this trend contradicts the proposed hypothesis of the effect of fillers on the matrix crosslink density. In comparison to the unfilled samples, the crosslink density of a nanocomposite containing 80 phr silica ($\phi \approx 21\%$) particles reduces to 45%. This finding shows that nano-sized filler particles do not act as physical crosslinkers. A possible interpretation of this finding is to assume that the crosslink agent, which is sulfur in our case, is partly deactivated due to its adsorption on large surfaces of the filler particles. Therefore, the deactivated sulfur no longer participates in the vulcanization process.

Comparing the two trends i.e., the filler reinforcement in Figure 6.1a and the average crosslink density in Figure 6.10, we conclude that the reinforcement in the plateau range is governed by the filler content and it is barely affected by the crosslink density of the rubber in the composite.

6.4.2 Filler Network

A standard experimental technique to quantify the contributions to reinforcement, in particular filler network contribution, is a strain sweep. A filler network is a solid percolating path formed by a continuous solid phase incorporating the filler particles in a composite material. Strain sweeps are performed on filled elastomer from small sinusoidal deformations to large deformations. As a result, a step in a real part and a maximum in an imaginary part of the shear modulus are observed for the filled elastomer composites due to breakdown of the filler network. This strain induced softening phenomenon is also known as Payne Effect and the details of this effect can be found in the chapter Section 2.3.

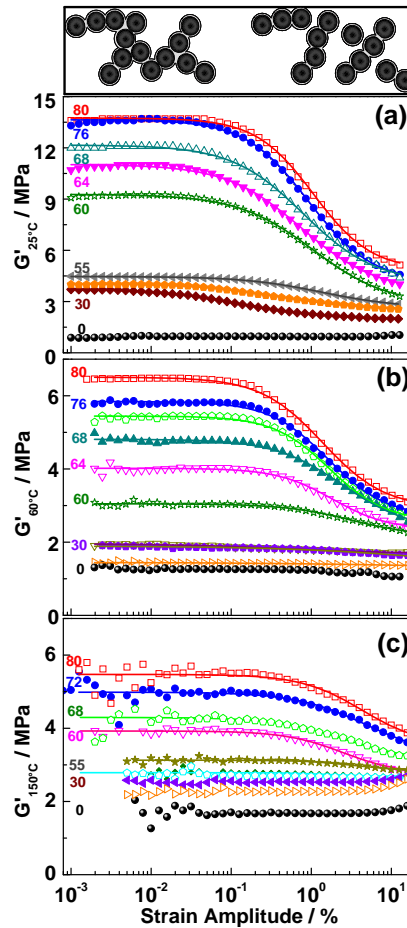


Figure 6.11: Storage modulus G' versus shear strain γ (Payne effect) for composites containing different amounts of silica. Measurements were performed at (a) 25°C, (b) 60°C and (c) 150°C and 10 rad/s. The lines are fits based on the Kraus model (Eq.2.12). Top inserts show sketches of the filler network before ($(\gamma \rightarrow 0)$, left) and after applying large deformations ($(\gamma \rightarrow \infty)$, right).

To see the contribution from a filler network to reinforcement, large sinusoidal

deformations were applied to the given composites and the shear moduli were recorded. Figure 6.11 shows the shear measurements performed at 25°C, 60°C and 150°C with strain amplitudes γ increasing from 0.001% to 20% at a frequency of 10 rads^{-1} . The results for different silica-filled composites show a sigmoidal decrease of storage modulus as a step of G' from low to high strain limits at 25°C. The strain sweeps measured at 60°C or higher temperatures for different silica-filled composites also show this feature but the magnitude of $G'(\gamma \rightarrow 0)$ is reduced compared to 25°C. This finding is in accordance with the temperature sweeps shown in Figure 6.1 where we discussed that the decreasing trend of $G'(T)$ is due to the relaxation of a filler network. From the Figure 6.11a, significant sigmoidal steps in $G'_{25^\circ\text{C}}$ appear in the composites containing fillers from 80 phr down to 60 phr. However this step is less pronounced for the composites containing fillers <60phr. Although, $G'_{60^\circ\text{C}}(\gamma)$ and $G'_{150^\circ\text{C}}(\gamma)$ show the decreasing step for 60phr or higher silica-filled composites, this feature is not observed at lower filled composites (<60 phr).

The phenomena of sigmoidal decrease of G' is interpreted due to the break down of the filler network after subjecting the composite under large amplitude deformations $\gamma > 1\%$ (cf. sketches shown as insets in Figure 6.11). The pure rubber without fillers, on the other hand, does not exhibit such phenomena as seen in strain sweeps (0 phr-black circles in Figure 6.11). Even, the composites filled up to 55 phr do not contain filler network due to the fact that they do not show a sigmoidal step in $G'(\gamma)$ (exception is found at 25°C and this finding will later discuss as a breakdown of aggregates containing occluded rubber but no filler network).

For a qualitative analysis of this strain-induced softening of the filled rubber, a Kraus model was used to obtain the absolute values of the G' at low ($\gamma \rightarrow 0$) and high strain ($\gamma \rightarrow \infty$) limits. The solid lines over each measured data in Figure 6.11a,b,c are the fits based on the Kraus model (Eq 2.12), details of which is mentioned already in the Section 2.3.

Kraus parameters at different temperatures are shown in Figure 6.12. The analysis in Figure 6.12 is based on two parameters extracted from the model: G'_∞ , which shows the absolute modulus values at $\gamma \rightarrow \infty$ and G'_0 , which is the sum of $\Delta G'$ and G'_∞ and regarded as $G'(\gamma \rightarrow 0)$. Comparing values for the storage modulus G'_0 , G'_∞ and theoretical predictions of Einstein-Smallwood (ES) (Eq 6.5) in Figure 6.12, one can conclude that hydrodynamic contributions of the nanosized silica particles alone are small at all temperatures and shear deformations.

$$G'_{ES} = G'_{matrix} (1 + 2.5\phi_{filler}) \quad (6.5)$$

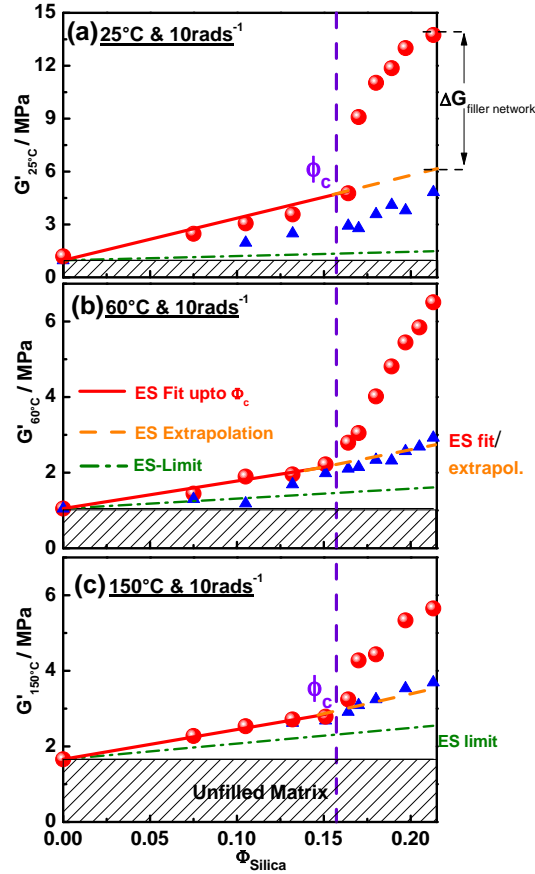


Figure 6.12: Analysis of nonlinear mechanical measurements (strain sweeps) as shown in the Figure 6.11 ($\omega = 10\text{rads}^{-1}$). Storage moduli at strain amplitude $\gamma \rightarrow 0$ (red circles) and $\gamma \rightarrow \infty$ (blue triangles) for different silica filled nanocomposites at (a) 25 °C, (b) 60 °C and (c) 150 °C. Thick-solid line (red), dash line (orange) and the dash-dotted line (green) represent the Einstein-Smallwood (ES) fit up to ϕ_c (over red circles), the extrapolation of ES fit to $\phi_{maximum}$ (extension of red line) and the prediction of Einstein-Smallwood model based on unfilled rubber respectively. The diagonal hatch illustrates the limit of unfilled SBR plateau modulus.

At constant temperature and frequency in Figure 6.12, G'_0 (red circles) increases linearly with the addition of filler up to a critical fraction $\phi_c \approx 0.155$. A change in slope is observed for large ϕ indicating the formation of a percolating filler network (as shown schematically in Figure 6.13) and ϕ_c is regarded as the percolation threshold.

Note that the percolation threshold is found to be independent of the temperature. It is schematically illustrated as a vertical dashed line in Figure 6.12. This observation gives a strong indication that the temperature has primarily no effect on the formation of the filler network. At certain filler fraction (ϕ_c), silica fillers due to strong filler-filler interaction form a filler network and no temperature-dependent medium (glassy/immobilized material) is necessary to aid the formation of the filler network.

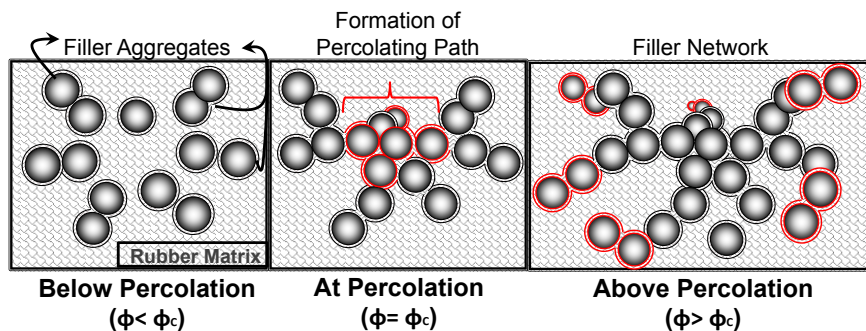


Figure 6.13: Schematic illustration of filler network formation. Additional filler aggregates at each of ϕ are encircled in red.

Hence, one can conclude that even during the linear-response measurements for high-filled composites, the structure of a percolating filler network within the matrix does not change with temperature. With increasing temperature, G'_0 is significantly reduced due to the relaxatory material properties of the SBR nanocomposite containing filler network (as discussed previously in Section 6.2). So from where does this filler network relaxation comes from? The answer of this question will be discussed in Section 6.5, once the filler network will be quantified in absolute values.

The modulus at high strain limit G'_∞ (blue triangles) in Figure 6.12 contains no contribution from the filler network as it breaks down under large deformations. At each temperature in Figure 6.12, G'_∞ increases linearly with the whole given range of filler fractions and the slope remains unchanged. The values of G'_∞ measured at 25°C and 60°C are significantly above the hydrodynamic limit as predicted by ES-relation (Eq 6.5) when considering $\phi_{filler} = \phi_{silica}$. Notably, the 150°C data can be fitted in this way when adding the Guth-Gold second-order term i.e., $14.1\phi_{silica}^2$. However this factor is still controversial and debatable and reported to be too high.

To quantify the gain in modulus due to the formation of a filler network, a specific ΔG needs to be defined which contains the information only about the filler network at small mechanical deformations. In the data set of the G'_0 (red circles) of each temperature in Figure 6.12, the ES-relation was used to fit the range from $\phi = 0$ to ϕ_c using $\phi_{eff} = f \cdot \phi_{silica}$. The factor f attributes to the model inadequacies and it is here interpreted as the experimental quantification factor for the occluded rubber at small strain limits. Typical values of the factor f is found to be 6 at 25°C, 3 at 60°C and 1.8 at 150°C. Based on the information from ϕ_{eff} , the ES-fit is extrapolated to the maximum of $\phi_{silica} \approx 0.213$. Finally the filler network contribution ($\Delta G_{filler\ network}$) to the modulus is determined at these given T and ω as the difference between the measured G'_0 and

ES extrapolation to above ϕ_c . Hence, by using the information from linear and nonlinear dynamic mechanical measurements, the filler network $\Delta G_{filler\ network}$ contribution to the reinforcement is quantified.

$$\Delta G_{filler\ network} = G'_0 - G'_{ES\ fit/extrapol} \quad (6.6)$$

From the analysis above, it is concluded from the linear-response measurements that the total reinforcement of filled composite consists of a hydrodynamic contribution h_0 and a filler network contribution ($\Delta G_{filler\ network}$). The hydrodynamic contribution (h_0) is a multiplicative factor to the unfilled modulus G_{matrix} . While the filler network contributes as an additive term to the overall modulus of the filler elastomer.

$$G'_0 = h_0 \cdot G_{matrix} + \Delta G_{filler\ network} \quad (6.7)$$

Concerning the large-scale deformation of the filled composite with an assumption that the filler network is completely destroyed and additionally there is no Payne effect for the pure matrix, the modulus at infinite strain limit (G_∞) of the composite can be written as:

$$G'_\infty = h_\infty \cdot G_{matrix} \quad (6.8)$$

where h_∞ is a potentially modified hydrodynamic factor that takes into account the amount of remaining filler aggregates. Broken filler aggregates comprise the effective filler fraction (ϕ_{eff}) which is associated with ‘‘occluded rubber’’ and which will be discussed in the next section.

6.4.3 Occluded Rubber

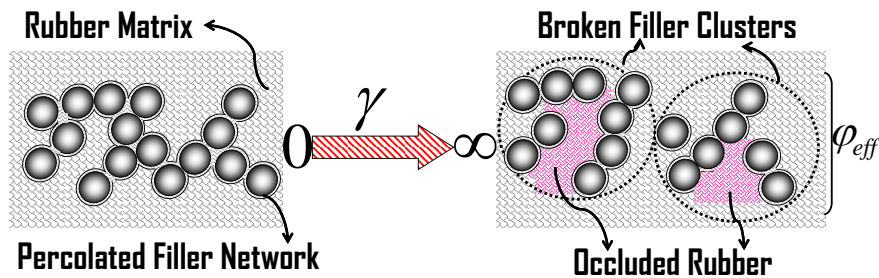


Figure 6.14: Schematic illustration of occluded rubber within the cavities of the broken filler aggregates.

In the previous section, we observed that the values G'_{∞} measured at 25 °C and 60 °C in Figure 6.12 are significantly above the hydrodynamic limit as predicted by the Einstein-Smallwood [96,97] even if the filler network is practically destroyed. The extra reinforcement ($G'_{\infty} - G'_{ES}$) at given temperature depends on the silica content as it increases linearly with the filler fraction. This observation indicates that at low temperatures there are additional contributions to the reinforcement, other than the filler network. In the previous section, we quantified the hydrodynamic contribution to the modulus (from $\phi=0$ to $\phi=\phi_c$) at low strain limits by assuming the ES-model as an approximate hydrodynamic approach. For G'_{∞} , we used the similar approach to estimate the ϕ_{eff} . The typical values for the factor f indicates that the volume fraction of the solid material ϕ_{solid} should be 5.5, 2.8 and 2 times higher than the original filler content ϕ_{silica} at 25 °C, 60 °C and 150 °C respectively in order to explain the obtained G'_{∞} values. It seems to be unrealistic to assume that the observed G'_{∞} values can be explained either by simple hydrodynamic effects of the filler particles or by filler particles plus additional immobilized layer alone. Additionally, the rigid/immobilized fraction is found only on the order of few percent of the polymer fraction at each temperature (see Figure 6.7b).

Additional hydrodynamic effects which are related to the presence of larger filler aggregates existing also for large strains ($\gamma \gg \gamma_c$) where filler network is destroyed, are obviously important. From hydrodynamic point of view, these remaining aggregates, after the breakdown of the filler network, act like bigger objects containing “occluded” rubber which is shielded from the shear flow. The whole assembly of aggregates and the occluded rubber shielded within the cavities of aggregates, as shown schematically in Figure 6.14, hence, leads to an effectively larger filler fraction and resulting in a stronger reinforcement. At high temperatures, the aggregates containing occluded rubber are

soft enough to move with the applied stress field and hence the reinforcement decreases.

6.5 Viscoelasticity of Filler Network

So far, we have found that the composites containing the filler network display relaxatory nature and the elastic moduli of those composites, either obtained from linear response temperature sweep or frequency sweep measurements, decrease with increasing temperature and decreasing frequency (see Figure 6.1 in Section 6.1 and Figure 6.5 in Section 6.2 respectively). Based on this observation, in previous sections we hypothesized that the relaxatory behaviour of the composite originates from the softening of the immobilized layer confined to the filler surfaces of the network. The $\Delta G_{filler\ network}$ of highly filled composites, which is defined in the previous section as the modulus of the filler network, must show viscoelasticity and depends on T and ω . To obtain the $\Delta G_{filler\ network}$, linear response temperature sweep measurements were performed at different frequencies for different silica filled composites containing $\phi_{silica} > \phi_c$. As an example Figure 6.15a shows $G'(T)$ for only 80 phr silica-filled composite measured at 1 rads^{-1} , 10 rads^{-1} and 100 rads^{-1} frequencies. At same frequencies, Figure 6.15b shows $G'(\phi_{silica})$ plotted for different degree of fillings at 25°C. Noteably, the less-filled composites ($\phi_{silica} < \phi_c$) do not show the ω dependence, allowing a linear ES-fit in the range of $\phi_{silica} = 0 - \phi_c$. Upon extrapolating the ES-fit to ϕ_{max} i.e., 0.213, the absolute values of the $\Delta G_{filler\ network}$ were determined at each isochrone as a difference between measured G'_0 and the ES-extrapolation.

The central result of the analysis mentioned above, is plotted in Figure 6.16a. The frequency- and temperature-dependent response of the filler network in terms of $\Delta G_{filler\ network}$ of the highest-filled sample is shown as a function of temperature for different frequencies ω . Significant dependence of the filler network reinforcement ($\Delta G_{filler\ network}$) on frequency is observed at each temperature. The observation that $\Delta G_{filler\ network}$ decreases monotonically with temperature as well as frequency is in support of the relaxatory, viscoelastic nature of the filler network.

An attempt is also made to establish a connection between the mechanical properties with the results obtained by the NMR measurements of the immobilized fraction of the matrix. Figure 6.16b shows a correlation of $\Delta G_{filler\ network}$ with NMR-determined rigid fraction (%) for different frequencies and temperatures for $\phi_{silica} > \phi_c$. It is observed that the ΔG as a function of immobilized volume (%) from samples with different ϕ_{silica} measured at different temperatures follow nearly the same nonlinear trend for all frequencies as compared to the Figure 6.16a. In other words, we can deduce an

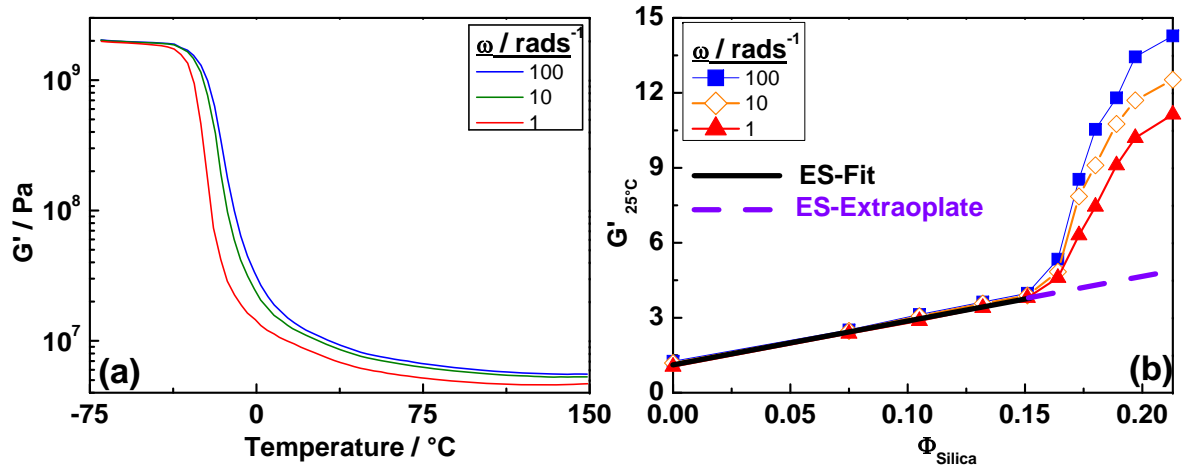


Figure 6.15: (a) Storage modulus of 80phr silica-filled composite as a function of temperature for 100 rads^{-1} (blue), 10 rads^{-1} (green) and 1 rads^{-1} (red) (b) Comparison of storage moduli as a function different silica loadings measured at 25°C and at 100 rads^{-1} (closed-squares), 10 rads^{-1} (open-diamonds) and 1 rads^{-1} (closed-triangles). Thick-solid line (black) is the ES fit up to ϕ_c and thick-dashed line (violet) is further the extrapolation up to $\phi \approx 0.213$.

apparent rigid fraction-temperature superposition property of $\Delta G(\phi_{\text{rig}}(T), T)$. This means that the filler network reinforcement is governed by two vital parameters. 1) Temperature, as $\Delta G_{\text{filler network}}$ decreases with increasing T and 2) the rigid fraction ϕ_{rig} , as $\Delta G_{\text{filler network}}$ increases with the increase of ϕ_{rig} due to the addition of solid/rigid component ($\phi_{\text{silica}} + \phi_{\text{immobilized}}$) inside the matrix.

Based on the experimental observations, the relaxatory behaviour of the highly filled ($\phi_{\text{silica}} > \phi_c$) composites was assumed to be originated from the softening of the immobilized polymer associated to the filler network. As suggested by many researchers in literature [54, 55] in the model systems, the strong reinforcement of the filler network is a result of “glassy bridges” formed within the percolating path of the filler particles/aggregates due to the presence of rigid/glassy layer on filler surfaces. Thus, the reinforcement increases with decreasing temperature due to the formation of thicker glassy layer. If this would be the case, then this phenomenon, however, should lead to a reduced percolation threshold at lower temperatures, where the aggregates (plus the thicker glassy layer) are effectively larger. Hence, they percolate at small filler fractions. However, our experimental results shows that the percolation threshold of the filler network does not change with temperature. The temperature-independent percolation behavior of the filler network strongly indicates that the “glassy bridges” are not directly responsible for the formation of the filler network. NMR investigations, however, revealed the presence of small fractions of immobilized components within a

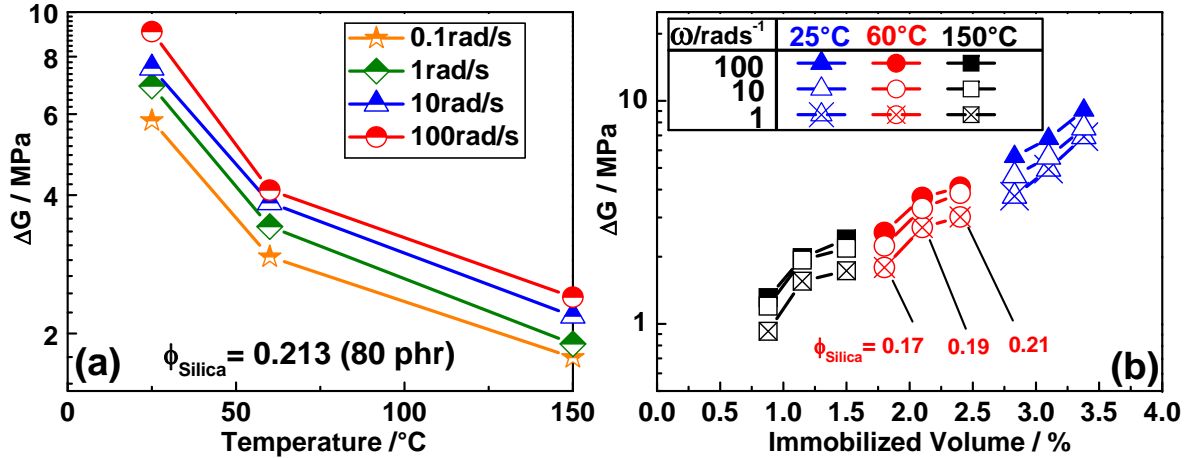


Figure 6.16: (a) Strength of filler network ΔG for 80phr composite as a function of temperature at different frequencies. (b) Immobilized volume dependence of filler network strength (ΔG) shown at three different frequencies 1rad/s^{-1} (crossed symbols), 10rad/s^{-1} (open symbols) and 100rad/s^{-1} (closed symbols) and at three different temperatures 25°C (triangles), 60°C (circles) and 150°C (squares).

composite (max. 3.5% of the matrix). Hence in this thesis, it is suggested that the fractions of rigid/immobilized polymer ($G' \approx 10^9$ Pa) is located in the highly confined regions of the filler network as shown schematically in Figure 6.17. This argument is well supported by the finite-element simulation work of Gusev [61, 123]. According to his simulation, only minute amounts of increased-Tg material (down to the permille level) located between filler particles can explain the enhanced storage modulus and the additional dissipation in filled elastomers. The immobilized polymer may or may not form the contiguous layer over the filler network, it is still an open question.

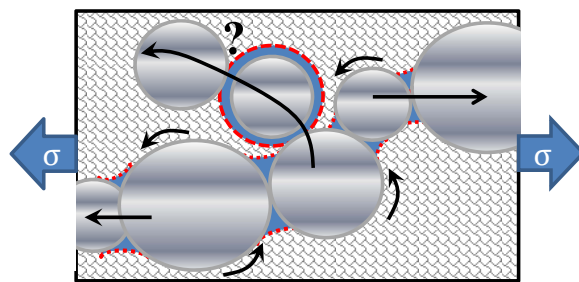


Figure 6.17: Schematic illustration of the complex deformation modes in the percolating filler aggregates containing immobilized fractions in highly confined regions.

The sketch in Figure 6.17 highlights the complex deformation modes of the percolated filler network, and provides a fundamental ground for the temperature-independent percolation threshold. Due to the strong filler-filler interaction in silica particles, the

filler network is formed at a certain critical filler fraction (ϕ_c) during the mixing process of fillers in an elastomer. The strong adsorption of the polymer in the highly confined regions of filler network results in the immobilization of the polymer. During the mechanical deformations, the confined immobilized polymer in the cavities of the filler network dominates the bending modes of the filler network. It has already been established that the elastic properties in the random percolating system is dominated by the bending modes of the filaments due to soft and rigid portions of the system [162]. Therefore, in case of near-spherical filler particles, the small amplitude shearing of the filler network causes the bending or dilating of the filler network possibly via the immobilized fractions in the interparticle gaps. At lower temperatures, network experiences a high bending rigidity of the viscoelastic filler-filler connections due to relatively high amount of rigid material in the cavities and thus an overall higher ΔG is observed.

6.6 Parameters Influencing Energy Dissipation in Filled Rubbers

According to Kramers-Kronig relation, real part of the modulus (G') is connected to the imaginary part (G'') of the complex function G^* provided that the measurement is performed under linear regime. Therefore in a linear response dynamic mechanical experiments if there is a relaxation in the form of a step in $G'(T)$ curve, there must be a dissipation peak in $G''(T)$.

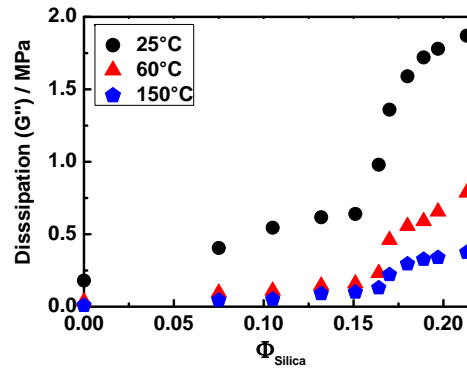


Figure 6.18: Loss modulus G'' at 25°C (circles), 60°C (triangles) and 150°C (pentagones) for composites containing different amounts of silica measured at 0.2% amplitude and 100 rads^{-1} angular frequency from linear response measurements.

Figure 6.18 shows the values of the loss modulus G'' obtained from the linear response measurements for the composites with different degree of silica fractions measured at 25°C, 60°C and 150°C. At a given temperature, loss modulus G'' increases strongly with increasing filler particles. A comparison of the data in Figure 6.18 with Figure 6.12 shows that G'' depends in a similar way on the filler fraction as the corresponding storage modulus G' . With increasing filler fraction, a change in slope of G'' is also observed around ϕ_c at each temperature indicating that the formation of a filler network strongly amplifies the loss modulus.

Similar behavior of loss modulus G'' was observed when the composites were subjected to large sinusoidal deformations. Figure 6.19 shows the Payne effect measurements for the loss modulus. At large deformations and given temperatures, G'' shows a similar significant decrease as compared to G' (shown in Figure 6.11).

At critical strain amplitude ($\gamma_c > 1\%$), the loss modulus of high silica-filled SBR composites exhibits a pronounced peak indicating an elevated dissipation of the applied energy due to the breaking process of the filler network. Once the filler network is broken down, the G'' values reduces significantly as compared to the values observed

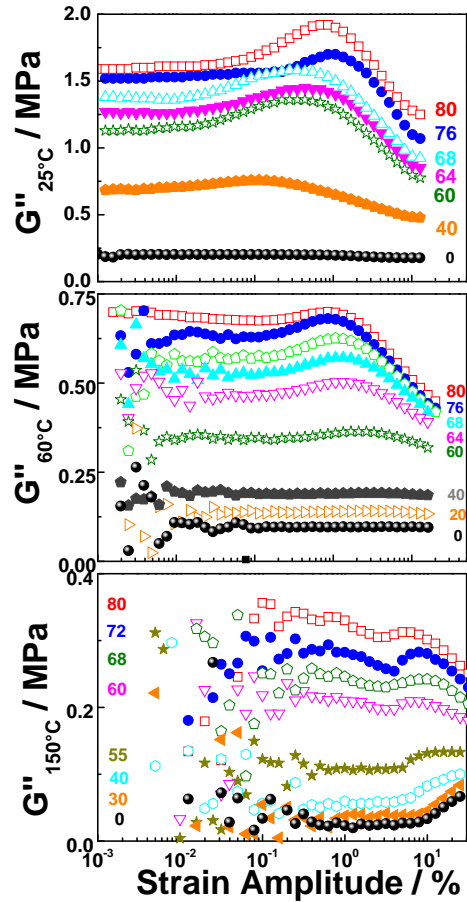


Figure 6.19: Loss modulus G'' versus shear strain γ (Payne effect) for composites containing different amount of silica. Measurements are performed at (a) 25°C, (b) 60°C and (c) 150°C and 10 rad/s. Note: the increasing values of G'' at 150°C and high amplitudes for samples 0 to 55 phr are purely instrumental effect, appeared due to softening of the samples.

at small deformations. Interestingly, a similar systematic trend of high deformation loss modulus G''_{∞} is observed with the addition of fillers as well as with the temperature as compared to the trends observed for G'_{∞} (c.f. Figure 6.11).

Comparison of Loss Factor and Loss Modulus

In the previous chapter 4, on the basis of the literature review it was concluded that the $\tan \delta$ might be a misleading parameter for the characterization of loss/dissipation during the wet skid and the rolling resistance. Additionally based on the studies of Robertson et al., G'' appeared to be an appropriate loss quantity in terms of analyzing the glass transition temperature of the rubber matrix which is not affected by addition of fillers. The values of the $\tan \delta$ peak and/or even glass-rubber transition region, which is the important temperature region for the wet skid resistance, are influenced

not only by local segmental motions, as shown in the loss modulus (G'') towards lower T, but also by filler reinforcement effects on both the storage modulus (G') and G'' at higher T. Similar results were obtained in this thesis (see Figure 6.1). Therefore to see the validity of this argument in silica filled composites, $\tan \delta$ vs temperature obtained from dynamic shear experiments is plotted below in Figure 6.20a.

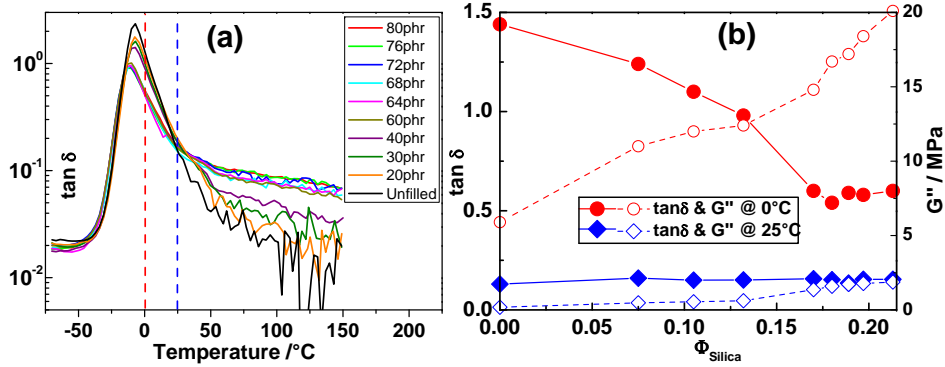


Figure 6.20: (a) $\tan \delta$ as a function of temperature of composites filled with 0 to 80 phr silica. Measurements were done at 0.2% strain amplitude and at an angular frequency of 100 rad/s. (b) Comparison between $\tan \delta$ (full symbols) and G'' (open symbols) as a function filler fraction at 0 $^{\circ}\text{C}$ (circles) and 25 $^{\circ}\text{C}$ (diamonds).

Figure 6.20a shows that the high temperature plateau region of the $\tan \delta$, which is the important region for the optimization of the rolling resistance of the tire, increases systematically with the addition of filler. However, this is not the case in the temperature range of 0 $^{\circ}\text{C}$ to 25 $^{\circ}\text{C}$ which has a considerable importance concerning the wet skid resistance of the tire. In order to compare both of the viscoelastic loss parameters i.e., $\tan \delta$ and G'' , a comparison is done in Figure 6.20b at 0 $^{\circ}\text{C}$ to 25 $^{\circ}\text{C}$. At 0 $^{\circ}\text{C}$, the $\tan \delta$ and G'' show opposite trends with increasing filler fraction. G'' systematically increases with the filler addition which is the expected behavior of the dissipation in case of addition of the fillers. However, $\tan \delta$ decreases with the filler loading upto ϕ_c (0.156) and then it remains nearly constant for the loading above ϕ_c . At 25 $^{\circ}\text{C}$, it is observed that the values of the $\tan \delta$ approximately remain unchanged over the whole range of filling. While G'' systematically increases with the addition of silica.

It is evident from the observations above, that the loss modulus G'' is related to the storage modulus G' not only in the linear range of small deformations (G'_0, G''_0) but also in the nonlinear range of large deformations (G'_∞, G''_∞). Therefore, if the behaviour of loss needs to be monitored in the tread rubber by varying the filler content, G'' gives the most systematic results as compared to the $\tan \delta$ particularly in the low temperature zone.

Chapter 7

Conclusion

In this work, solution polymerized Styrene Butadiene rubber (S-SBR) vulcanizates filled with different amounts of silica nanoparticles with high specific surface are studied. To study the temperature- (T) and frequency-dependent (ω) mechanical response of the composites, the dynamic mechanical analysis (DMA) were used to quantify and to understand different factors contributing to the reinforcement (defined here as plateau storage modulus G'_p). DQ-NMR approach was used to study the network topology with and without the presence of fillers. Additionally magic-sandwich-echo (MSE)-sequence of the low-field NMR was used to quantify the confined rigid-immobilized components of the matrix.

The temperature-dependent mechanical properties of the composites filled with different amounts of silica nanoparticles show that the plateau storage modulus (G'_p) increases systematically with the fillers. The filler-induced reinforcement (G'_p) is strongly increased over the silica loadings of 60 phr ($\phi_{silica}=0.156$). This notable increase in G'_p is, assumed at this point, appeared due to a filler network formed at such high filler loadings. The softening of the composites (>60 phr) are observed at high temperatures based on the observations of T-dependent decreasing modulus of those composites. Similarly the loss modulus (G''_p) also systematically increases with the addition of the fillers. Furthermore, similar to the observation for G'_p for high silica-filled samples, the G''_p also decreases with increasing temperature.

In order to obtain the wide-range ω -dependent shear modulus for the composites, isothermal frequency curves of shear modulus (limited ω -range 0.1-100 rads^{-1}) were obtained from DMA at different temperatures. The master curve of unfilled SBR, which fulfills time-temperature superposition principle (TTS), was constructed over the wide frequency range by using WLF-horizontal shift factors. It is further demonstrated that

by using the shift factors of the pure SBR, a master curve of high silica-filled composite cannot be constructed which is an expected result as already discussed in literature. Additional vertical shift factors are used, according to the procedures mentioned in literature [55,56], to create master curve of G' . However these vertical shift factors do not master a simultaneous curve for G'' . For the first time, it is shown in this thesis that the master curve of the composites containing silica > 60 phr can be constructed using single set of horizontal shift factors. Such master curves are constructed by horizontal shifting of each isotherm and the corresponding shift factor is recorded separately. The apparent-single set of shift factors obtained for the filled composites follow WLF-behavior for the composites filled with silica < 60 phr. However the shift factors obtained for the composites with high amount of silica (>60 phr) deviate from the WLF-trend at high temperatures ($T > T_g$). Systematic trends of the shift factors obtained from the addition of fillers (over 60 phr) support the idea of the presence of filler network whose relaxation dynamics is dominant over the rubber network at such high filler loadings. The master curves of G' obtained for high silica-filled composites show the presence of low frequency relaxations which is indicated as a negative slope of G'_p vs ω . Due to the fact that this feature is not seen in the low silica-filled composite, hence the negative slope of G'_p at high filler loadings is interpreted due to relaxation of the filler network.

The T- and ω -dependent mechanical results show the high-temperature softening and low-frequency relaxation of the G'_p respectively at high filler loadings. From these results, the presence of a rigid-immobilized fraction of the soft polymer matrix was assumed which has modulus that is considerably higher than the matrix and presumably this fraction is associated with the filler network. To confirm the presence of the immobilized component of the matrix, a low-field NMR was used with a particular MSE-sequence to detect an apparent minimum fraction of an immobilized material (a_{rig}) of the matrix. The a_{rig} for a given filler loading decreases significantly with temperature. This result explains the softening and the relaxation of G'_p in high silica filled composites. At constant temperature, a_{rig} increases with the addition of silica fillers. This result indicates that the immobilized-rigid component of the matrix is associated with the filler surface.

A different NMR technique was used to study the effect of fillers on the crosslink density of the filled composites. The DQ-NMR spectroscopy measurements on unfilled rubbers with variable content of crosslink agent and crosslink density allow, in combination with shear measurements on these samples, to determine the crosslink density ν of rubbers in *absolute units*. According to classical theories describing rubber elas-

ticity, the crosslink density ν was estimated from the plateau modulus G_p^0 of unfilled elastomers [88]. The D_{res} values from independent DQ NMR measurements on these unfilled rubbers are found proportional to the ν values determined from shear data. This allows to determine the proportionality constant between both quantities for our Sprintan[®] SLR-4602 - Schkopau samples with a specific microstructure. Based on a combination of DQ NMR measurements and shear data for unfilled rubbers, for the first time the crosslink density of the rubber matrix is estimated in composites in absolute units (m^{-3}). The results for different silica-filled composites show clearly that the crosslink density decreases systematically with increasing U7000GR filler content. We interpret this as a consequence of a strong absorption of the cross-linking agent on the surface of filler particles. With this observation, it is evident from T-sweep mechanical measurements that the reinforcement is primarily induced by the fillers and it is absolutely not affected by the network topology.

Different contributions to the reinforcement were quantified based on nonlinear mechanical behavior of SBR composites. It is concluded from this analysis that the hydrodynamic component of the filler reinforcement is the multiplicative term to the unfilled storage modulus. The contribution from the filler network is an additive quantity to the overall modulus of the filled composite. At small deformations, the filler network is formed at critical filler fraction $\phi_c \approx 0.156$ (60 phr). The ϕ_c is considered as the percolation threshold of the formation of the filler network. The G'_0 measured at 25°C, 60°C and 150°C show that the value of the percolation threshold (ϕ_c) do not change with temperature. The storage modulus (G'_∞) measured at large sinusoidal deformations increases linearly with the addition of filler and do not show a percolation threshold, indicating the absence of the filler network at high mechanical deformations. The G'_∞ observed at all measured temperatures are observed higher than theoretical hydrodynamic model of Einstein-Smallwood (ES). The remaining reinforcement ($G'_\infty - G'_{ES}$) and its systematic temperature-dependent behavior is interpreted as a contribution from the occluded rubber within the broken aggregates, which is shielded from the applied stress-field and hence it increases the effective filler volume (ϕ_{eff}) of the composite.

From the linear response mechanical measurements, the filler network contribution ($\Delta G_{filler\ network}$) were isolated at different temperatures and frequencies as the difference between the measured G'_0 and the ES extrapolation to above ϕ_c . $\Delta G_{filler\ network}$ decreases monotonically with temperature as well as with frequency. This result confirms the idea presented in T- and ω -dependent G'_p measurements for high silica-filled samples that the filler network ($\Delta G_{filler\ network}$) has a relaxatory nature and holds vis-

coelastic properties. By combining the results obtained from the NMR and the DMA measurements, it is proposed that the viscoelasticity of the filler network originates from the rigid-immobilized fractions of the matrix confined in the isolated cavities of the filler network. Upon increasing the temperature, the softening of confined-immobilized component leads to a lower bending rigidity of the viscoelastic filler-filler connections and hence lower the overall $\Delta G_{filler\ network}$.

Appendix A

Isothermal Frequency Sweeps (80 phr Silica-filled)

To construct a master curve of the SBR composite filled with 80 phr of the silica, frequency sweeps were measured at temperatures from -35°C to 150°C with a given strain amplitude 0.2%. The isothermal curves of storage and loss moduli are plotted against the given frequency window in Figure A.1.

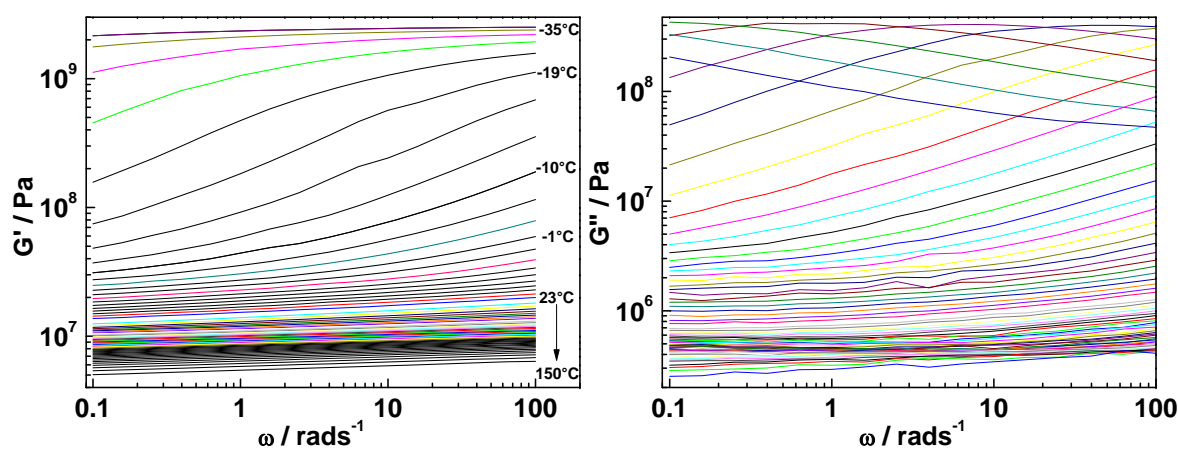


Figure A.1: Isothermal storage (a) and loss (b) modulus curves of SBR plotted against the given frequency measured at temperatures from -35°C to 150°C (as indicated few of them).

To obtain the master curves of G' and G'' , the isothermal frequency curves shown in Figure A.1 were shifted horizontally along the frequency scale with the reference curve of 0°C . The resultant viscoelastic master curves $G^*(\omega)$ are shown in Figure 6.5. The obtained temperature-dependent horizontal shift factors a_T are shown in Figure 6.6.

Bibliography

- [1] G. Kraus, *Reinforcement of elastomers*. Interscience Publishers, 1965.
- [2] J. E. Mark, B. Erman, and F. R. Eirich, eds., *Science and Technology of Rubber*. Elsevier, Amsterdam, 2006.
- [3] A. I. Medalia, “Effects of carbon black on abrasion and treadwear,” in *The Second international conference on carbon black*, pp. 295–304, Universite de Haute-Alsace, 1993.
- [4] C. Robertson and C. Roland, “Glass transition and interfacial segmental dynamics in polymer-particle composites,” *Rubber Chem Technol*, vol. 81, no. 3, pp. 506–522, 2008.
- [5] M. Gerspacher and C. P. O’Ferrell, “Tire compound materials interaction,” *KGK*, vol. 54, pp. 153–158, 2001.
- [6] M.-J. Wang, “Effect of filler-elastomer interaction on tire tread performance part 1,” *Kautsch Gummi Kunstst*, vol. Issue 9, pp. 438–443, 2007.
- [7] M.-J. Wang, “Effect of filler-elastomer interaction on tire tread performance part 2,” *Kautsch Gummi Kunstst*, pp. 33–42, 2008.
- [8] G. Heinrich, M. Klüppel, and T. A. Vilgis, “Reinforcement of elastomers,” *Curr Opin Solid State Mater Sci*, vol. 6, no. 3, pp. 195–203, 2002.
- [9] M. Klüppel and G. Heinrich, “Rubber friction on self-affine road tracks,” *Rubber Chem. Technol.*, vol. 73, no. 4, pp. 578–606, 2000.
- [10] B. Persson, “Theory of rubber friction and contact mechanics,” *J Chem Phys*, vol. 115, pp. 3840–3861, 2001.
- [11] B. Persson, “On the theory of rubber friction,” *Surface Science*, vol. 401, pp. 445–454, 1998.

- [12] C. Angell, “Formation of glasses from liquids and biopolymers,” *Science*, vol. 267, pp. 1924–1935, 1995.
- [13] R. Böhmer, R. Chamberlin, G. Diezemann, B. Geil, A. Heuer, G. Hinze, S. Kuebler, R. Richert, B. Schiener, H. Sillescu, H. Spiess, U. Tracht, and M. Wilhelm, “Nature of the non-exponential primary relaxation in structural glass-formers probed by dynamically selective experiments,” *J noncryst solids*, vol. 235-237, pp. 1–9, 1998.
- [14] E. Donth, *The glass transition: Relaxation dynamics in liquids and disordered materials*. Springer, Heidelberg, 2001.
- [15] G. P. Debenedetti and F. H. Stillinger, “Supercooled liquids and the glass transition,” *Nature*, vol. 410, no. 6825, pp. 259–267, 2001.
- [16] L. Berthier, G. Biroli, J. Bouchaud, L. Cipelletti, D. El Masri, D. L’Hôte, F. Ladieu, and M. Pierno, “Direct experimental evidence of a growing length scale accompanying the glass transition,” *Science*, vol. 310, no. 5755, pp. 1797–1800, 2005.
- [17] G. B. McKenna, “Glass dynamics - diverging views on glass transition,” *Nature Physics*, vol. 4, no. 9, pp. 673–674, 2008.
- [18] K. Dawson, K. Kearns, L. Yu, W. Steffen, and M. Ediger, “Physical vapor deposition as a route to hidden amorphous states,” *Proceedings of the National Academy of Sciences of the United States of America*, vol. 106, no. 36, pp. 15165–15170, 2009.
- [19] K. Ngai, *Relaxation and diffusion in complex systems*. Springer, Heidelberg, 2011.
- [20] M. Alcoutlabi and G. B. McKenna, “Effects of confinement on material behaviour at the nanometre size scale,” *J Phys Cond Matter*, vol. 17, no. 15, pp. R461–R524, 2005.
- [21] C. Alba-Simionesco, B. Coasne, G. Dosseh, G. Dudziak, K. Gubbins, R. Radhakrishnan, and M. Sliwinska-Bartkowiak, “Effects of confinement on freezing and melting,” *J Phys Cond Matter*, vol. 18, no. 6, pp. R15–R68, 2006.
- [22] E. Hempel, S. Vieweg, A. Huwe, K. Otto, C. Schick, and E. Donth, “Characteristic length of glass transition from calorimetry in different confinements,” *J.Phys.IV France*, vol. 10, no. Pr7, pp. 79–82, 2000.

- [23] M. Beiner and H. Huth, “Nanophase separation and hindered glass transition in side-chain polymers,” *Nat Mat*, vol. 2, no. 9, pp. 595–599, 2003.
- [24] C. J. Ellison and J. M. Torkelson, “The distribution of glass-transition temperatures in nanoscopically confined glass formers,” *Nat Mat*, vol. 2, no. 10, pp. 695–700, 2003.
- [25] J. Dutcher and M. Ediger, “Materials science - glass surfaces not so glassy,” *Science*, vol. 319, no. 5863, pp. 577–578, 2008.
- [26] A. Serghei, M. Tress, and F. Kremer, “The glass transition of thin polymer films in relation to the interfacial dynamics,” *J Chem Phys*, vol. 131, no. 15, pp. 154904–+, 2009.
- [27] V. Boucher, D. Cangialosi, A. Alegria, J. Colmenero, J. Gonzalez-Irun, and L. Liz-Marzan, “Accelerated physical aging in pmma/silica nanocomposites,” *Soft Matter*, vol. 6, no. 14, pp. 3306–3317, 2010.
- [28] A. Papon, K. Saalwächter, K. Schäler, L. Guy, F. Lequeux, and H. Montes, “Low-field nmr investigations of nanocomposites: Polymer dynamics and network effects,” *Macromolecules*, vol. 44, no. 4, pp. 913–922, 2011.
- [29] K. Saalwächter, “Proton multiple-quantum nmr for the study of chain dynamics and structural constraints in polymeric soft materials,” *Progress in nuclear magnetic resonance spectroscopy*, vol. 51, pp. 1–35, 2007.
- [30] J. L. Valentin, J. Carretero-Gonzalez, I. Mora-Barrantes, W. Chasse, and K. Saalwächter, “Uncertainties in the determination of cross-link density by equilibrium swelling experiments in natural rubber,” *Macromolecules*, vol. 41, no. 13, pp. 4717–4729, 2008.
- [31] J. L. Valentin, P. Posadas, A. F. Torres, M. A. Malmierca, J. Carretero-Gonzalez, W. Chasse, and K. Saalwächter., “Inhomogeneities and chain dynamics in diene rubbers vulcanized with different cure systems,” *Macromolecules*, vol. 43, no. 9, pp. 4210–4222, 2010.
- [32] J. L. Valentin, I. Mora-Barrantes, J. Carretero-Gonzalez, M. A. Lopez-Manchado, P. Sotta, D. R. Long, and K. Saalwächter, “Novel experimental approach to evaluate filler-elastomer interactions,” *Macromolecules*, vol. 43, no. 1, pp. 334–346, 2010.

- [33] A. Medalia, "Effect of carbon black on dynamic properties of rubber vulcanizates," *Rubber Chem. Technol.*, vol. 51, pp. 437–523, 1978.
- [34] M. J. Wang, "Effect of polymer-filler and filler-filler interactions on dynamic properties of filled vulcanizates," *Rubber Chem Technol*, vol. 71, no. 3, pp. 520–589, 1998.
- [35] J. L. Leblanc, "Rubber-filler interactions and rheological properties in filled compounds," *Prog Polym Sci*, vol. 27, pp. 627–687, 2002.
- [36] D. Kohls and G. Beaucage, "Rational design of reinforced rubber," *Current Opinion in Solid State and Materials Science*, vol. 6, no. 3, pp. 183 – 194, 2002.
- [37] E. M. Dannenberg, "The effects of surface chemical interactions on the properties of filler-reinforced rubbers," *Rubber Chem Technol*, vol. 48, pp. 410–444, 1975.
- [38] R. Christensen, *Mechanics of composite materials*. New York: Wiley, 1979.
- [39] A. R. Payne, "The dynamic properties of carbon black-loaded natural rubber vulcanizates. part-1," *J App Polym Sci*, vol. 6, Issue. 19, pp. 57–63, 1962.
- [40] A. R. Payne, "Dynamic properties of heat treated butyl vulcanizates," *J App Polym Sci*, vol. 7, pp. 873–885, 1963.
- [41] A. R. Payne and W. F. Watson, "Carbon black structure in rubber," *Rubber Chem. Technol.*, pp. 147–155, 1963.
- [42] G. Kraus, "Mechanical losses carbon-black filled rubbers," *App. Polym. Sci.: App. Polym. Symp.*, vol. 39, pp. 75–92, 1984.
- [43] M. Klüppel, R. H. Schuster, and G. Heinrich, "Structure and properties of reinforcing fractal filler networks in elastomers," *Rubber Chem. Technol.*, vol. 70, no. 2, pp. 243–255, 1997.
- [44] M. Klüppel, "The role of disorder in filler reinforcement of elastomers on various length scales," *Adv Polym Sci*, vol. 164, pp. 1–86, 2003.
- [45] M. Klüppel and G. Heinrich, "Physics and engineering of reinforced elastomers: From mechanical mechanisms to industrial applications," *Kautsch. Gummi Kunstst.*, vol. 58, pp. 217–224, 2005.

- [46] T. Vilgis and G. Heinrich, “Disorder-induced enhancement of polymer adsorption—a model for the rubber-polymer interaction in filled rubbers,” *Macromolecules*, vol. 27, pp. 7846–7854, 1994.
- [47] P. Mele, S. Marceau, D. Brown, Y. Puydt, and N. D. Alberola, “Reinforcement effects in fractal-structure-filled rubber,” *Polymer*, vol. 43, pp. 5577–5586, 2002.
- [48] C. Gauthier, E. Reynaud, R. Vassoille, and L. Ladouce-Stelandre, “Analysis of the non-linear viscoelastic behaviour of silica filled styrene butadiene rubber,” *Polymer*, vol. 45, pp. 2761–2771, 2004.
- [49] L. Guy, S. Daudey, P. Cochet, and Y. Bomal, “New insights in the dynamic properties of precipitated silica filled rubber using a new high surface silica,” *Kautsch. Gummi Kunstst.*, vol. Jul/Aug, pp. 383–391, 2009.
- [50] Y. Fukahori, “New progress in the theory and model of carbon black reinforcement of elastomers,” *J App Polym Sci*, vol. 95, pp. 60–67, 2005.
- [51] J. Diani, P. Gilormini, Y. Merckel, and F. Vion-Loisel, “Micromechanical modeling of the linear viscoelasticity of carbon-black filled styrene butadiene rubbers: The role of the filler–rubber interphase,” *Mech Mat*, vol. 59, pp. 65–72, 2013.
- [52] P. G. Maier and D. Göritz, “Molecular interpretation of the payne effect,” *Kautsch. Gummi Kunstst.*, vol. 49, pp. 18–21, 1996.
- [53] A. P. Meera, S. Said, Y. Grohens, and S. Thomas, “Nonlinear viscoelastic behavior of silica-filled nr nanocomposite,” *J Phys Chem C*, vol. 113, pp. 17997–18002, 2009.
- [54] S. Merabia, P. Sotta, and D. R. Long, “A microscopic model for the reinforcement and the nonlinear behavior of filled elastomers and thermoplastic elastomers (payne and mullins effects),” *Macromolecules*, vol. 41, no. 21, pp. 8252–8266, 2008.
- [55] M. Klüppel, “Evaluation of viscoelastic master curves of filled elastomers and applications to fracture mechanics,” *Journal of Physics-Condensed Matter*, vol. 21, p. 35104, 2009.
- [56] J. Fritzsche and M. Klüppel, “Structural dynamics and the interfacial properties of filled-reinforced elastomers,” *J of Phys: Cond. Matter*, vol. 23, p. 035104, 2011.

- [57] A. Papon, H. Montes, M. Hanafi, F. Lequeux, L. G. L., and K. Saalwächter, “Glass-transition temperature gradient in nanocomposites: Evidence from nuclear magnetic resonance and differential scanning calorimetry,” *Phys Rev Lett*, vol. 108, p. 065702, 2012.
- [58] A. Papon, H. Montes, F. Lequeux, J. Oberdisse, K. Saalwächter, and L. Guy, “Solid particles in an elastomer matrix: impact of colloid dispersion and polymer mobility modification on the mechanical properties,” *Soft Matter*, vol. 8, pp. 4090–4096, 2012.
- [59] A. Papon, T. Chaussee, L. Guy, K. Saalwächter, J. Oberdisse, S. Merabia, D. Long, P. Sotta, H. H. Frielinghaus, A. Radulescu, B. Deme, L. Noirez, H. Montes, and F. Lequeux, “Studying model samples to understand mechanical properties of filled elastomers,” *Kautsch Gummi Kunstst*, vol. 9, pp. 52–58, 2013.
- [60] C. Robertson, C. Lin, R. Bogoslovov, M. Rackaitis, P. Sadhukhan, J. Quinn, and C. Roland, “Flocculation, Reinforcement, and Glass Transition Effects in Silica-Filled Styrene-Butadiene Rubber,” *Rubber Chem. Technol.*, vol. 84, pp. 507–519, 2011.
- [61] A. A. Gusev, “Micromechanical mechanism of reinforcement and losses in filled rubbers,” *Macromolecules*, vol. 39, pp. 5960–5962, 2006.
- [62] D. Long and P. Sotta, “Stress relaxation of large amplitudes and long timescales in soft thermoplastic and filled elastomers,” *Rheo. Acta*, vol. 46, pp. 1029–1044, 2007.
- [63] I. Morozov, B. Lauke, and G. Heinrich, “A new structural model of carbon black framework in rubbers,” *Comput. Mat. Sci.*, vol. 47, pp. 817–825, 2010.
- [64] G. Tsagaropoulos and A. Eisenberg, “Direct observation of two glass transitions in silica-filled polymers. implications for the morphology of random ionomers,” *Macromolecules*, vol. 28, no. 1, pp. 396–398, 1995.
- [65] D. Fragiadakis, L. Bokobza, and P. Pissis, “Dynamics near the filler surface in natural rubber-silica nanocomposites,” *Polymer*, vol. 52, no. 14, pp. 3175–3182, 2011.
- [66] E. Donth, “Characteristic length of the glass transition,” *J Polym Sci B: Polym Phys*, vol. 34, no. 17, pp. 2881–2892, 1996.

- [67] J. Berriot, H. Montes, F. Lequeux, D. Long, and P. Sotta, "Evidence for the shift of the glass transition near the particles in silica-filled elastomers," *Macromolecules*, vol. 35, no. 26, pp. 9756–9762, 2002.
- [68] A. Wurm, M. Ismail, B. Kretzschmar, D. Pospiech, and C. Schick, "Retarded crystallization in polyamide/layered silicates nano-composites caused by an immobilized interphase," *Macromolecules*, vol. 43, pp. 1480–1487, 2010.
- [69] N. Jouault, J. F. Moll, D. Meng, K. Windsor, S. Ramcharan, C. Kearney, and S. K. Kumar, "Bound polymer layer in nanocomposites," *Macro Lett*, vol. 2, pp. 371–374, 2013.
- [70] C. G. Robertson and M. Rackaitis, "Further consideration of viscoelastic two glass transition behavior of nanoparticle-filled polymers," *Macromolecules*, vol. 44, pp. 1177–1181, 2011.
- [71] H. Montes, F. Lequeux, and J. Berriot, "Influence of the glass transition temperature gradient on the nonlinear viscoelastic behavior in reinforced elastomers," *Macromolecules*, vol. 36, pp. 8107–8118, 2003.
- [72] A. Mujtaba, M. Keller, S. Ilisch, H.-J. Radusch, T. Thurn-Albrecht, K. Saalwächter, and M. Beiner, "Mechanical properties and cross-link density of styrene-butadiene model composites containing fillers with bimodal particle size distribution," *Macromolecules*, vol. 45, no. 16, pp. 6504–6515, 2012.
- [73] J. E. Mark, B. Erman, and F. R. Eirich, eds., *Science and Technology of Rubber*. Elsevier 3rd Edition, 2005.
- [74] W. Hofmann, *Rubber Technology Handbook*. Hanser Publishers, 1989.
- [75] M. K. H. Nordsiek, "The integral rubber concept- an approach to an ideal tire tread rubber.," *Kautsch. Gummi Kunstst.*, vol. 38, pp. 178–185, 1984.
- [76] M. Rubinstein and S. Panyukov, "Nonaffine deformation and elasticity of polymer networks," *Macromolecules*, vol. 30, pp. 8036–8044, 1997.
- [77] T. A. Vilgis, G. Heinrich, and M. Klüppel, *Reinforcement of polymer nanocomposites*. Cambridge University Press, 2009.
- [78] R. Ullman, "An essay on the molecular theory of rubber elasticity," *J Polym Sci: Polym Symp*, vol. 72, pp. 39–44, 1985.

- [79] J. J. Hermans, "Deformations and swelling of polymer networks containing comparatively long chains.," *Transactions of the Faraday Society*, vol. 43, pp. 591–600, 1947.
- [80] F. T. Wall and P. J. Flory, "Statistical thermodynamics of rubber elasticity," *J Chem Phys*, vol. 19, pp. 1435–1439, 1951.
- [81] H. M. James and E. Guth, "Theory of elastic properties of rubber," *J Chem Phys*, vol. 11, pp. 455–481, 1943.
- [82] H. M. James and E. Guth, "Theory of the increase in rigidity of rubber during cure," *J Chem Phys*, vol. 15, pp. 669–683, 1947.
- [83] G. Ronca and G. Allegra, "An approach to rubber elasticity with internal constraints," *J Chem Phys*, vol. 63, pp. 4990–4997, 1975.
- [84] S. F. Edwards, "The statistical mechanics of polymerized material," *Proceedings Phys Soc*, vol. 92, p. 9, 1967.
- [85] P. G. Higgs and R. J. Gaylord, "Slip-links, hoops and tubes: tests of entanglement models of rubber elasticity," *Polymer*, vol. 31, pp. 70–74, 1988.
- [86] M. Gottlieb and R. J. Gaylord, "Experimental tests of entanglements models of rubber elasticity," *Macromolecules*, vol. 17, pp. 2024–2030, 1984.
- [87] J. E. Mark and J. L. Sullivan, "Model networks of end-linked pdms chains: a comparison between experimental and theoretical values of elastic modulus and equilibrium degree of swelling.," *J Chem Phys*, vol. 66, pp. 1006–1011, 1977.
- [88] M. Rubinstein and R. H. Colby, *Polymer Physics*. Oxford University Press, Oxford, 2003.
- [89] A. I. Medalia, "Morphology of aggregates: I. calculation of shape and bulkiness factors; application to computer-simulated random flocs," *J Colloid Interface Sci*, vol. 24, pp. 393–404, 1967.
- [90] A. I. Medalia, "Effective degree of immobilization of rubber occluded within carbon black aggregates," *Rubber Chem. Technol.*, vol. 45, p. 1171, 1972.
- [91] G. Kraus, "A structure-concentration equivalence principle in carbon black reinforcement of elastomers," *Polym Lett*, vol. 8, pp. 601–606, 1970.

- [92] S. Wolff and M. J. Wang, "Filler elastomer interactions. part 4. the effect of the surface energies of fillers on elastomer reinforcement," *Rubber Chem Technol*, vol. 65, no. 2, pp. 329–342, 1992.
- [93] M. P. Wagner, "Reinforcing silica and silicates," *Rubber Chem Technol*, vol. 49, pp. 703–774, 1976.
- [94] S. Wolff, "Chemical aspects of rubber reinforcement by fillers.," *Rubber Chem Technol*, vol. 69, p. 325, 1996.
- [95] J. Fröhlich, W. Niedermeier, and H. D. Luginsland, "The effect of filler-filler and filler-elastomer interaction on rubber reinforcement.," *Compos. Part A: Appl. Sci. Manuf.*, vol. 36, p. 449, 2005.
- [96] A. Einstein, "Eine neue bestimmung der molekül dimension," *Ann. Physics*, pp. 289–306, 1906.
- [97] H. M. Smallwood, "Limiting law of the reinforcement of rubber," *J App Phys*, vol. 15, no. 11, pp. 758–766, 1944.
- [98] E. Guth and O. Gold, "On the hydrodynamical theory of the viscosity of suspensions," *Phys. Rev.*, vol. 53, p. 322, 1938.
- [99] E. Guth, "Theory of filler reinforcement," *J. App. Phys.*, vol. 16, pp. 20–25, 1944.
- [100] A. I. Medalia, "Heat generation in elastomer compounds: causes and effects," *Rubber Chem. Technol.*, vol. 64, pp. 481–492, 1990.
- [101] G. K. Batchelor and J. T. Green, "The determination of the bulk stress in a suspension of spherical particles to order c^2 ," *J Fluid Mech*, vol. 56, pp. 401–427, 1972.
- [102] D. G. Thomas, "Transport characteristics of suspension: A note on the viscosity of newtonian suspensions of uniform spherical particles," *J Colloid Sci*, vol. 20, pp. 267–277, 1965.
- [103] B. Hinkelmann, "The analytical description of the filler influence on the flow behaviour of the polymer melt," *Rheol Acta*, vol. 21, p. 491, 1982.
- [104] H. Eggers and P. Schümmer, "Reinforcement mechanisms in carbon black and silica loaded rubber melts at low stresses.," *Rubber Chem. Technol.*, vol. 69, pp. 253–265, 1996.

- [105] S. Wolff and J.-B. Donnet, "Characterization of fillers in vulcanizates according to the einstein-guth-gold equation," *Rubber Chem Technol*, vol. 63, pp. 32–45, 1990.
- [106] M.-J. Wang, S. X. Lu, and K. Mahmud, "Carbon-silica dual phase filler," *J Polym Sci B: Polym Phys*, vol. 38, pp. 1240–1249, 2000.
- [107] R. W. Sambrook *J Inst Rubber Ind*, vol. 4, p. 210, 1970.
- [108] F. Clement, L. Bokobza, and L. Monnerie, "Investigation of the payne effect and its temperature dependence on silica-filled pdms networks. part i: Experimental results," *Rubber Chem. Technol.*, vol. 78, pp. 211–231, 2005.
- [109] F. Clement, L. Bokobza, and L. Monnerie, "Investigation of the payne effect and its temperature dependence on silica-filled pdms networks. part ii: Test of quantitative models," *Rubber Chem. Technol.*, vol. 78, pp. 232–244, 2005.
- [110] K. E. Gui, C. S. Wilkinson, and S. D. Gehmann, "Vibration characteristics of tread stocks," *Ind Engg Chem*, vol. 44, pp. 720–723, 1952.
- [111] P. P. A. Smit, "The glass transition in carbon black reinforced rubber," *Rheol Acta*, vol. 5, pp. 277–283, 1966.
- [112] S. Vieweg, R. Unger, K. Schröter, and E. Donth, "Frequency and temperature dependent of the small-strain behaviour of carbon-black filled vulcanizates," *Polym Net Blends*, vol. 5, pp. 199–204, 1995.
- [113] S. Vieweg, R. Unger, G. Heinrich, and E. Donth, "Comparison of dynamic shear properties of styrene-butadiene vulcanizates filled with carbon black or polymeric fillers," *J.Appl.Polym.Sci.*, vol. 73, no. 4, pp. 495–503, 1999.
- [114] G. Heinrich and M. Klüppel, "Recent advances in the theory of filler networking in elastomers," *Ad Polym Sci*, vol. 160, 2002.
- [115] S. Kaufman, W. P. Slichter, and D. D. Davis, "Nuclear magnetic resonance study of rubber-carbon black interactions," *J Polym Sci*, vol. 9, pp. 829–839, 1971.
- [116] J. O'Brien, E. Cashell, G. E. Wardell, and V. J. McBrierty, "An nmr investigation of the interaction between carbon black and cis-polybutadiene," *Macromolecules*, vol. 9, pp. 653–660, 1976.

- [117] S. Asai, H. Kaneki, M. Sumita, and K. Miyasaka, "Effect of oxidized carbon black on the mechanical properties and molecular motions of natural rubber studied by pulse nmr," *J App Polym Sci*, vol. 43, pp. 1253–1257, 1991.
- [118] N. K. Dutta, N. R. Choudhury, B. Haidar, A. Vidal, and J. B. Donnet, "High resolution solid-state nmr investigation of the filler-rubber interaction: High speed 1h magic-angle spinning n.m.r, spectroscopy in carbon black filled styrene butadiene rubber," *Polymer*, vol. 35, pp. 4293–4299, 1994.
- [119] J. Berriot, H. Montes, F. Lequeux, D. Long, and P. Sotta, "Gradient of glass transition temperature in filled elastomers," *Europhys Lett*, vol. 64, no. 1, pp. 50–56, 2003.
- [120] N. Jouault, P. Vallat, F. Dalmas, S. Said, J. Jestin, and F. Boue, "Well-dispersed fractal aggregates as filler in polymer-silica nanocomposites: Long-range effects in rheology," *Macromolecules*, vol. 42, no. 6, pp. 2031–2040, 2009.
- [121] V. M. Litvinov and P. A. M. Steeman, "Epdm-carbon black interactions and the reinforcement mechanisms, as studied by low-resolution 1h nmr," *Macromolecules*, vol. 32, pp. 8476–8490, 1999.
- [122] J. Liu, S. Wu, L. Zhang, W. Wang, and D. Cao, "Molecular dynamics simulation for insight into microscopic mechanism of polymer reinforcement," *Phys Chem Chem Phys*, vol. 13, pp. 518–529, 2011.
- [123] A. A. Gusev and S. A. Lurie, "Loss amplification effect in multiphase materials with viscoelastic interfaces," *Macromolecules*, vol. 42, pp. 5372–5377, 2009.
- [124] C. G. Robertson, R. Bogoslovov, and C. M. Roland, "Structural arrest and thermodynamic scaling in filler-reinforced polymers," *Rubber Chem Technol*, vol. 82, no. 2, pp. 202–213, 2009.
- [125] C. G. Robertson, C. J. Lin, R. B. Bogoslovov, M. Rackaitis, P. Sashukhan, J. D. Quinn, and C. M. Roland, "Flocculation, reinforcement, and glass transition effects in silica-filled sbr," *Rubber Chem Technol*, vol. 84, pp. 507–519, 2011.
- [126] I. M. Ward and H. D. W., *An introduction to the mechanical properties of solid polymers*. John Wiley & Sons, 1993.

- [127] S. Pankaj, *Confined dynamics, side-chain crystallization and long term behavior of nanophase separated poly(3-alkyl thiophenes)*. PhD thesis, Martin-Luther-Universität Halle-Wittenberg, 2011.
- [128] J. D. Ferry, *Viscoelastic properties of polymers*. New York: Wiley, 1980.
- [129] K. Schäler, *Low-Field NMR Studies Of Structure and Dynamics in Semicrystalline Polymers*. PhD thesis, Martin-Luther-Universität Halle-Wittenberg, 2012.
- [130] M. Mauri, Y. Thomann, H. Schneider, and K. Saalwächter, “Spin-diffusion nmr at low field for the study of multiphase solids,” *Solid State Nucl. Magn. Reson*, vol. 34, pp. 125–141, 2008.
- [131] W. Chasse, *Structure, formation and thermodynamic properties of polymer networks as studied by NMR*. PhD thesis, Martin-Luther-Universität Halle-Wittenberg, 2012.
- [132] K. Saalwächter and J. Sommer, “Nmr reveals non-distributed and uniform character of network chain dynamics,” *Macromolecular Rapid Communications*, vol. 28, no. 14, pp. 1455–1465, 2007.
- [133] W. Kuhn and F. Grün, “Beziehungen zwischen elastischen konstanten und dehnungsdoppelbrechung hochelastischer stoffe.,” *Colloid & Polym Sci*, vol. 101, pp. 248–271, 1942.
- [134] K. Saalwächter, “Artifacts in transverse proton nmr relaxation studies of elastomers,” *Macromolecules*, vol. 38, pp. 1508–1512, 2005.
- [135] M. J. Duer, *Solid-state NMR spectroscopy - principles and applications*. Blackwell Science., 2002.
- [136] R. Bond and G. F. Morton, “A tailor-made polymer for tyre applications,” *Polymer*, vol. 25, pp. 132–140, 1984.
- [137] A. Lechtenboehmer, H. G. Money Penny, and F. M. F., “A review of polymer interfaces in tyre technology,” *J Brit Polym*, vol. 22, pp. 265–301, 1990.
- [138] K. Y. Saito, “New polymer development for low rolling resistance tyres,” *Kautsch Gummi Kunstst*, vol. 39, pp. 30–32, 1985.
- [139] A. K. Chandra, *Current topics in Elastomer Research*. CRC Press, 2008.

- [140] A. H. Tullo, "Stretching tire's magic triangle," *Chemical and Engineering News (C&EN)*, vol. 87:46, pp. 10–14, 2009.
- [141] R. A. L. H. J. F. S. L. Aggarwal, I. G. Hargis, *Advances in elastomers and rubber elasticity*. Plenum Press, 1986.
- [142] "Wet grip basics-continental-tires."
- [143] J. A. Greenwood, H. Minshall, and D. Tabor, "Hysteresis losses in rolling and sliding friction," *Rubber Chem. Technol.*, vol. 259, pp. 480–507, 1960.
- [144] F. S. Conant and J. W. Liska, "Friction studies on rubberlike materials," *Rubber Chem. Technol.*, vol. 33, pp. 1218–1258, 1960.
- [145] D. Bulgin, G. Hubbard, and M. Walters, "Road and laboratory studies of friction and elastomers," in *Paper presented at the 4th Rubber Technology Conference, London*, 1962.
- [146] K. A. Grosch, "The relation between the friction and visco-elastic properties of rubber," *Proc. R. Soc., Lond*, vol. A274, p. 21, 1963.
- [147] G. Heinrich and H. B. Dumler, "Wet skid properties of filled rubbers and the rubber - glass transition," *Rubber Chem. Technol.*, vol. 71, no. 1, pp. 53–61, 1998.
- [148] C. Robertson, C. Lin, M. Rackaitis, and C. Roland, "Influence of particle size and polymer-filler coupling on viscoelastic glass transition of particle-reinforced polymers," *Macromolecules*, vol. 41, no. 7, pp. 2727–2731, 2008.
- [149] D. F. Moore, "A review of hysteresis theories for elastomers," *Wear*, vol. 30, pp. 1–34, 1974.
- [150] D. F. Moore, *The Friction and Lubrication of Elastomers*. Pergamon Press, Oxford, 1972.
- [151] B. Choubane, C. R. Holzschuher, and S. Gokhale, "Precision of locked wheel testers for measurements of roadway surface friction characteristics," *Research Report FL/DOT/SMO/03-464*, 2003.
- [152] R. Engehausen, A. Rawlinson, and J. Trimbach *Tire Technol. Int. Ann. Review*, p. 36, 2001.

- [153] G. Heinrich, "The dynamics of tire tread compounds and their relationship to wet skid behavior," *Prog. Colloid Polym. Sci.*, vol. 90, pp. 16–26, 1992.
- [154] R. R. Rahalkar, "Dependence of wet skid resistance upon the entanglement density and chain mobility according to the rouse theory of viscoelasticity," *Rubber Chem. Technol.*, vol. 62, p. 246, 1988.
- [155] *Styron GmbH, SPRINTAN SLR 4602 - Schkopau, Technical information 2010, Form No. 850 - 00901.*
- [156] *Evonik GmbH, Ultrasil U7000GR - Technical information.*
- [157] M. Keller, A. Wutzler, A. Mujtaba, H. H. Le, S. Ilisch, and H.-J. Radusch in *Proceedings of Symposium 'Polymer Blends and Nanocomposites with Biobased Components'*, 14-15th of September 2011, Halle (Saale), ISBN 978-3-86829-391-3.
- [158] J. S. Dick, *Compounding Processing Characteristics and Testing, in Rubber Technology: Compounding and Testing for Performance.* Hanser Publisher, 2001.
- [159] G. P. Baeza, A. C. Genix, and J. Oberdisse, "Multiscale filler structure in simplified industrial nanocomposite silica/sbr systems studies by saxs and tem," *Macromolecules*, vol. 46, pp. 317–329, 2012.
- [160] D. Long and F. Lequeux, "Heterogeneous dynamics at the glass transition in van der waals liquids, in the bulk and in thin films," *Euro Phys E*, vol. 4:3, pp. 371–387, 2001.
- [161] A. Bansal, H. Yang, C. Li, K. Cho, B. Benicewicz, S. K. Kumar, and L. Schadler, "Quantitative equivalence between polymer nanocomposites and thin polymer films," *Nat Mat*, vol. 4, pp. 693–698, 2005.
- [162] Y. Kantor and I. Webman, "Elastic properties of random percolating systems," *Phys Rev Lett*, vol. 52,21, pp. 1891–1894, 1984.

Erklärung

Hiermit versichere ich, dass ich die vorliegende Arbeit selbstständig durchgeführt und verfasst habe. Außer den in der Arbeit genannten, standen mir keinerlei Hilfsmittel oder Hilfen zuteil. Die benutzten fremden Quellen habe ich vollständig aufgelistet und inhaltliche oder wörtliche Zitate als solche gekennzeichnet.

Anas Mujtaba

Acknowledgement

First, I would like to thank my supervisors, Prof. Dr. T. Thurn-Albrecht and Prof. Dr. K. Saalwächter , who not only induced scientific orientation into me but also set himself as an example of commitment and passion for research. Being my most critical audience, both of them have contributed to this research in invaluable ways. I have really enjoyed our countless inspiring discussions through this time which helped me to shape my intellectual development through these profitable interactions with them.

I would like to thank warmly to Prof. Dr. M. Beiner for his help, guidance, patience and advice. His enthusiastic and unremitting support during this course of time, and his teaching will benefit me in future, to which I show my greatest respect and most sincere gratitude from the core of my heart.

At the end, obviously I cannot forget the entire moral support from my parents and especially from my wife over the last four years. I really feel necessary to acknowledge the bundles of prayers and regards which I often felt at times of desperation here. Of course it is not out of place to mention the force of motivation which I received from my daughter to perform better for her future.

Halle (Saale), January 2014

Publications

1. A. Mujtaba, M. Keller, S. Ilisch, H.J. Radusch, T. Thurn-Albrecht, K. Saalwächter, and M. Beiner, 'Mechanical properties and cross-link density of styrene-butadiene model composites containing fillers with bimodal particle size distribution', *Macromolecules*, 45(16):2012
2. A. Mujtaba, M. Keller, S. Ilisch, H.J. Radusch, M. Beiner, T. Thurn-Albrecht and K. Saalwächter, 'Detection of surface-immobilized components and their role in viscoelastic reinforcement of rubber-silica nanocomposites', *ACS Macro Lett.*, 2014,3,481-485.
3. G. P. Baeza, A.-C. Genix, C. Degrandcourt, J. Gummel, A. Mujtaba, K. Saalwächter, T. Thurn-Albrecht, M. Couty and J. Oberdisse, 'Evidence for a unique structure-determining parameter in simplified industrial styrene-butadiene/silica nanocomposites', *ACS Macro Lett.*, 2014,3,448-452.

Curriculum vitae

First Name	Anas
Family Name	Mujtaba
Date of Birth	April 03, 1980
Place of Birth	Lahore, Pakistan
Nationality	Pakistan
E-mail	anasmujtaba@hotmail.com

EDUCATION

Apr. 1998 - Jul. 2002	Bachelor of Engineering: Chemical Engineering University of the Punjab Lahore, Pakistan
Oct. 2007 - Nov. 2009	Master of Science: Applied Polymer Science Martin-Luther-Universität Halle Wittenberg Halle, Germany
Dec. 2009 - Jan. 2014	Ph.D in Institut für Physik Experimental Polymer Physics Martin-Luther-Universität Halle-Wittenberg (Supervised by Prof. Thomas Thurn-Albrecht and Prof. Dr. Kay Saalwächter)

PROFESSIONAL EXPERIENCE

Feb 2003 - May 2006	Noon Industries of Ethanol Fermentation and Distillation. Sargodha, Pakistan (Shift Engineer)
Feb 2014 - Present	Wiss. Mitarbeiter Gruppe Polymerbasiertes Materialdesign Fraunhofer-Institut für Werkstoffmechanik IWM Halle (Saale)
